NASA
MSFC
BOEING

FOLDER 1
CATALOG OF ADVANCED
PROPULSION CONCEPTS
D180-26680-1

ADVANCED PROPULSION SYSTEMS CONCEPTS FOR ORBITAL TRANSFER

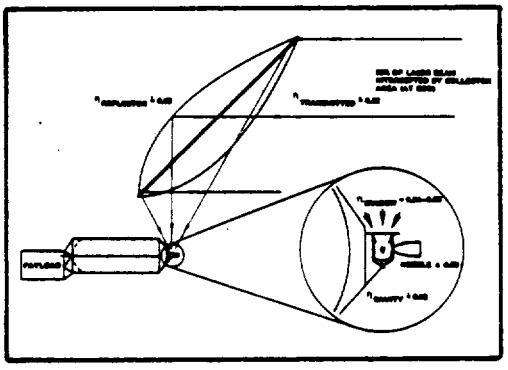

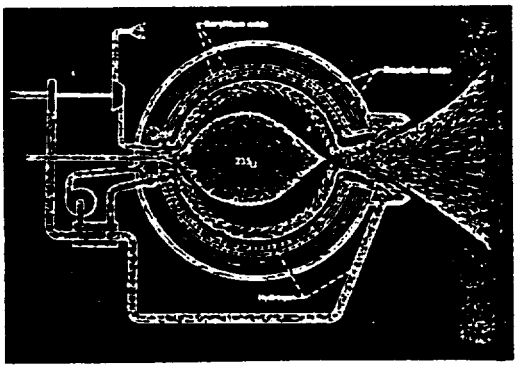

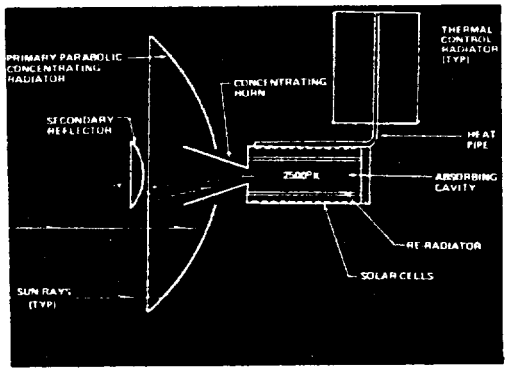

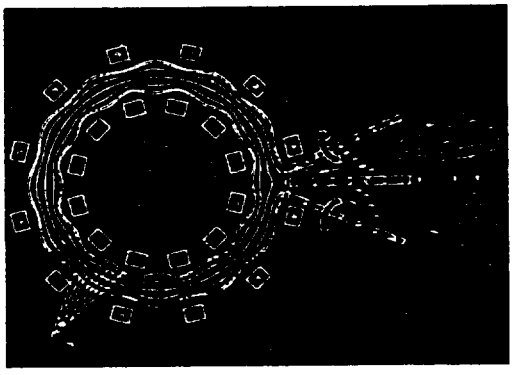

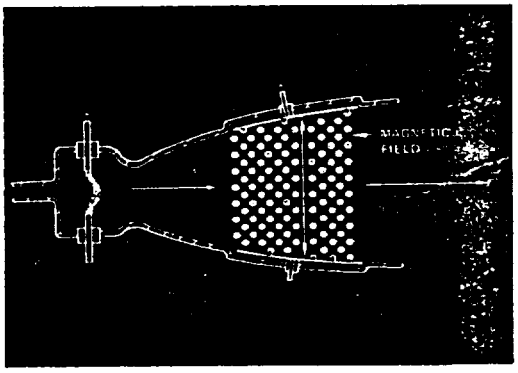

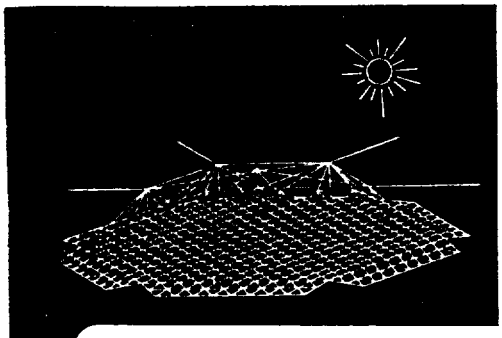

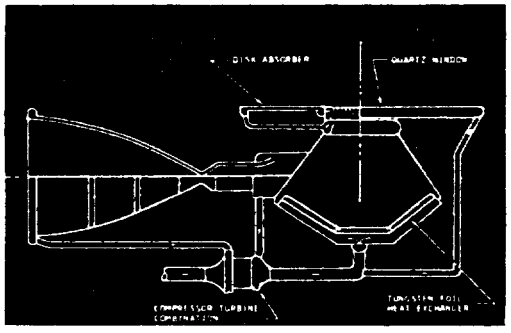

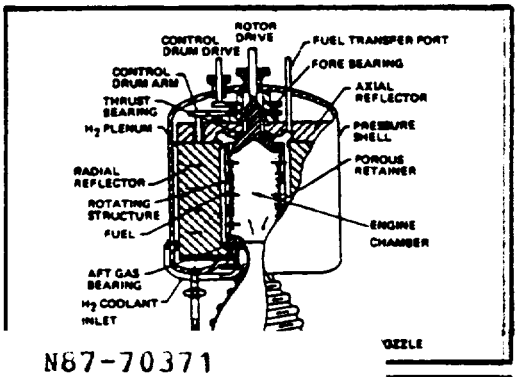

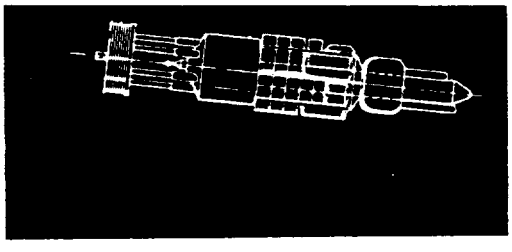

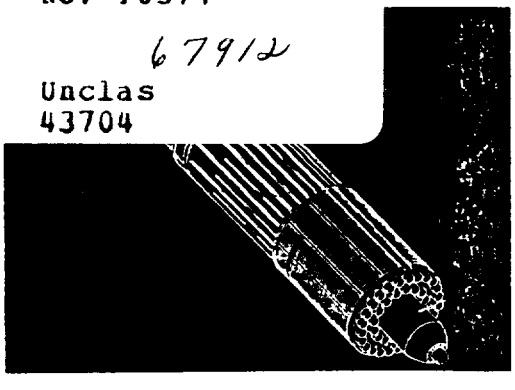

ADVANCED PROPULSION SYSTEMS CONCEPTS FOR ORBITAL TRANSFER STUDY

Final Report
Volume I

CATALOG OF ADVANCED PROPULSION CONCEPTS

D180-26680-1

1981

DPD Number 592
DR Number 6
Contract NAS8-33935

Submitted to
National Aeronautics and Space Administration
George C. Marshall Space Flight Center

by

Boeing Aerospace Company
Seattle, Washington 98124

FOREWORD

This final report of the Advanced Propulsion Systems Concepts for Orbital Transfer Study was prepared by the Upper Stages and Launch Vehicles Preliminary Design organization of the Boeing Aerospace Company (BAC) for the National Aeronautics and Space Administration's George C. Marshall Space Flight Center in accordance with Contract NAS9-33935. The study was conducted under the direction of the NASA study manager, Mr. William Galloway, during the period from July 1980 through July 1981. The final report is organized according to the following three documents:

Volume I:	Catalog of Advanced Propulsion Concepts
Volume II:	Study Technical Results
Volume III:	Life Cycle Cost Estimates

Key personnel during the performance of this study were:

Dr. Dana G. Andrews - Study manager, responsible for nonelectric concepts

Mr. Don Grim - Deputy study manager, responsible for electric vehicle concepts

Supporting personnel during this study were:

Structures and Weights	R. T. Conrad
Electrical Power	R. J. Gewin
Systems Analysis	E. E. Davis and R. P. Reinert
Cost and Programmatics	J. C. Jenkins
Constructive Criticism	V. A. Caluori

CONTENTS

		Page
1.0	INTRODUCTION	1
2.0	THERMODYNAMIC ROCKET CONCEPTS	5
	2.1 Advanced Chemical Rockets	5
	2.1.1 High-Energy Chemical Propellants	5
	2.1.2 Free Radical Rocket	7
	2.1.3 Metastable Electron States	8
	2.2 Nuclear Fission Thermodynamic Rockets	9
	2.2.1 Solid-Core Nuclear Rocket	9
	2.2.2 Rotating Fluidized-Bed Rocket	16
	2.2.3 Liquid-Core Nuclear Rocket	20
	2.2.4 Gas-Core Nuclear Rocket	24
	2.2.4.1 Open-Cycle Gas-Core Rocket	24
	2.2.4.2 Closed-Cycle Gas-Core Nuclear Rocket	28
	2.2.5 Operational Issues of Fission Rockets	30
	2.3 Nuclear Fission Pulse Propulsion (Project ORION)	34
	2.4 Fusion Rockets	37
	2.4.1 Magnetic Confinement Concepts	40
	2.4.2 Inertial Confinement Concepts	46
	2.5 Laser-Powered Rockets	50
	2.5.1 Pulsed-Laser Concepts	50
	2.5.2 Continuous-Wave Laser Concepts	52
	2.6 Solar Thermal Rocket	64
3.0	ELECTRIC ROCKET CONCEPTS	77
	3.1 Solar Electric Power Sources	78
	3.1.1 Solar Photovoltaic (SPV) Powerplant	78
	3.1.2 Solar Thermophotovoltaic (TPV) Powerplant	79
	3.1.3 Solar Thermoionic (STI) Powerplant	82

		Page
3.2	Nuclear Electric Power Systems (NEPS)	84
3.2.1	Nuclear Thermionic (NTI)	84
3.2.2	Nuclear Thermoelectric (NTE)	86
3.2.3	Nuclear Brayton Cycle (NBC)	89
3.3	Electrostatic Ion Thrusters	91
3.3.1	Advanced Ion Thruster	91
3.3.2	Colloid Thrusters	99
3.4	Magnetoplasmadynamic (MPD) Thrusters	100
3.4.1	Princeton MPD Thruster	100
3.4.2	Pulse Formation and Energy Storage Systems	103
3.4.3	Magnetohydrodynamic (MHD) Thrusters	104
3.5	Arc-Jet Thrusters	113
3.6	Electromagnetic (EM) Thrusters	115
3.6.1	Mass Driver Reaction Engine	115
3.6.2	Rail Gun Reaction Engine	117
3.6.3	Induction Thruster	119
4.0	OTHER PROPULSION CONCEPTS	122
4.1	Solar Sail	122
4.2	Antimatter Rocket	123
5.0	OBSERVATIONS	125
6.0	REFERENCES	128

FIGURES

		Page
1.0-1	Effect of I_{sp} on Single-Stage Mission Performance	2
1.0-2	Specific Impulse Categories for Advanced Propulsion Concepts	3
1.0-3	Specific Impulses Available With Advanced Propulsion Concepts	4
2.0-1	Available Energy Sources	5
2.2-1	Properties of Selected Matrix Carbides	10
2.2-2	Melting Points of Termary Carbide Fuels	11
2.2-3	Carbide Superheater Solid-Core Rocket Reactor	12
2.2-4	Small Nuclear Rocket Engine Characteristics	13
2.2-5	Gamma Engine Mass Statement	14
2.2-6	General Layout of Proposed Nuclear Engine	14
2.2-7	Schematic of Fuel Elements, Support Elements, and Hot-End Support Hardware	15
2.2-8	Rotating Fluidized-Bed Nuclear Rocket	16
2.2-9	Rotating Fluidized-Bed Reactor Rocket Characteriscs	18
2.2-10	Rotating-Bed Reactor Internal Arrangement	18
2.2-11	Multiplayer Fuel Particles	19
2.2-12	Multielement Liquid-Core Nuclear Rocket	21
2.2-13	Typical Fuel Element for Multielement Liquid-Core Reactor	22
2.2-14	Pressure Temperature Dependence of Kinetic Equilibrium I_{sp} From Hydrogen Propellant in Flow Through a Finite Nozzle	22
2.2-15	Specific Impule Optimization of Liquid-Core Nuclear Rocket	23
2.2-16	Conceptual Open-cycle Gas-Core Rocket Engine	25
2.2-17	Gas-Core Engine Weight and Specific Impulse	27
2.2-18	Nuclear Light Bulb Rocket Features and Risks	28
2.2-19	Technology Boundaries for Nuclear Light Bulb Engine	30
2.2-20	Predicted Worldwide Health Effects as a Function of Upper Atmosphere Release of Modified PW-4b in Cermet Form	33

2.3-1	Summary of Nuclear Fission Pulsed Rocket (Orion) Characteristics	34
2.4-1	Important Fusion Cross-Sections	39
2.4-2	Tandem-Mirror Conceptual Configuration	42
2.4-3	Schematic of Direct Converter for Mirror Reactor	43
2.4-4	Artist's Concept of D-T Fueled Riggatron	45
2.4-5	Direct Fusion Rocket Based on Toroidal Fusion Reactor	46
2.4-6	Nuclear Pulse Propulsion Using Fusion Microbombs	47
2.4-7	Pulsed Fusion Rocket Using Two-Stage Ignition Process	48
2.5-1	Acoustically Valved Ground-Launched Laser Rocket	50
2.5-2	Laser-Sustained Detonation Wave Rocket Engine	52
2.5-3	Inverse Bremsstrahlung Coupled-Laser Rocket	54
2.5-4	Equilibrium Chemistry of 10-atm H_2 and 1-atm CO Versus Temperature	56
2.5-5	Equilibrium Chemistry of 10-atm H_2 and 1-atm H_2O Versus Temperature	57
2.5-6	Absorption per cm Versus Temperature, 1-atm CO in 10-atm H_2	58
2.5-7	Measured ku Versus Temperature (T)	59
2.5-8	Results of Simulated Propellant Heating Tests Using Carbon Seed Material	61
2.5-9	Variation of Bulk Exit Temperature with Radiation Incident on Test Section for Propellant Heating Tests	62
2.5-10	Propellant Heating Test Configuration	63
2.6-1	Principal Solar Thermal Rocket Elements	65
2.6-2	Nonrigidized, Inflatable, Off-Axis Concentrator Configuration	66
2.6-3	Windowless Heat Exchanger Cavity	67
2.6-4	Windowed Heat Exchanger Cavity	68
2.6-5	Windowed Molecular or Particulate Direct-Solar-Absorption Concept	69
2.6-6	Theoretical Vacuum Specific Impulse Variation With Carbon Concentration and Gas Temperature for Hydrogen/Carbon	70
2.6-7	Windowed Vortex Flow Direct-Solar-Absorption Concept	70
2.6-8	Rotating-Bed Direct-Solar-Absorption Concept	71
2.6-9	Solar Rocket Coated-Window Transmission Properties	74

2.6-10	Solar Rocket Coated-Window Reflection Properties	75
2.6-11	Rotating-Bed Absorber Solar Rocket	75
3.0-1	Morphology of Electric-Powered Rocket Concepts	77
3.1-1	Sclar Array Specific Mass	79
3.1-2	Photovoltaic Systems Comparison	80
3.1-3	TPV-Ion Propulsion Vehicle Concept	81
3.1-4	Key Elements of the Thermophotovoltaic Concentrator	82
3.2-1	NEP Spacecraft Using MPD Thrusters	84
3.2-2	Thermionic Converter Concept	85
3.2-3	Thermionic System Heat-Rejection Concept	86
3.2-4	High-Power-Density thermoelectric Module	87
3.2-5	Radiator Segments	88
3.2-6	400-kW_e Reference Power System Brayton Cycle State Points	89
3.2-7	Predicted Specific Weight for Nuclear Brayton Cycle Power Systems	90
3.3-1	50-cm Ion Thruster	91
3.3-2	J-Thruster Characterization Program Block Diagram	93
3.3-3	Discharge Control Optimization - 50-cm Argon Ion Thruster	94
3.3-4	Discharge Optimization - 50-cm Argon Thruster	94
3.3-5	Life Trends for a 50-cm Argon Thruster	95
3.3-6	50-cm Argon Ion Thruster Power Requirements	95
3.3-7	50-cm Argon Ion Thruster Performance Characterization	96
3.3-8	50-cm Argon Ion Thruster Life Trends	97
3.3-9	CDVM PPU for 50-cm Argon Ion Thruster	98
3.3-10	Colloid Thruster	99
3.4-1	Princeton Pulsed Self-Field Thruster	101
3.4-2	Self-Field MPD Operating Map	101
3.4-3	MPD Thruster Performance Charcterization	102
3.4-4	Comparison of Electric Thruster Options	103
3.4-5	Trapezoidal Wave Shape Assumed for Five-Section Guillemin Voltage-Fed Pulse-Forming Network	104
3.4-6	MPD Thruster Voltage-Current Characteristics	105
3.4-7	Five-Section Guillemin Voltage-Fed Pulse-Forming Network of Z_n 10.065-Milliohms, 1.16-Millisecond Pulse	106

3.4-8	PFN Charging Current for Low-Voltage System	107
3.4-9	Low-Voltage Resistive Charge	108
3.4-10	Low-Voltage Thruster System Performance Summary	108
3.4-11	High-Voltage Resistive Charge	109
3.4-12	High-Voltage Thruster System Performance Summary	110
3.4-13	Pulse-Forming/Energy Storage Concepts Summary	111
3.4-14	MDH or Cross-Field Accelerator	112
3.5-1	25-kW Thermal Arc-Jet Concept	114
3.6-1	Mass-Driver Linear Synchronous Motor	116
3.6-2	Mass-Driver Features and Risks	117
3.6-3	Simple Rail Gun Schematic	118
3.6-4	Solar Electric Rail Gun Rocket	119
3.6-5	Schematic of Pulsed Inductive Thruster	120
3.6-6	Effect of Coil Diameter on Efficiency	121
4.1-1	Solar Sail Configuration	123
5.0-1	Propulsion System Performance	125
5.0-2	Upper-Stage Vehicle and Mission Chronology	126

1.0 INTRODUCTION

This study was established to examine alternatives to the hydrogen-oxygen rocket, to determine their availability and usefulness, and to estimate their cost effectiveness as a replacement or partner for the chemical rocket. The study was divided into four tasks. The first, to survey and characterize possible advanced propulsion concepts, is covered in this volume. In the remaining tasks, the propulsion concepts recommended here were assessed as vehicles, sized for our best prediction of future mission requirements, and then subjected to life cycle cost estimates over a future operations scenario. Results of these tasks are included under a separate cover as Volume II. The logic used to justify the diversity of propulsion concepts chosen for characterization follows.

The ability to move payloads from place to place in space is fundamentally dependent on the capability to control and apply energy. The practicality of any propulsion concept is determined by the size, mass, efficiency, and cost of the method of energy conversion from its initial form, such as high-temperature combustion gases or high-energy nuclear reactions, to the production of force or thrust. The historical dependence of transportation progress on advancements in propulsion technology also has its analog in space.

The hydrogen-oxygen rocket engine is about 20 years old. Its latest application in the Space Transportation System (shuttle orbiter) requires that its near ultimate theoretical potential be realized in practical application, especially with respect to efficiency and endurance. Although it is reasonable to expect this performance, it is also evident that further progress in propulsion technology is highly desirable to more effectively perform currently visualized missions.

The most likely future needs are to operate heavier, more complex and capable spacecraft in cislunar space for both manned and unmanned purposes and to perform larger and faster science missions to the planets. The impact of engine efficiency on the mass ratio required to perform some of these more

ambitious missions is shown in Figure 1.0-1. A single-stage vehicle carrying a typical near-Earth-type payload has a maximum mass ratio of about 4 to 5. A deep-space probe is a much lighter payload and the propulsive vehicle could have a mass ratio as high as 10.

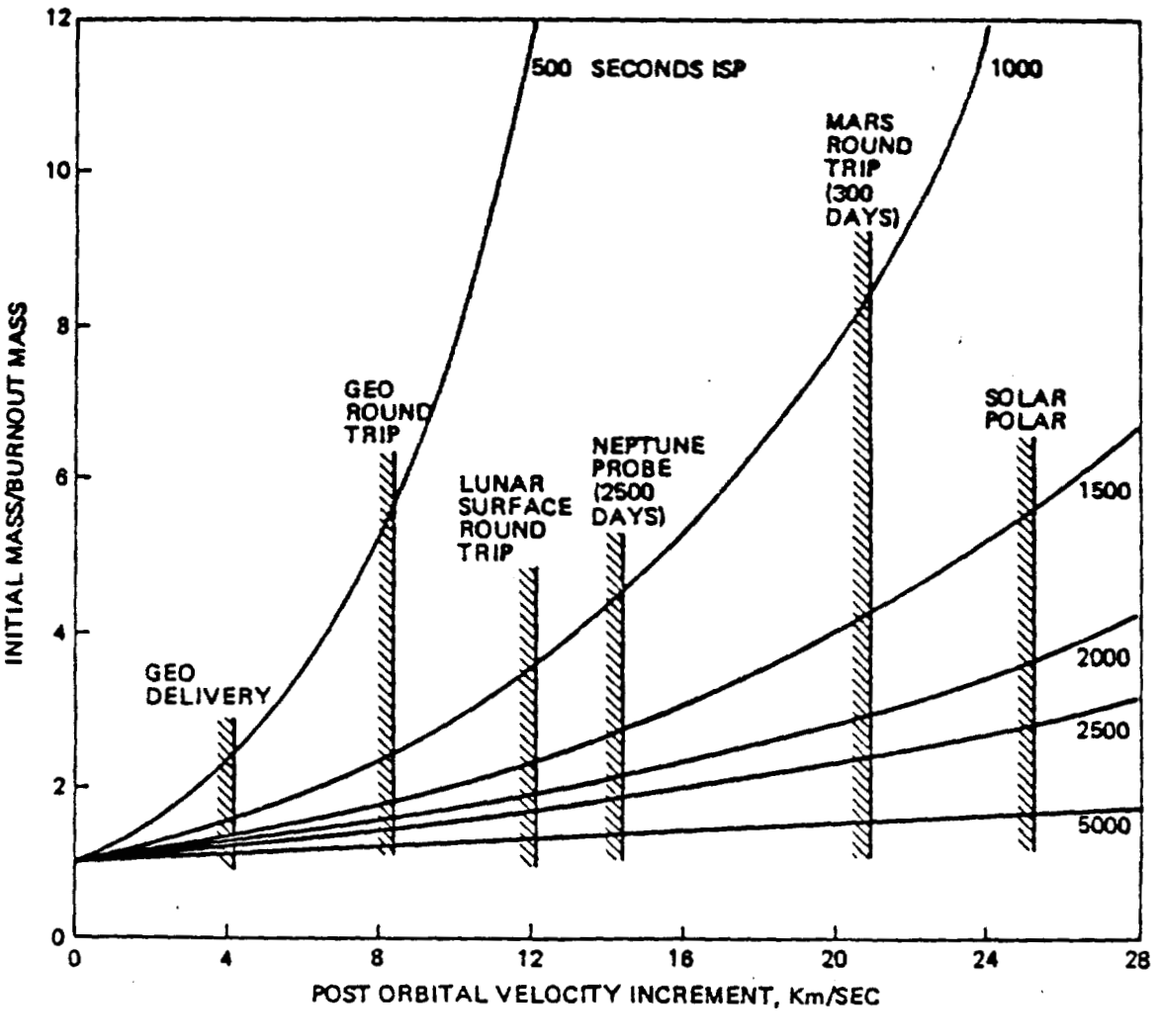

Figure 1.0-1: Effect of Isp on Single-Stage Mission Performance

In general practice, it is desirable to accomplish space missions with a single-stage rocket.

The hydrogen-oxygen rocket, with a maximum theoretical specific impulse of almost 500 sec, has reasonable single-stage mass ratio requirements for missions to geosynchronous orbit and back. However, a round trip to the lunar surface and back would require a specific impulse of 800 to 1000 sec (single stage), and a manned fast round trip to Mars using a single-stage vehicle

would require a specific impulse of 1500 sec or better. Similarly, the very ambitious planetary probe missions, such as the fast trip to Neptune or the fast solar polar missions, will also require a single-stage vehicle to have a specific impulse of 1000 to 1500 sec. Note that this first-order analysis ignores the effect of staging vehicles and also of vehicle thrust to weight, both of which could impact specific impulse requirements.

The interrelationships between advanced propulsion technologies and mission capabilities have been explored in detail in several previous studies. References 1-1 through 1-4 are examples of the results of such studies. This particular study is less mission oriented and more technology and systems oriented than these previous studies, especially in that it will examine and compare a larger number of different advanced propulsion concepts. The propulsion concepts examined in this study have been roughly categorized with respect to specific impulse in Figure 1.0-2. Note that many of the propulsion

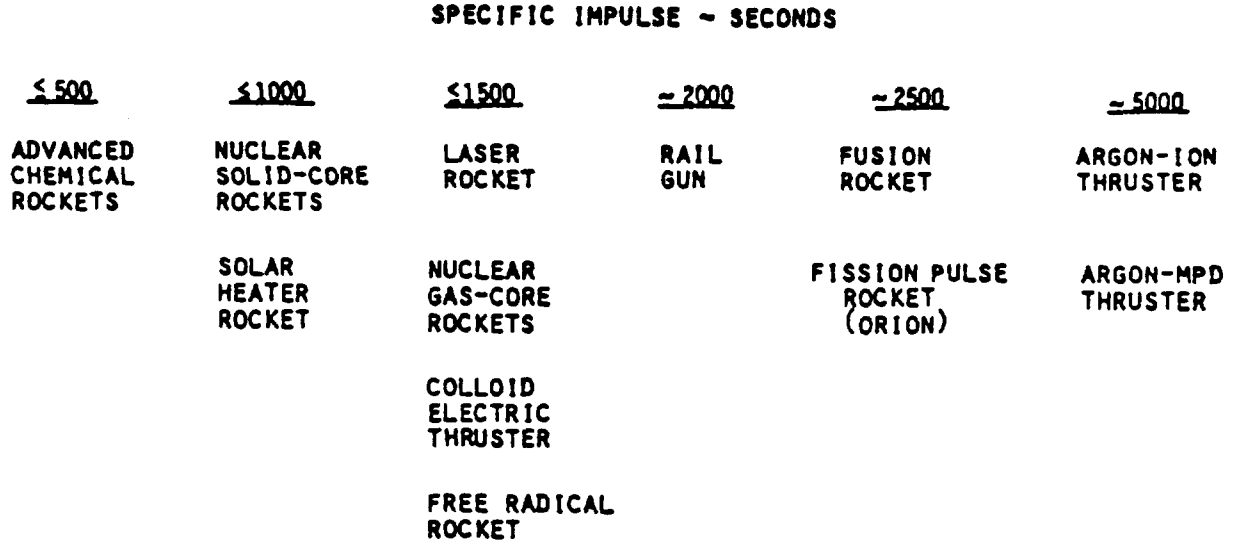

Figure 1.0-2: Specific Impulse Categories for Advanced Propulsion Concepts

options listed are actually thruster concepts and must be paired with an energy source to be a complete propulsion system. The combinations of thruster concepts and energy sources available to this study are shown in Figure 1.0-3, along with specifc impulses available for each combination. Each propulsion option in Figure 1.0-3 will be catagorized and its technology requirements evaluated in the sections which follow.

THRUSTER CONCEPT \ ENERGY SOURCE	CHEMICAL	METASTABLE ELECTRON STATES	NUCLEAR FISSION	NUCLEAR FUSION	SOLAR FLUX	LASER BEAM
THERMODYNAMIC (ROCKET)	530-1,500	2,750	850-2,500	2,500 - 200,000	800-1,200	1,000-3,000
MAGNETOPLASMADYNAMIC (MPD)	—	—	1,200 - 5,000	—	1,200 - 5,000	1,200 - 5,000
ELECTROSTATIC (ION)	—	—	5,000 - 10,000 (ARGON)	—	5,000 - 10,000 (ARGON)	5,000 - 10,000 (ARGON)
MOMENTUM REFLECTOR (e.g., Solar Sail)	—	—	—	—	(1)	(1)
ELECTROMAGNETIC (MASS DRIVER/RAIL GUN)	—	—	1,000 - 10,000	—	1,000 - 10,000	—
PULSE PROPULSION	(2)	(2)	1,500-6,000	6,000 - 1,000,000	—	(2)

(1) NOT DIRECTLY CHARACTERIZABLE IN TERMS OF Isp.

(2) MAY BE APPLICATION

Figure 1.0-3: Specific Impulses Available with Advanced Propulsion Concepts

2.0 THERMODYNAMIC ROCKET CONCEPTS

The key to an excellent space transportation system is the effective use of more advanced energy sources than the simple combustion of a fuel and oxidant. In the foreseeable future, the most likely sources of energy for this purpose are nuclear fission and fusion reactions, either directly from an onboard reactor or indirectly via collection of energy transmitted from a remote reactor (e.g., the Sun). Present concepts for conversion and application of these alternative energy sources are still primitive; but even at this early stage, nuclear energy offers large benefits for space transportation. The energy density available for various chemical and nuclear reactions is compared in Figure 2.0-1. This section covers potential uses of high-energy chemical reactions and nuclear energy for advanced space propulsion.

ENERGY TYPE	POTENTIAL SPECIFIC ENERGY (Cal/g)
• CHEMICAL (H_2-O_2)	3.6×10^3
• FREE RADICAL (H + H→H_2)	5.3×10^4
• NUCLEAR FISSION	1.7×10^{10}
• NUCLEAR FUSION	1.8×10^{11}
• MATTER ANNIHILATION	2.2×10^{13}

Figure 2.0-1: Available Energy Sources

2.1 Advanced Chemical Rockets

2.1.1 High-Energy Chemical Propellants

The performance of a thermodynamic rocket is usually stated in terms of

specific impulse or exhaust velocity (in a vacuum: $I_{sp} = V_{exhaust/g}$). A rocket engine requires a high chamber temperature (T_c) and/or a low molecular weight of the exhaust products (M_e) to achieve a high specific impulse. The vacuum specific impulse, in seconds, of a 1990 technology rocket can be approximated by the equation $I_{sp} = 30.5\sqrt{T_c/M_e}$.

The H_2-O_2 rocket, at a mixture ratio of 6:1, has a chamber temperature of 3500°K and molecular weight of 13 for a vacuum specific impulse approaching 500 sec. An H_2-O_2 rocket is usually operated hydrogen rich to keep the molecular weight low and achieve maximum performance. Note that nuclear rockets can achieve even higher specific impulses by using hydrogen alone as the working fluid ($M_e = 2$), but in chemical rockets we must find a chemical reactant for the energy. The element fluorine is a very energetic oxidizer, combining with hydrogen to form HF and releasing about 3.2 kcal/g. This results in an appreciably higher combustion temperature than H_2-O_2 and about 20 sec of increased specific impulse. In addition to increased performance, the hydrogen-fluorine rocket runs at a mixture ratio of 12:1, thereby decreasing by a factor of 2 the amount of low-density liquid hydrogen which must be carried. This permits a shorter, lighter vehicle and simplifies shuttle integration. On the negative side, fluorine is hypergolic with most materials, very corrosive, and deadly poisonous.

Previous attempts to develop hydrogen-fluorine engine technology resulted in destruction of the prototype engines and test facilities in two out of the three attempts; therefore, any future fluorine engine development should be viewed as a high risk program and planned accordingly.

Fluorine also reacts with lithium to form LiF and release 5.6 kcal/g. This very energetic reaction can be used to heat hydrogen that has been injected into the combustion chamber to provide a working fluid. This tripropellant combination gives a specific impulse of 560 sec at a mixture ratio of 1:1 (F_2: L_i + H_2). Unfortunately, the lithium must be heated to over 500°K to be injected into a chamber as a liquid, which complicates the feed system. Also the exhaust product LiF melts and vaporizes in the chamber, which absorbs energy for the heats of fusion and vaporization. As a result, the F_2 + L_i + H_2 tripropellant rocket does not offer performance in proportion to its very high heating value.

The oxidizer which provides the maximum energy release with any fuel is ozone (O_3). With hydrogen, ozone combines to release 4.2 kcal/g which results

in a specific impulse of approximately 570 sec. In addition, ozone at any significant concentration provides hypergolic ignition with hydrogen and most other fuels. A major difficulty with ozone is that concentrations greater than 55% in oxygen are in danger of spontaneous detonation. In addition, mixtures between 25% and 55% ozone have a characteristic of splitting into a light phase, 25% ozone, and a heavy phase, 55% ozone, and then exploding. Some work 10 years ago by the Air Reduction Company (ref. 2-1) showed that addition of 8% to 10% fluorine homogenizes the ozone-oxygen system and protects against phase separation. Reference 2-1 proposes a mixture of 10% F_2, 40% O_3, and 50% O_2 as a candidate oxidizer to upgrade performance and reduce problems of pure fluorine systems. It is possible, but not likely, that further studies can find some way to safely handle mixtures with more than 55% ozone and permit use of this high-energy oxidizer.

The chemical combustion reaction with the highest known specific energy is beryllium with ozone which liberates approximately 6.2 kcal/g. The resultant material is beryllium oxide, which remains a solid at combustion chamber temperatures and hence cannot provide thrust. By running about 25% hydrogen by weight as the working fluid, this tripropellant combination can provide a theoretical specific impulse approaching 600 sec. Unfortunately, current technology has not found a way to get 100% combustion of the beryllium; the best to date is 85%. Beryllium has a high melting point ($1560^{\circ}K$) which prevents injecting it as a liquid like lithium. When it is injected in particulate form, a thin layer of BeO slag forms on each particle and prevents further oxidation. Data presented in reference 2-2 show that 95% combustion efficiency is required if the O_3 + Be + H_2 system is to be competitive with H_2-F_2 rockets, which is not likely in the near future.

2.1.2 Free Radical Rocket

An ideal rocket propellant is pure hydrogen at a very high temperature. One way to obtain very high temperatures is to store the hydrogen as a free radical (i.e., as monatomic hydrogen). The energy released by recombining dissociated hydrogen atoms is 51,700 g-cal/g. Pure monatomic hydrogen would generate specific impulse values of about 1500 sec if recombined and expanded through a high-expansion ratio nozzle. Monatomic hydrogen is currently produced by blowing ordinary hydrogen through a high-temperature arc discharge or high-power radiofrequency discharge. The dissociated gas can then be

captured as a gas in a bottle lined with superfluid liquid helium ($0.2^{\circ}K$). To suppress the strong tendency of the hydrogen to recombine and to form H_2, the atomic hydrogen is held in a high state of polarization with a strong magentic field ($\sim$ 10T). Recent experiments (refs. 2-3 and 2-4) have shown the capability of storing monatomic hydrogen gas at a density of more than 10^{17} atoms/cm^3 for periods of several hours. The time limit was determined more by equipment limitations than by recombination. This is an inefficient way to store monatomic hydrogen because it requires a cubic meter to store 10g. The problem is that spin-polarized atomic hydrogen is expected to remain as a low-density gas at pressures below 50 atm, even when cooled to absolute zero. At some as yet undetermined combination of very low temperature and very high pressure and magnetic field strength, it is possible that monatomic hydrogen could be stored as a solid; however, theorists currently do not agree on this.

Further experimental work is required to determine whether monatomic hydrogen can ever be stored safely at a density required for propulsion applications. Until such time that the basic feasibility of storing significant amounts of solid monatomic hydrogen has been shown experimentally, this concept should not be pursued as a propulsion option.

An alternate method of using monatomic hydrogen has been proposed, in which the monatomic hydrogen is produced onboard, as required, by one of the methods discussed earlier. This eliminates the low density storage problem and leads to a device with the characteristics of a high-performance low-efficiency hydrogen arc jet. The efficiency of producing atomic hydrogen in a device of this type is not well documented (efficiencies of 30% to 50% have been mentioned) but appears to be considerably less than the 60% to 90% efficiency available with arc jets. Because the maximum practicable performance from either device is about 1200 seconds, there appears to be no reason at this time to favor development of the free radical rocket over the arc jet.

2.1.3 Metastable Electron States

An alternative high performance monopropellant could be helium with one of its electrons in an excited energy state. If radiofrequency energy is added to a helium atom, one of its electrons can be moved to a higher orbit. If this process is done in a strong magnetic field, it can be arranged that

the electrons are no longer "spin paired" and hence cannot return directly to the unexcited ground state by photon emission. The helium atom must first reverse the spin of one electron in an intermediate collision with another atom. If the helium is very cold, collisions can be minimized and this excited state becomes metastable. Helium in this state is called triplet helium and could theoretically store 114 kcal/g. As a rocket propellant, metastable helium could provide I_{sp}'s as high as 2700 sec. However, unlike monatomic hydrogen, no one has yet demonstrated that significant quantities of triplet liquid helium can be manufactured or stored for more than 10^{-2} sec (reference 2-5). Until this process has been experimentally proven, this concept should not be pursued as a propulsion option.

2.2 Nuclear Fission Thermodynamic Rockets

Various concepts for nuclear fission rockets have evolved from nearly two decades of research and development. The desire for enhanced performance led to investigating increased operating temperatures until the temperature limits of solid materials were exceeded and fission rockets were designed using liquid and gaseous nuclear fuels. The ultimate upper limit on specific impulse for a fission thermodynamic rocket is determined by the ability to cool the walls of the chamber and nozzle throat. Hydrogen above 6000°K radiates like a black body and this radiation must be absorbed in the boundary layer to protect the structural walls of the rocket. Also, to obtain a critical mass of uranium in a gaseous state, the physical size and weight of the reactor must grow, which results in a serious degradation in engine thrust-to-weight ratio. These and other key characteristics of nuclear thermodynamic rockets are summarized below.

2.2.1 Solid-Core Nuclear Rocket

The most straightforward method of heating a gaseous working fluid is to pass it through a solid-structured heat exchanger. If this heat exchanger is constructed of appropriate materials, it can be made to contain the fissionable material which forms the core of a nuclear reactor. In this heat exchanger/core region, the fissionable fuel is distributed in a manner to yield a desirable distribution of fission power, and the coolant (propellant) is heated in its passage through many flow channels in the core structure.

The only way to achieve better performance from solid-core reactors is to operate them at higher temperatures; the ability to do this depends upon the materials, geometry, and reactor core design. There are three metallic carbides which offer promise for ultrahigh-temperature use. They are zirconium carbide (ZrC), niobium carbide (NbC), and tantalum carbide (TaC). All three are compatible with uranium carbide and with each other. Selected properties of these carbides are shown in Figure 2.2-1. There is no compelling reason to select one carbide matrix over another; but for nuclear and density reasons, ZrC and uranium zirconium carbide (UZrC) have had an edge even though TaC has significantly higher temperature capability.

Figure 2.2-1. Properties of Selected Matrix Carbides

Item (at ambient standard conditions)	ZrC	NbC	TaC
Melting point (^{o}K)	3680	3780	4280
Density (g/cm^3)	6.8	7.8	14.5
Thermal conductivity ($g\text{-}cal/sec\text{-}cm\text{-}^{o}K$)	0.049	0.034	0.053
Microscopic neutron absorption (b/atom)	0.18	1.16	21
Macroscopic neutron absorption (cm^{-1})	0.007	0.05	0.95
Microscopic neutron scattering (b/atom)	7	7.3	6.7
Macroscopic neutron scattering (cm^{-1})	0.277	0.326	0.304

The addition of large amounts of fissionable fuel (uranium) to the carbide matrix severely lowers the melting point (see Fig. 2.2-2). Figure 2.2-2 shows that ternary fuels have a variable melting point depending upon

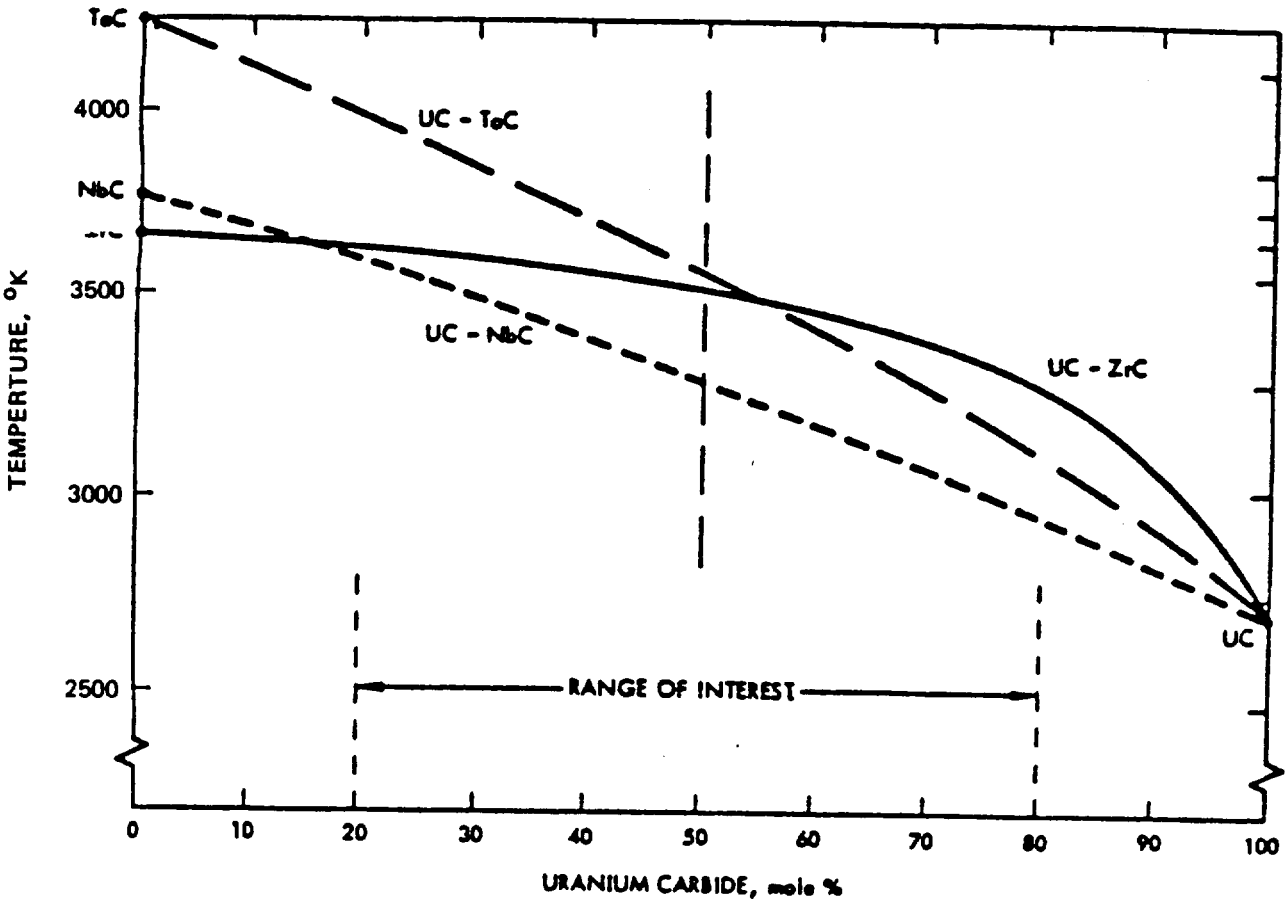

Figure 2.2-2: Melting Points of Ternary Carbide Fuels

the percentage of UC present. The fuel content can be varied from 0% to 100% UC, but the mixture should not go below 20% UC or there will not be enough fissile material present to be classified as fuel. If the ternary system goes beyond 80% UC, the melting point drops off rapidly and engine performance suffers.

UZrC is the preferred ternary fuel for temperature and nuclear reasons. Its temperature advantage over UNbC (within the range of interest) is self-evident in Figure 2.2-2. The UTaC system is very attractive at mixtures of less than 50% UC content, but its neutron absorption cross-section is too large to allow a reasonable size core. This can be avoided and the chamber exit temperature increased by use of a two-section core, in which a highly loaded lower temperature section provides neutrons to help cause fissions in a lightly loaded carbide superheater section (ref. 2-6). The best geometry (neutronically speaking) is one in which the superheater is wrapped around the highly loaded core in such a way that it is thin and sandwiched between the

reflector and core, as shown in Figure 2.2-3. According to reference 2-6, the possible range of specific impulses attainable with this arrangement is from 1000 sec with UZC and H_2 at 100 atm to 1200 sec with UTaC and H_2 at 10 atm. Still higher specific impulses may be attained by operation at still lower pressures, but the thrust-to-weight ratio will decrease roughly linearly with chamber pressure.

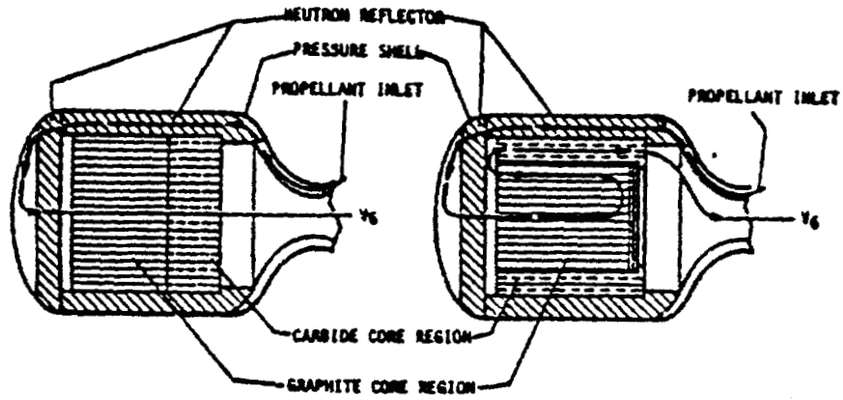

Figure 2.2-3: Carbide Superheater Solid Core Rocket Reactor

Another method for increasing the specific impulse of a solid-core rocket is to use the solid fuel in the form of small pellets (500 m in diameter) suspended in a rotating fluidized bed. The advantage of this concept lies in the reduction of thermal stresses in the fuel elements and the possiblility of attaining temperatures fairly close to the solid-fuel melting point. The temperature gain available with this concept may yield another 50- to 100-sec increase in specific impulse.

Dual-Mode Small Nuclear Rocket. Early nuclear rocket studies focused on the requirements for manned planetary missions. A 5000-MW, 900,000N (200,000-lbf) thrust engine was optimum for these missions and technology readiness for this engine was demonstrated early in the NERVA program (Phoebus 2A, 1968). As it became apparent that manned planetary missions were going to be deferred indefinitely, a smaller 330,000N (75,000-lb_f) NERVA engine was designed. This engine was sized to serve as a high-performance replacement for the Saturn S-IVB stage and support a variety of lunar and deep-space missions. When the Saturn V vehicle was phased out in favor of the reusable space shuttle, the

nuclear rocket engine design was sized down again to 70,000N (15,000-lbf) to match the orbiter payload requirements. This engine was designated the small nuclear rocket engine (SNRE) by Los Alamos Scientific Laboratories (LASL) where it was designed. SNRE technology is characterized in Figure 2.2-4 from reference 1-1, which shows estimated characteristics of several SNRE's. The

Parameter	Alpha Engine	Beta Engine	Gamma Engine
Thrust (N)	73000	71700	65500
Effective jet velocity (m/sec)	8580	8430	9479
Propellant flow rate (kg/sec)	8.52	8.51	6.81
Power (MW)	365	354	365
Engine mass (kg)	2570	2570	2742
Core length (m)	0.889	0.889	0.889
Engine length (nozzle folded) (m)	3.16	3.16	3.12
Chamber pressure (N/cm^2)	310	310	310
Chamber temperature (K)	2690	2633	3335
I_{SP} (sec)	875	860	970
Fuel life (hr)	1	2	unlimited
Operating cycles	3	20	unlimited
Fuel element material	composite	composite	carbide

Figure 2.2-4. Small Nuclear Rocket Engine Characteristics

Alpha engine design used NERVA technology and served as the baseline for SNRE studies. The Beta engine design used Alpha components but was modified to include an auxiliary electrical power generating system. The Gamma engine was an evolutionary development of the Alpha and Beta designs incorporating the carbide fuel elements discussed earlier. The Gamma engine would be capable of operating at temperatures sufficient to provide 1000 sec of specific impulse for up to 10 hr plus be capable of providing up to 40 kW_e of auxilliary electrical power for a number of years.

The Gamma SNRE has been selected as the reference solid-core nuclear rocket engine for this study. The basic design has been well defined and its operating characteristics have been estimated (refs. 2-7 through 2-13). The estimated weight statement for the Gamma engine is shown in Figure 2.2-5, a

Reactor core and hardware	960
Reflector and hardware	570
Internal shield (attenuation factor)	240
Pressure vessel	150
Turbopump	40
Nozzle and skirt assembly	225
Propellant lines	15
Thrust structure and gimbal	30
Valves and actuators	210
Instrumentation and electronics	160
	2700
Contingency	50
Total	2750

Figure 2.2-5. Gamma Engine Mass Statement (kg)

general layout is shown in Figure 2.2-6, and a schematic of the fuel element

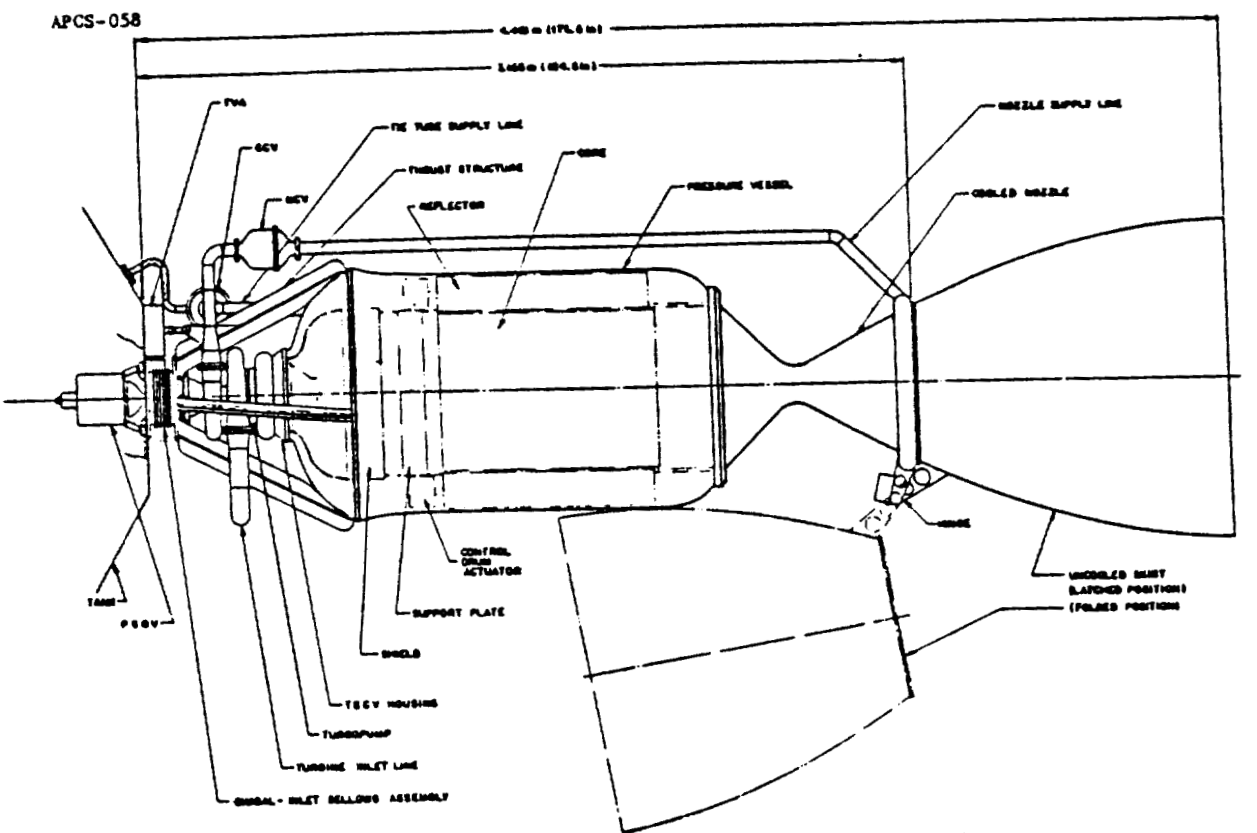

Figure 2.2-6: General Layout of Proposed Nuclear Engine

arrangement is shown in Figure 2.2-7. Using the carbide fuel elements in the Gamma engine extends the chamber operating temperature limits from 2750°K to roughly 3350°K; but the carbide material is more brittle and cracks more easily under thermal stresses than the composite materials used to date. The core design must account for this brittleness factor and for the increased density of the carbide fuel which will tend to increase the mass of the core. The concept characterized in the next subsection directly addresses this problem of brittle fuel and thermal stress buildup.

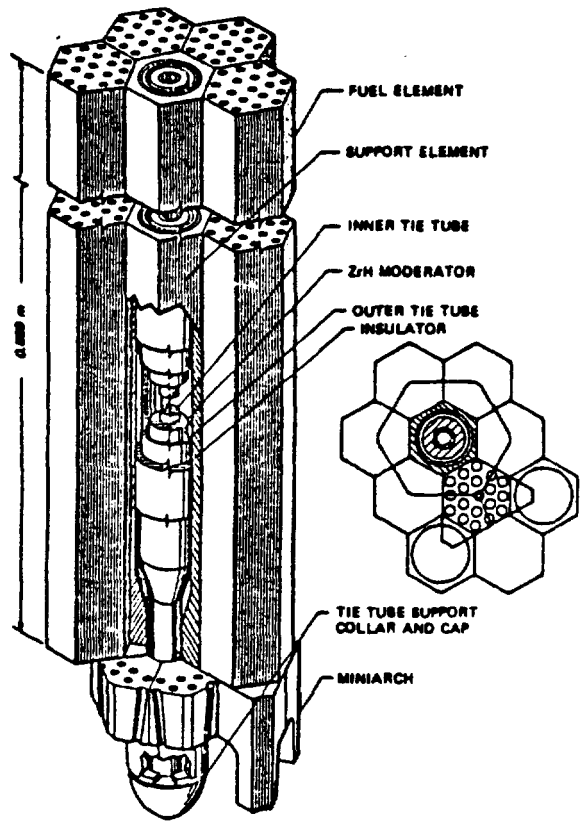

Figure 2.2-7: Schematic of Fuel Elements, Support Elements, and Hot-End Support Hardware

The technical risks of the solid-core nuclear rocket relate to the desired level of performance and fuel element life. Fuel element life of 10 hr at a specific impulse of 825 sec has essentially been proven. On the other hand, the fuel element life at a specific impulse of 1000 sec is a matter of conjecture and further testing is required. Overall, the technical and development risks of the solid-core nuclear rocket are thought to be quite minimal relative to most other advanced propulsion concepts in this volume.

2.2.2 Rotating Fluidized-Bed Rocket

The rotating fluidized-bed reactor concept was originally proposed as a propulsion device in 1960 (ref. 2-14). A schematic drawing of the concept is shown in Figure 2.2-8. Fuel (UC-ZrC) in the form of small particles (100 to

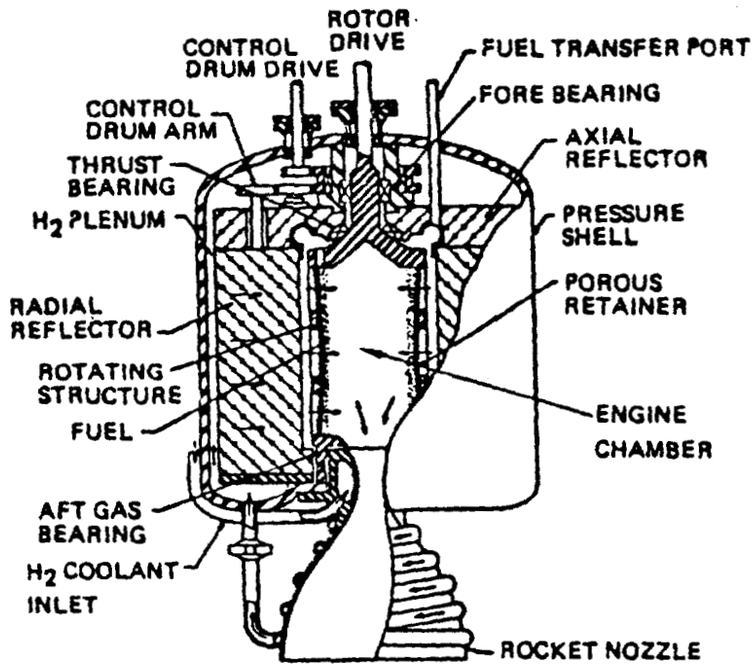

FEATURES

- ISP ≥ 1000 SECS
- INITIAL T/W ≥ 6
- MANNED MISSION CAPABILITY

RISK/FEASIBILITY ISSUES

- RADIATION HAZARD

Figure 2.2-8: Rotating Fluidized-Bed Nuclear Rocket

500 μm in diameter) is retained by centrifugal force in a rotating cylinder to form an annular core. The cylinder is made of porous material known as a frit, backed up by a squirrel-cage-type support structure. The engine uses an expander-type cycle in which the hydrogen propellant goes from the tank to the turbopump, where the pressure is raised, then through the cooling passages in the rocket nozzle and into the reflector. All (or part) of the hydrogen passes

through the turbine of the turbopump unit and enters the core chamber where it flows radially inward through the frit at a velocity sufficient to fluidize the bed (lift and separate the particles). The weight of the bed can be adjusted to match any flow rate by varying the r/min of the frit. The superheated gas finally flows through the nozzle, generating the desired thrust.

Advantages of this concept over other nuclear solid-core rockets are summarized below:

a. The high surface-to-volume ratio of the fuel pellets and the high fuel-to-coolant-to-heat transfer coefficients result in very high heat-transfer rates and a small temperature differential between the fuel pellets and gas stream. This results in minimum core size for any thrust level.

b. Because the core support structure remains cool with this concept, core design requirements are dictated by the high temperature stability of the fuel elements instead of thermal stress and other structural factors. This results in the highest specific impulse available to a solid-core fuel element.

c. The volume and mass of the material that must be handled in loading and unloading fuel elements are reduced by about a factor of 6 relative to the more conventional solid-core rocket. Refueling the core is greatly simplified and the core can now be removed for routine maintenance.

A series of analytical and experimental studies of the rotating-bed nuclear rocket were performed at the Brookhaven National Laboratory between 1960 and 1973 (refs. 2-15 through 2-17). These studies refined and optimized the design of the rotating-bed nuclear rocket until the program was abruptly cancelled in January 1973 along with all other nuclear rocket work. The results of the final study on the rotating-bed rocket (RBR) were reported in ref. 2-18 and the resultant engine design is summarized in Figure 2.2-9. The

Reactor power (MW)	420
Engine mass (less shield) (kg)	1370
Chamber pressure (MN/M^2)/(atm)	3.94/38.9
Exit temperatures (^oK)	3400
Specific impulse (sec)	1000
Thrust (N)/(lbf)	90,000/20,000
Particle diameter (m)	500
Total fuel mass (UC-ZrC) (kg)	140
Propellant flow rate (kg/sec)	9.2

Figure 2.2-9. Rotating Fluidized-Bed Reactor Rocket Characteristics

engine internal configuration is shown in Figure 2.2-10.

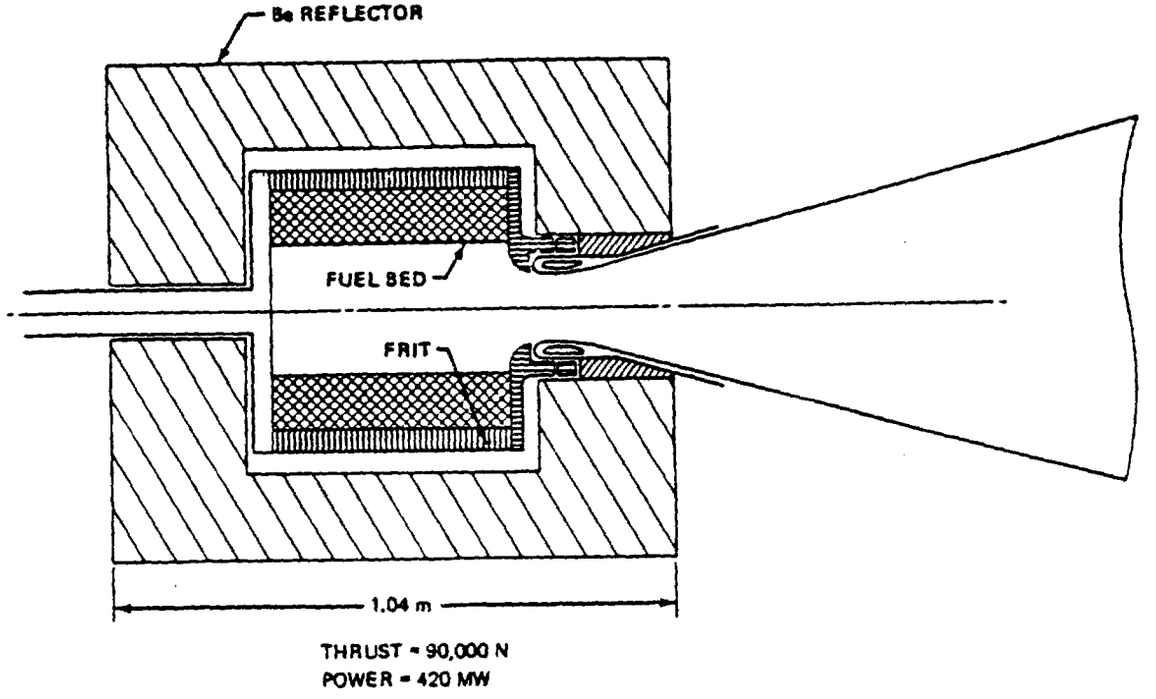

Figure 2.2-10: Rotating-Bed Reactor Internal Arrangement

The fuel particles themselves could be engineered through the proper use of coatings to improve fuel element temperatures and reduce fuel vaporization losses. The approach would be to surround each fuel particle with several layers of coatings and drive the fuel temperature into the molten state. These coatings would be sufficiently thick and with sufficient high-temperature structural capability to contain the molten fuel and its

vapor pressure. Figure 2.2-11 shows a scheme for multilayer coating of fuel particles for the RBR. In this figure, the first coating adjacent to the fuel

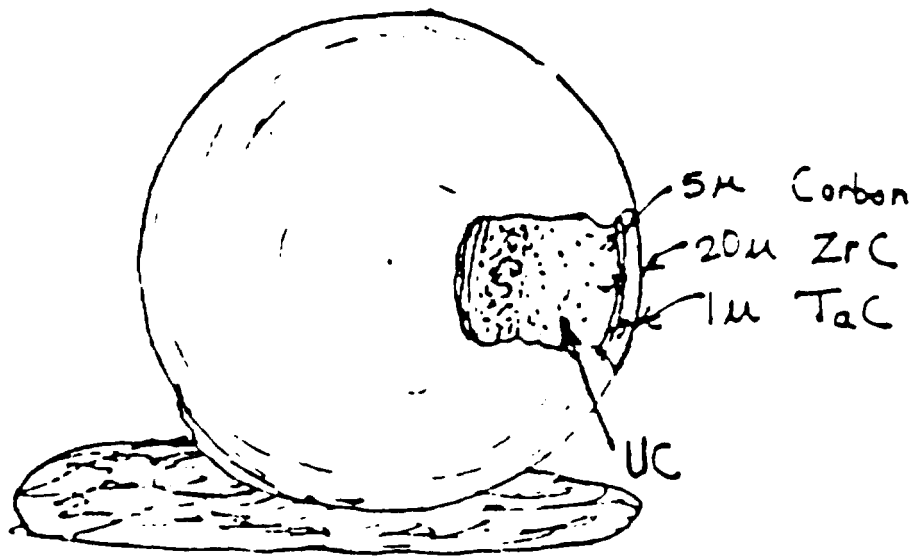

Figure 2.2-11: Multiplayer Fuel Particle

is an armor shell, only thick enough to slow down the fission fragments so they come to rest in the stopping zone outside the armor. For coating materials of interest (ZrC), fission fragment stopping distances average about 5μm, so this would be the thickness of the first coating. The second coating in the figure is a stopping zone of about 15- to 20-μm thick, where fission fragments would give up their kinetic and thermal energy. The first and second coatings are a graduated cushion zone, about 25-μm thick, with high thermal conductivity for good heat distribution and controlled porosity for fission product diffusion. The primary purpose for the third coating is to provide impact protection while multiple collisions occur in the fluidized bed. The upper limit on temperature is dependent upon the strength of the coating material. The vapor pressure of the molten fuel increases with temperature and could eventually burst the coating shell and release the molten mixture.

If the core consisted of particles of uncoated uranium-carbide alloy (1U-10Zr)C, the upper limit on specific impulse would be determined by the vaporization loss of uranium fuel. It has been estimated (ref. 2-19) that the fuel vaporization rate for a 90,000N-thrust dust-bed rocket operating at 3300^{o}K and 100 atm is 100 g/sec. The propellant flow rate at these conditions

would be 10 kg/sec. The fuel flow rate is 1/100 of the propellant flow rate and a vehicle using 15 metric tons of propellant would consume 150 kg of enriched uranium. The RBR will operate at about the same temperature as the dust reactor in the above example; but by using coated fuel particles, the effective fuel vaporization rate should be reduced to negligible levels. The vapor pressure of UC_2 at 3500°K is approximately 2000 N/m^2 (1/40 atm) which should not overly stress the particle shell.

The principal advantage of RBR over the conventional solid-core nuclear rocket is the increase in engine thrust-to-weight ratio from 2.4 to 6.5. The RBR is inherently lighter because of its improved heat-transfer characteristics and reduced core fuel loading, and this advantage becomes even more pronounced with increasing power levels. For instance, a 6.5-GW RBR generating a thrust of 1.8 MN would have an estimated thrust-to-weight ratio of 17 while a NERVA-type rocket of this size would be hard pressed to produce a thrust-to-weight of 4. The technical risks of the RBR relate to the fact that, unlike the NERVA concept, the RBR has never had its criticality and heat transfer tested. This should be a straightforward test program but every previous nuclear propulsion program has encountered surprises. Key technology requirements are (1) development of the superhigh temperature fuel elements desired and (2) development of fuel-handling techniques and equipment to fuel and unfuel and a reactor core in orbit.

2.2.3 Liquid-Core Nuclear Rocket

For nuclear rocket performance beyond 1000 to 1200 sec, it is necessary for the core to operate above the melting point of any known fuel elements. The first step toward this improved performance would be to operate with a liquid core, where the upper temperature limit would be set by the vapor pressure (boiling point) of the fuel rather than the melting point. The best liquid fuel would have a low melting point, to allow containment of the melting fuel with available structural materials, and a high boiling point, to maximize performance before fuel vaporization losses mount.

Furthermore, a liquid fuel mixture should be able to contain fissionable materials in fairly uniform solution to avoid separation of immiscible liquids. The logical candidate fuel is a mixture of uranium carbide (UC_2) with zirconium carbide (ZrC) for which data were presented in the previous

section. A reasonable mixture would melt about 3500°K and operate up to about 4800°K, the temperature at which the uranium carbide would begin to boil out of the mixture.

Efficient heat transfer at high power densities requires the propellant gas to be bubbled through the hot liquid fuel. The best concept proposed for accomplishing this is a rotating cavity core surrounded by an external reflector. This is identical to the rotating-bed reactor discussed in the last section except the fluidized bed is replaced by molten fuel and the hydrogen propellant is bubbled radially inward. The rotating liquid core differs from the RBR in that the propellant flow per unit area is much more limited because of problems with frothing and liquid-vapor entrainment (ref. 2-20). To counter this problem, it has been proposed (ref. 2-21) that the liquid-core rocket consist of multiple rotating cylinders to increase the flow area (see Figs. 2.2-12 and -13). It is also necessary to operate at high pressure (100 atm) to maintain the high flow rates without the use of excess centrifugal forces (ref. 2-22).

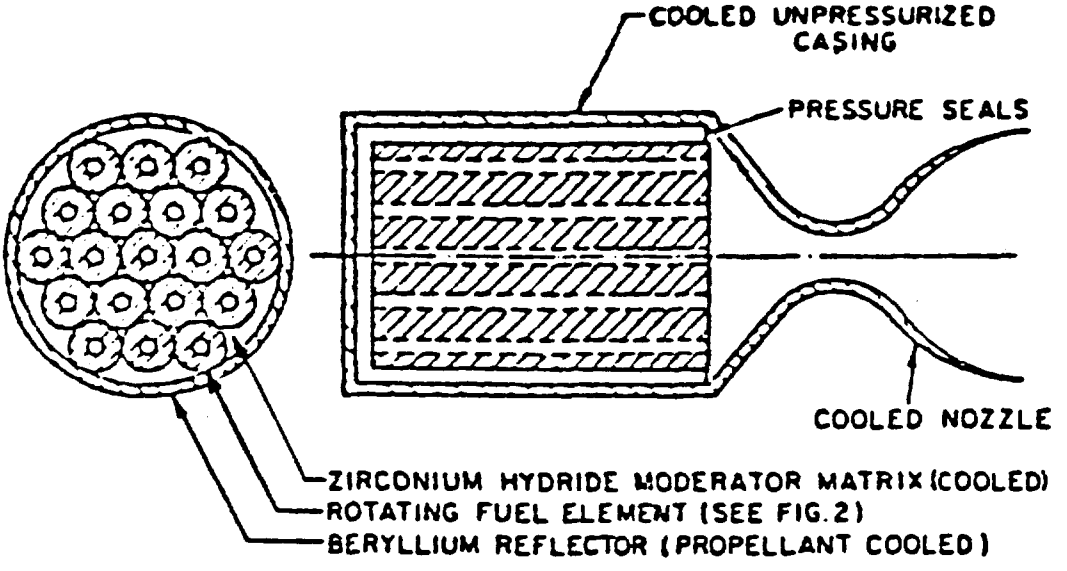

Figure 2.2-12: Multielement Liquid-Core Nuclear Rocket

The maximum propellant temperature gain available through use of liquid instead of solid fuels is about 1000°K. Although this is not large, it is significant in terms of specific impulse because this is the temperature regime where molecular dissociation and recombination of hydrogen become very important as an energy source to the expanding gas in the rocket nozzle. As discussed previously, there are 51,700 g-cal/g of energy available when

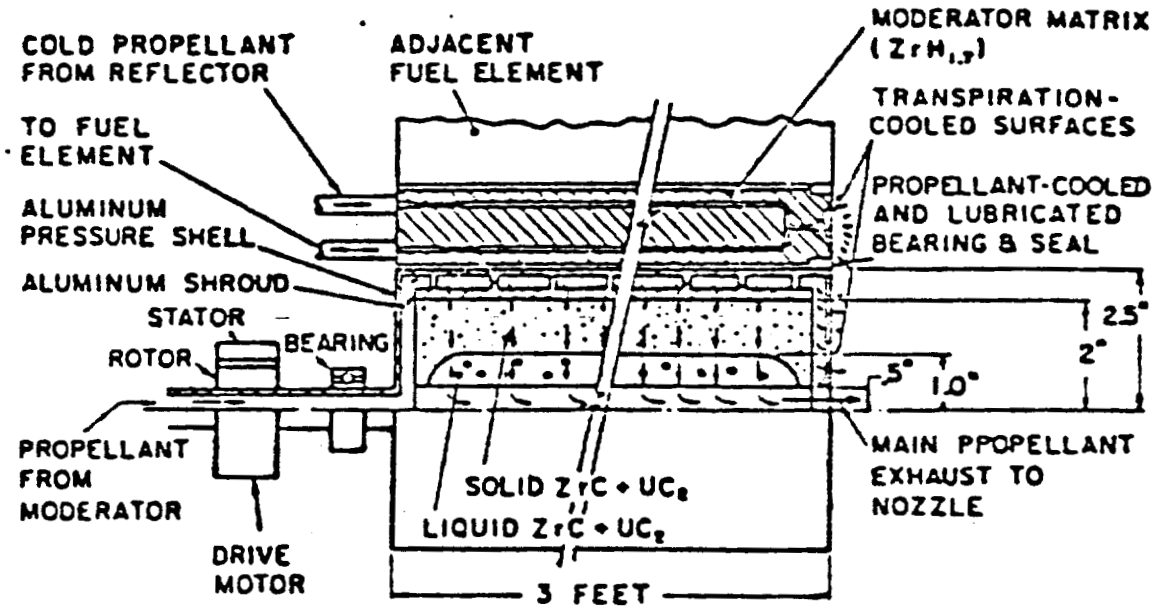

Figure 2.2-13: Typical Fuel Element for Multielement Liquid-Core Reactor

dissociated atomic hydrogen recombines. If the fuel is hot enough to dissociate molecular hydrogen, the energy of dissociation is absorbed from the fuel and becomes available to the propellant as it expands in the nozzle flow. For example, at 4500°K, hydrogen at a few atmospheres pressure can yield a specific impulse of 1600 sec, nearly twice that attainable from 2500°K gas (see Fig. 2.2-14).

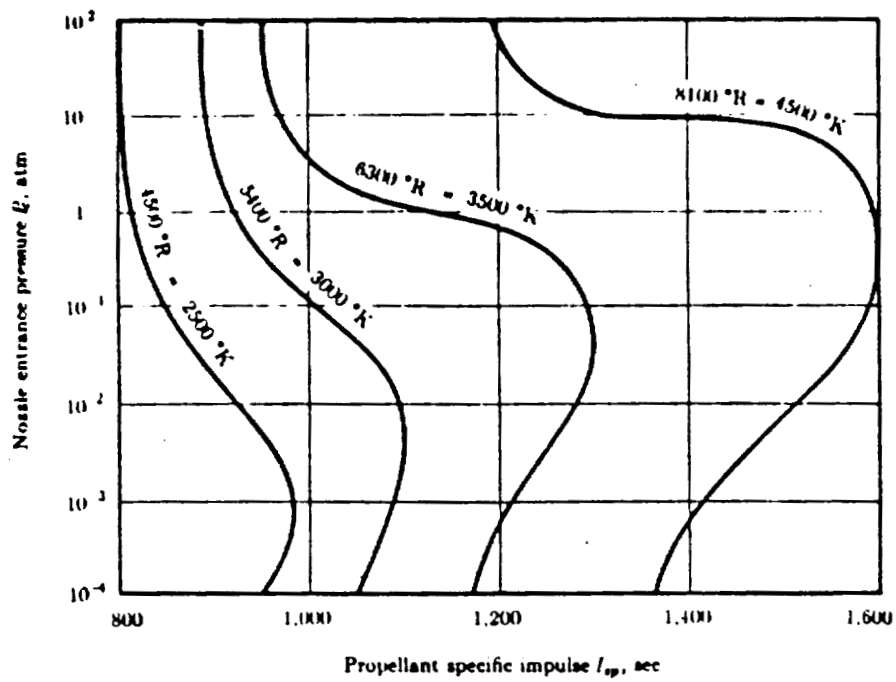

Figure 2.2-14: Pressure Temperature Dependence of Kinetic Equilibrium Isp for Hydrogen Propellant Flow Through a Finite Nozzle

There appear to be many formidable technical risks for the liquid-core nuclear rocket. Chief among these is the potentially high fuel-loss rate caused by high vapor pressures and vapor-liquid entrainment at high propellant flow rates. Reference 2-21 discusses these problems at some length and concludes that evaporation of the fuel elements will limit the specific impulse available to approximately 1500 sec (see Fig. 2.2-15). The multiple cylinder design shown in Figure 2.2-12 operates at a dilution ratio (moles ZrC/moles UC_2) of about 500 which results in a fuel-loss ratio (MU_{235}/MH_2) of

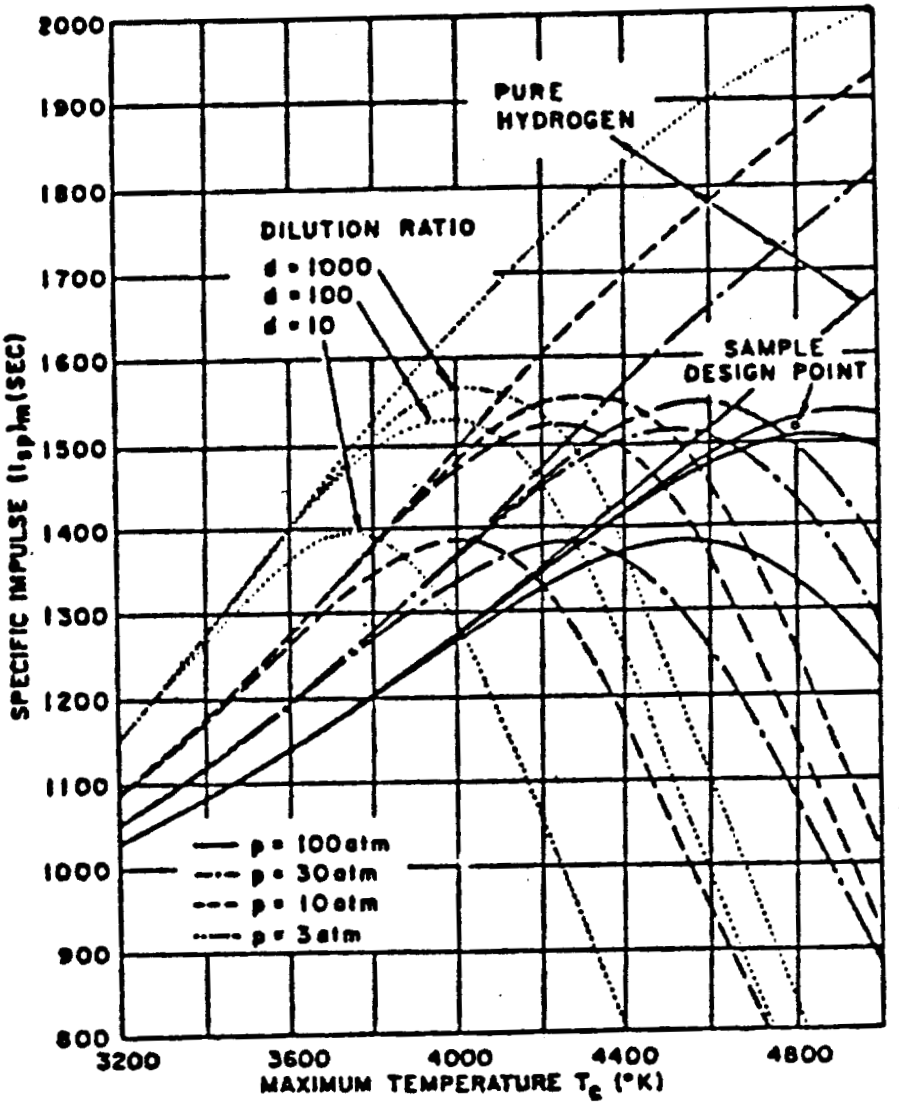

Figure 2.2-15: Specific Impulse Optimization of Liquid-Core Nuclear Rocket

approximately 1/5000. At the pressures and flow rates per unit area used in the sample point design, the vapor-liquid entrainment losses will be a small percentage of the evaporation losses (ref. 2-20). The point design engine in

reference 2-21 had an engine thrust-to-weight of just over 1 for a thrust of 35 kN and a specific impulse of 1500 sec. This engine operates at a pressure of 100 atm and an outlet temperature of 4800°K.

Other technical risks for this concept include:

a. Startup and shutdown where the core must undergo changes of state from solid to liquid and vice versa

b. Cooling of the core containment structure during fuel solidification

c. Contamination caused by lack of containment of fission products

d. Reuse and refueling of a reactor core which loses an amount of uranium equal to its critical mass each mission

Until these risks are resolved or at least quantified, this concept should be held in abeyance.

2.2.4 Gas-Core Nuclear Rocket

The ultimate step in increasing the performance of a nuclear fission thermodynamic rocket is use of a gas-core nuclear reactor, where the fuel is maintained as a fissioning plasma with a surface temperature of approximately 10,000°K and an interior plasma temperature approaching 100,000°K. At these temperatures, the plasma radiates like a black body and the reactor energy is transferred to the propellant primarily by radiation. In theory this concept could achieve very high specific impulses for a reasonable engine size and weight. Two gas-core engine concepts have emerged as principal candidates: the open cycle or coaxial flow gas-core concept and the closed cycle or nuclear lightbulb gas-core concept. Both concepts are characterized in the following subsections.

2.2.4.1 Open-Cycle Gas-Core Rocket

Description. In the open-cycle gas-core rocket, (Fig. 2.2-16), the uranium plasma is confined by the enveloping flow of the hydrogen working

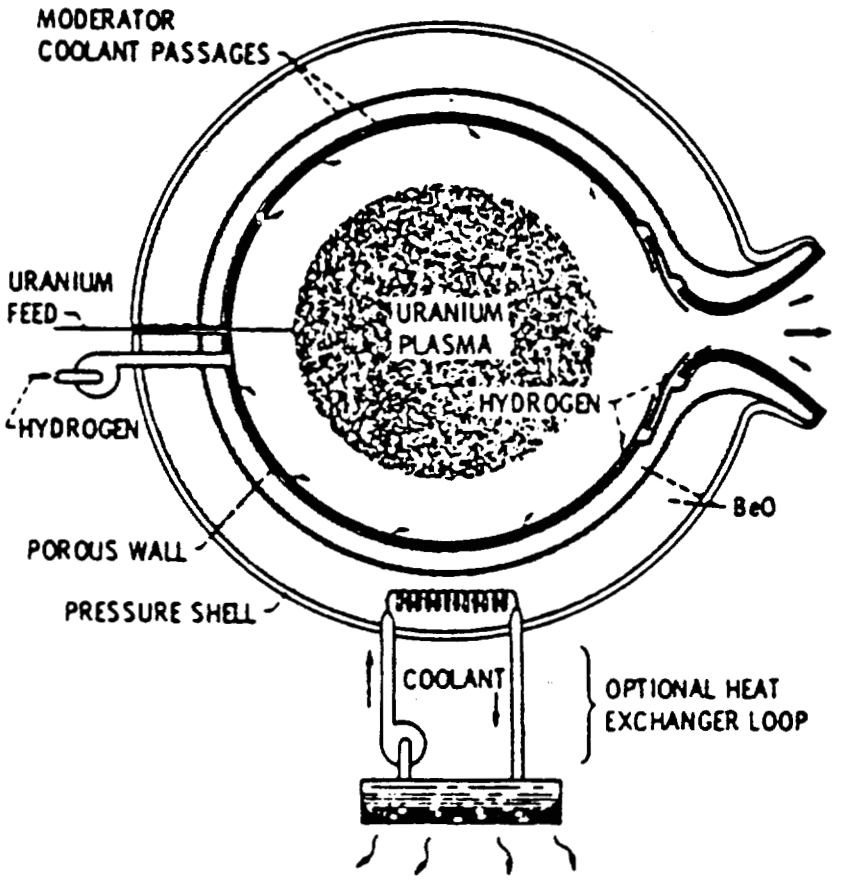

Figure 2.2-16: Conceptual Open-Cycle Gas-Core Rocket Engine

fluid which has been seeded with submicrometer-sized carbon or tungsten particles to absorb 99+% of the thermal radiation to protect the reactor walls. The cavity containing the fuel and propellant is surrounded by a moderator region to reflect the neutrons created by the fission process back into the cavity to sustain the nuclear chain reaction. The hot hydrogen, along with the seed material and a small quantity of unburned fuel and fission products, is exhausted through a transpiration-cooled nozzle to provide thrust.

Extensive analyses of this concept were conducted during the late 1960's and early 1970's to optimize engine size, pressure, specific impulse, etc. (refs. 2-23 through 2-29). A representative configuration (ref. 2-30), shown schematically in Figure 2.2-16 might have a spherical cavity almost 4m in diameter containing 50 kg of uranium 233. The reactor would generate 22 GW of thermal energy, which would be transfered to 100 kg/sec of hydrogen, resulting in a thrust of 1800 kN at a specific impulse of 1800 sec. The pressure

2.2.4.2 Closed-Cycle Gas-Core Nuclear Rocket

Description. The nuclear lightbulb engine, as currently defined, comprises seven separate unit cavities (Fig. 2.2-18). Each cavity contains a

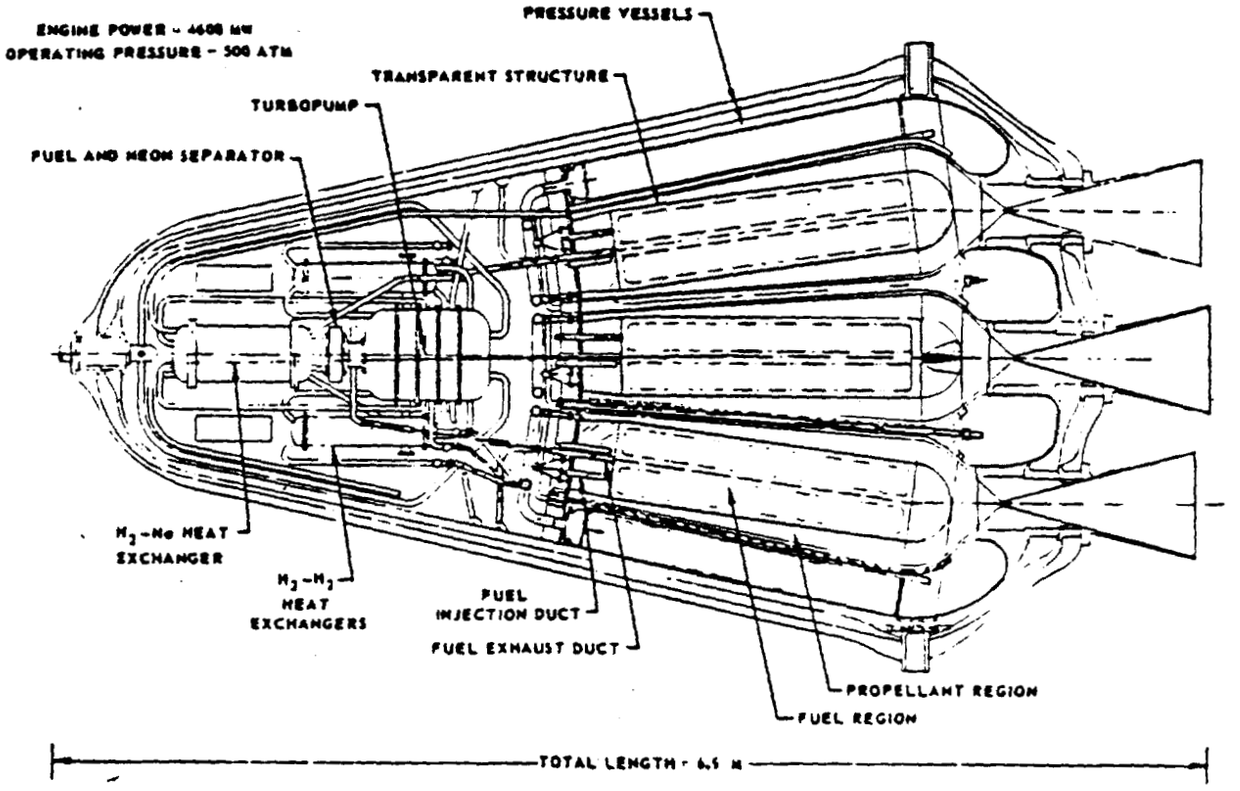

FEATURES

- ISP = 1,500 -2,500 SECS
- INITIAL T/W = 1.0

RISK/FEASIBILITY ISSUES

- TECHNICAL FEASIBILITY OF "BULB" CONCEPT
- SURVIVABILITY OF 0,12 MM GLASS WALL AT 500 ATM
- SEED MATERIAL ADHERING TO GLASS WALL

Figure 2.2-18: Nuclear Light Bulb Rocket Features and Risks

central region of fissioning uranium plasma which heats seeded hydrogen propellant by thermal radiation as in the open-cycle engine. However, an internally cooled transparent wall has been added between the fuel and the propellant regions. The fuel plasma would be isolated from the transparent wall by a neon vortex. The neon flow would pass through ports located at the

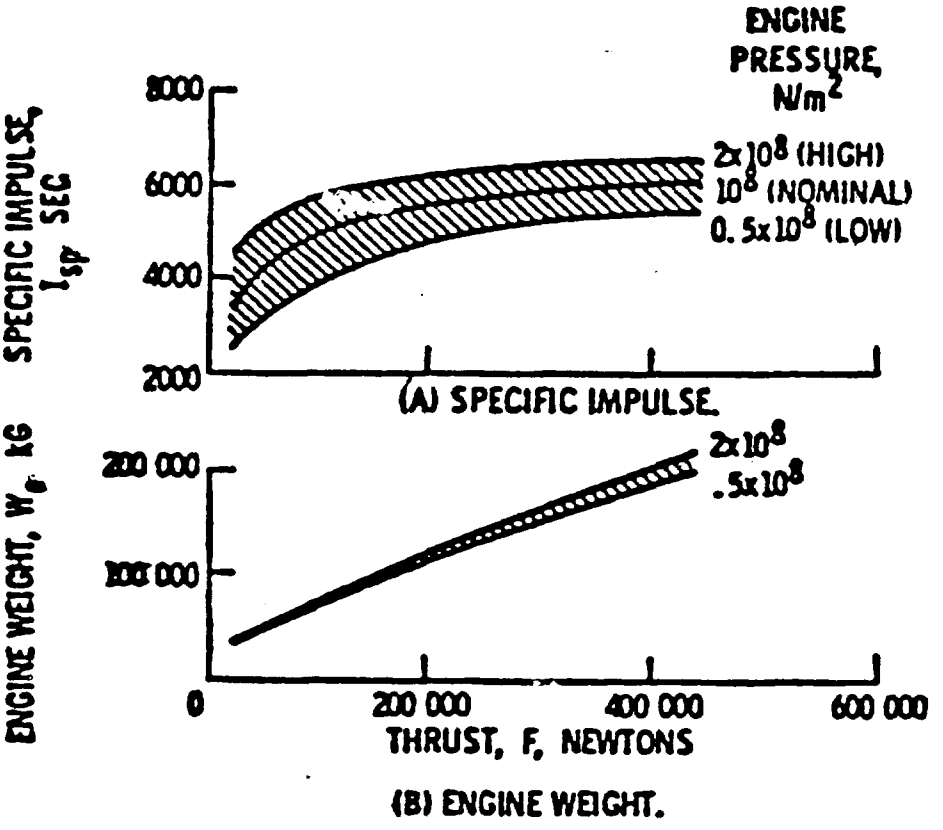

Figure 2.2-17: Gas-Core Engine Weight and Specific Impulse

Recommendation. Preliminary performance data indicate that the open-cycle gas-core rocket is too heavy and too expensive to operate to be competitive in the current mission model. Even if missions were much larger in scope, many unanswered questions remain concerning the technical feasibility of this concept. Some resolved technical issues are listed below:

- appropriate seeding to protect engine walls
- radiation from the fission fragments in the plume
- uranium loss rate
- engine throttlability

For these reasons the open cycle gas core rocket should not be pursued further at this time.

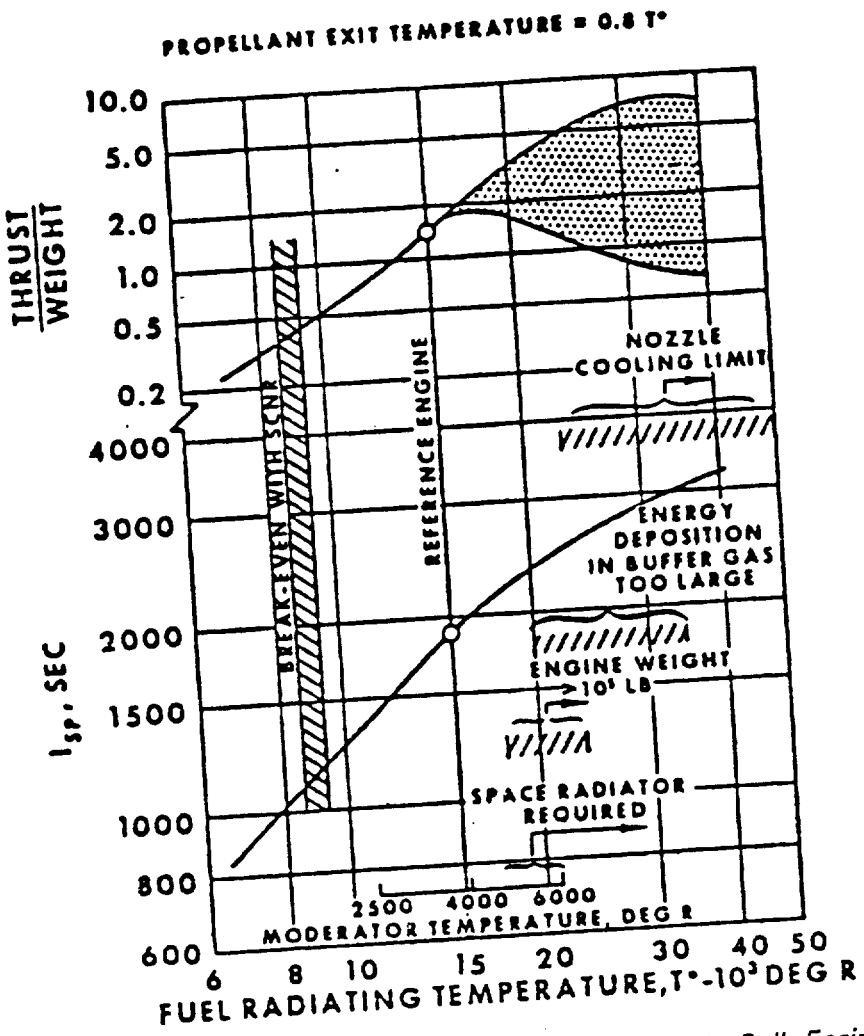

Figure 2.2-19: Technology Boundaries for Nuclear Light Bulb Engine

thin wall must span a distance of 1m to 2m and must withstand a very severe neutron flux plus the acoustic environment in a large thrust chamber operating at 500 atm. In addition, if just one particle of seeding material added to the propellant flow adheres to the transparent wall, the wall will melt through at that point.

These two problems appear unsolvable using current or extrapolated advanced technologies.

For this reasons, the nuclear lightbulb rocket does not appear feasible.

2.2.5 Operational Issues of Fission Rockets

A principal operational consideration for any nuclear rocket concept is the impact of neutron and gamma-ray radiation on the vehicle and its payload.

centerline of the end wall of each cavity to a fuel recycle system where the uranium entrained in the neon would be condensed to its liquid state, centrifugally separated from the neon, and pumped back into the fuel region.

The reference engine (Fig. 2.2-18 from ref. 2-33) has a total volume of 4.3 m^3. The total amount of fuel contained within the seven cavities would be approximately 14 kg, and the designed power level would be 4600 MW. The critical mass of the lightbulb reactor would be less than that for the open-cycle reactor because of the reduced engine size and the beneficial effect of the moderating walls between the unit cavities. The total pressure in the engine cavity was estimated to be 500 atm. A propellant flow rate of 22 kg/sec would be heated to 6670°K, providing a specific impulse of 1870 sec. The resulting engine thrust would be 410 kN. The engine total mass would be approximately 32,000 kg with the following breakdown:

Moderator (graphite and beryllium oxide)	12,000 kg
Pressure vessel (filament-wound fiberglass)	14,000 kg
Turbopumps	1,500 kg
Miscellaneous (includes fuel recycle system)	4,500 kg
Total	32,000 kg

The technology boundaries of the closed-cycle nuclear engine are summarized in Figure 2.2-19 from reference 2-34. The reference engine design point was chosen to provide the highest specific impulse compatible with regenerative cooling (no space radiator). The large uncertainty in engine thrust to weight at higher temperatures is due to the uncertainty in weight of the space radiator. The lower line assumes the radiator has meteoroid protection sufficient for deep-space mission times while the upper line assumes no meteoroid protection.

Recommendation. In theory, the nuclear lightbulb engine offers the possibility of perfect containment of nuclear fuel because of its internally cooled transparent wall between fuel and propellant and because of its fuel recycle system. In fact, however, the thermal radiation which must pass through the transparent wall would be very intense (27.6 kW/cm^2) and even the best wall material absorbs about 1% of the energy transmitted; therefore the wall must be extremely thin (0.12 mm) to keep from melting. This extremely

required in the cavity to reach adequate fuel densities in 1000 atm and the fuel-loss rate would be on the order of 0.5% of the propellant flow rate. The moderator/reflector surrounding the cavity would be composed of beryllium oxide, with a total thickness of 76 cm. The total mass of ths configuration was estimated to be 128,000 kg with the following mass breakdown: moderator/reflector, 55,000 kg; pressure shell, 63,000 kg; turbopump, 9000 kg; and exhaust nozzle structure, 1000 kg. The reference engine above has a thrust-to-weight ratio of 1.42.

The open-cycle reactor relies on fluid mechanics phenomena to provide preferential containment of the gaseous nuclear fuel. Tests to date (refs. 2-30 through 2-32) indicate that aerodynamic confinement will result in a uranium mass flow rate of 1% to 2% of the propellant mass flow. In addition, every time the engine is started and stopped, the entire critical mass inventory (50 kg) will be lost out the nozzle. Hence, a normal geosynchronous Earth orbit (GEO) delivery mission using a gas-core rocket will consume 600 to 1000 kg of 98% enriched U_{233} worth $100 million or more.

The upper limit on specific impulse for a gas-core reactor would be determined by either: (1) the hydrogen flow rate necessary to keep the BeO moderator below 2500°K (7% to 8% of the total reactor power goes into the moderator in the form of high energy neutrons) or (2) the maximum propellant temperature for which the nozzle throat can be kept intact. Criteria number (1) can be overcome by using a heat-pipe space-radiator to dispose of waste heat not regeneratively removed by the hydrogen propellant as shown in Figure 2.2-16. Criteria number (2) is much harder to quantify since the heat transfer rate to the nozzle wall is a function of boundary layer thickness, transpiration coolant injection, and seeding rate. Figure 2.2-17 taken from reference 2-26, indicates that a specific impulse of 5000 sec (T_c = 22,000°K) is the upper limit. More recent analysis of laser-generated plasmas indicates that a maximum specific impulse of 1500 to 2000 sec might be more reasonable.

The four basic ways in which reactor radiation can compromise the feasibility or performance of a nuclear rocket vehicle are as follows:

a. Engine components in or near the reactor can overheat from absorbed radiation energy.

b. Neutron and gamma-ray integrated flux during a mission can result in prohibitive radiation damage to sensitive engine or avionics components.

c. Energy deposition in the propellant can lead to boiloff or to pump-inlet boiling, especially in the case of liquid hydrogen propellant.

d. The total radiation dosage to the payload (particularly if manned) can be unacceptable.

The first three problems imply design limitations and result in minimum shielding and cooling requirements for each nuclear rocket concept. They are unavoidable requirements and not operational issues. The last problem of radiation dosage to the payload can be approached many ways and is therefore an appropriate operational issue. Unfortunately, this issue cannot be addressed without using a detailed vehicle definition and a fairly detailed mission model. This makes it a Task 2 configuration design issue and it will be addressed in Volume II of this study. It should be noted that the shielding penalty required for unmanned payloads appears to be quite minimal and that the nuuclear rockets (including all shielding) appear to be the only advanced propulsion concept with sufficient thrust to weight to perform manned missions.

Other potential considerations include the problem of containment and disposition of radioactive byproducts of a fission or fusion reactor. If the byproducts are retained in the reactor and the engine is reusable, adequate shielding must be provided to protect nearby personnel from the gamma-ray flux generated by decay products. If the byproducts are not retained but are mixed with the propellant gas, as in the liquid-core, gas-core, or pulsed rockets,

the final disposition of these radioactive materials must be determined and the resultant health hazard assessed.

If the decay products are retained in the reactor, as in the case of NERVA, then reference 2-35 indicates the maximum allowed dose of gamma radiation (25 rad) could be obtained at a distance of 100m in 1 hr even if the reactor had been shut down for 1 day. This radiation problem indicates that a used reactor core will probably not be allowed near any manned base unless the fuel elements have been removed.

If the decay products are mixed with the propellant during thrusting, two things happen: (1) the payload is exposed to gamma radiation from the fission fragments in the plume and (2) approximately half of the fission fragments enter the Earth's upper atmosphere (for geosynchronous delivery missions). Reference 2-36 discusses this plume radiation problem in some depth and determines that 5 cm of lead shielding is more than adequate to protect a manned capsule during a fast Mars mission using an open-cycle gas-core reactor. A GEO delivery mission generates less than 1% of the fission fragments generated during the Mars mission and would probably require no shielding beyond that required for the Van Allen belt and solar radiation fluxes.

Approximately 1 kg of fission fragments will reenter the Earth's upper atmosphere for every 180 metric tons of payload delivered to GEO using an open-cycle gas-core rocket (180 metric tons equals 6 sorties). Assuming 180 tons per year as a GEO delivery rate, use of an open-cycle nuclear rocket would result in less than one additional cancer death per year according to Figure 2.2-20 from the Space Disposal of Nuclear Waste Study (ref. 2-37). For comparison, it has been estimated that 10,000 to 20,000 additional lung cancer deaths per year could be caused by radon gas buildup if all homes in this country are weatherstripped to currently recommended standards.

In summary, a preliminary analysis of the operational issues of nuclear rockets indicates that reactor radiation will be a problem, but there appear to be no unsurmountable problems with respect to operating a nuclear rocket in cislunar space.

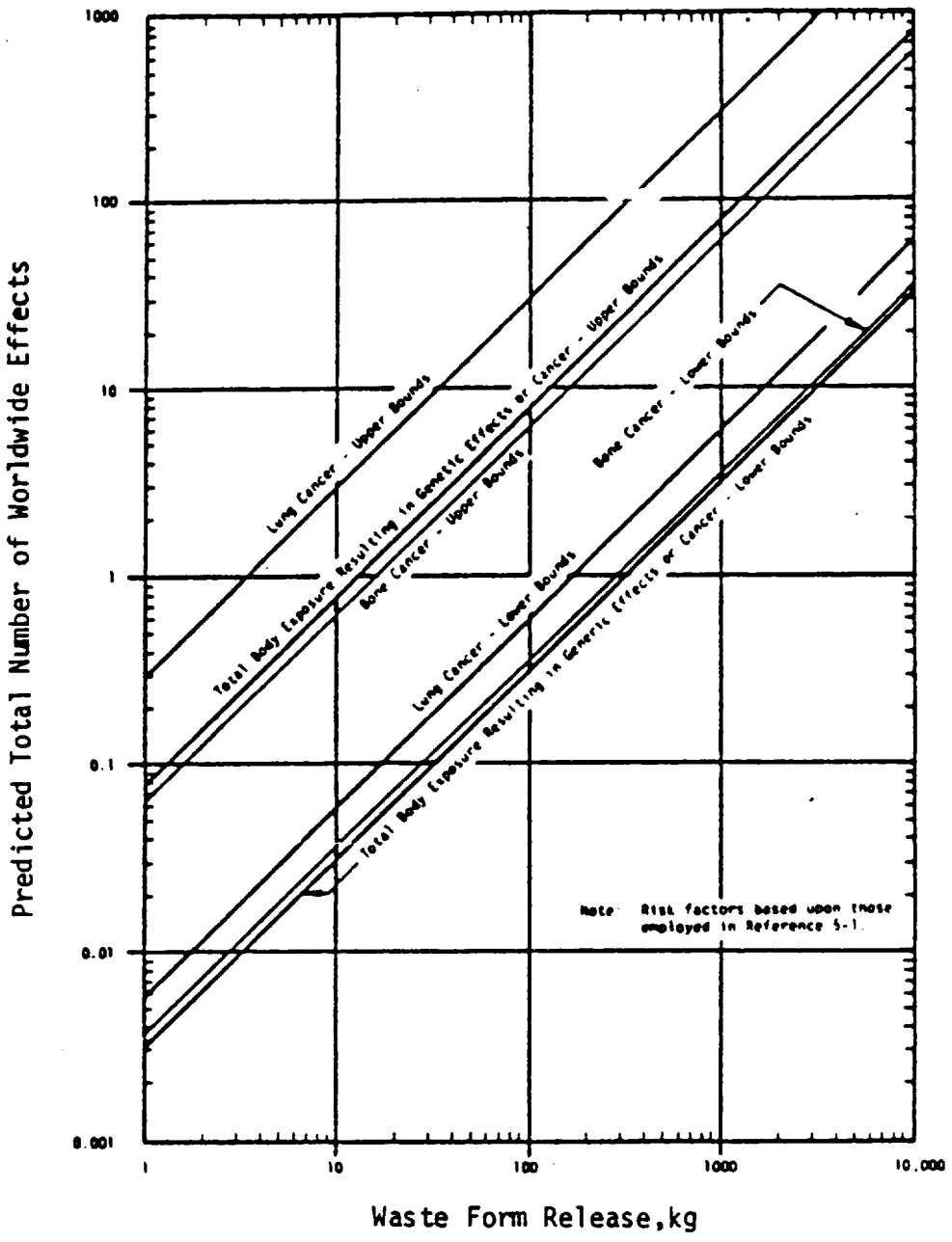

Figure 2.2-20: Predicted Worldwide Health Effects as a Function of Upper Atmosphere Release of Modified PW-4b in Cermet Form

2.3 Nuclear Fission Pulse Propulsion

Background. Nuclear fission pulse propulsion was studied extensively as a space transportation device from 1958 until 1965 under project Orion. An illustration of the NASA Orion vehicle, sized for compatibility with the Saturn V launch vehicle, is shown in Figure 2.3-1. This vehicle, according to

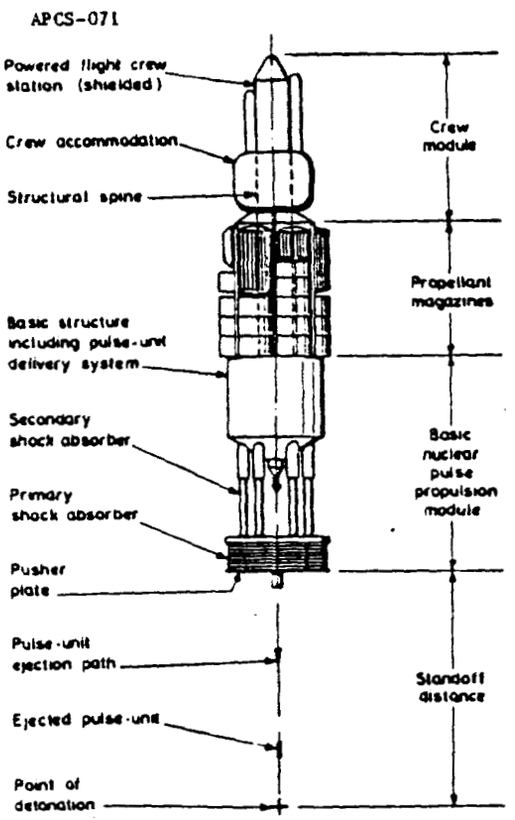

PERFORMANCE
- I_{sp} = 2000-6000 SEC
- ENGINE T/W~4

DEPENDS ON DIAMETER OF PUSHER PLATE

OPERATIONAL CAPABILITY
- VERY LONG LIFETIME
- CAN BE MAINTAINED
- OPERATION BELOW GEO QUESTIONABLE (PROJECT STARFISH)

RISK/FEASIBILITY ISSUES
- DATA BASE BELIEVED GOOD (CLASSIFIED)
- NUCLEAR TEST BAN TREATY PROHIBITS TESTING
- HIGH DEVELOPMENT COST MODERATE RADIATION HAZARD

RECOMMENDATION

THIS CONCEPT HAD THE BEST ALL-AROUND PERFORMANCE OF ANY CONCEPT EXAMINED, BUT FEASIBILITY FOR NEAR EARTH MISSIONS NEEDS FURTHER INVESTIGATION. THIS CONCEPT RECOMMENDED FOR FUTURE STUDY CONSIDERATION

Figure 2.3-1: Summary of Nuclear Fission Pulsed Rocket (Orion) Characteristics

reference 2-38, would be capable of completing a manned Mars surface-excursion mission from a single Earth launch, using a Saturn first stage. For this mission, the nuclear pulse propulsion would begin suborbitally, starting at an altitude greater than 100 km (50 nmi). The vehicle shown has an estimated specific impulse of 2500 sec, a dry mass of 90,000 kg (200,000 lb), and an effective thrust level of 3,470,000N (780,000 lbf).

Description. The data base for the nuclear fission pulse propulsion concept is extensive, although most of it is still classified. Reference 2-39 is an

excellent historical review of nuclear pulse propulsion and the source of most data presented here. The propulsion concept itself is quite simple, although its design and operation can become exceedingly complex.

The thrust operation begins with the ejection of a pulse unit (i.e., shaped nuclear charge) from the vehicle body and its detonation beneath the vehicle to create a cloud of rapidly expanding debris. A portion of the debris would be intercepted by the base of the vehicle, transfering momentum and providing thrust.

The expansion velocity of atomic explosion may be in excess of 10^6 m/sec; therefore, if a large majority of the pulse unit debris could be directed toward the vehicle base plate, a specific impulse approaching 10^5 sec should be possible. For obvious economic reasons, it would be better to reduce the average expansion velocity of the debris by loading the pulse unit with cheap radiation-absorbing propellant which would increase the vehicle thrust and reduce radiation damage at the expense of a higher launch mass. Lead, tungsten, and polyethylene are candidate propellant materials.

Interaction time between the expanding plasma debris and the vehicle base plate of a "a millisecond or less" is quoted in reference 2-39. Hence, the total interaction time (resulting from the detonation of a large number of pulse units) for all propulsive phases of a mission would be on the order of 1 sec or less. This short period and the high momentum transfer involved would result in excessive shock loading to the vehicle structure; therefore, a special "pusher plate" would be deployed below the vehicle which could be set into instantaneous motion by the expanding debris. This pusher plate would be gradually slowed by shock absorbers (which spread out the momentum pulse to the vehicle) and returned to its starting point ready for the next pulse. In theory, it should be possible to smooth out the momentum pulses to the point where the vehicle proper would experience only gradual variations in thrust transmitted by the shock-absorber system.

The pusher-plate surface would be subject to very hot ($\sim$80,000°K) debris along with the high shock loading, and prevention of surface erosion or spalling would be a major design issue. Work by General Atomic (ref. 2-39) indicated that a thin coat ($\sim$ 25 μm) of silicone grease on an aluminum pusher plate could effectively eliminate pusher-plate ablation. The report also states that correct shaping of the pusher plate thickness would prevent the plate from being destroyed by shock waves caused by the impact loading. The

ideal pusher-plate would be tapered in thickness, becoming thinner toward the edges.

The shock-absorber system designed by the Orion team consisted of two parts. Immediately ahead of the pusher plate was a series of toroidal gas-filled bags which absorbed the initial momentum pulse and corrected for off-axis detonations. These bags served as the primary shock absorber and trasferred the momentum to a set of telescoping pneumatic pistons which served as the secondary shock absorber (see Figure 2.3-1). The natural period of the secondary system was about an order of magnitude longer than the primary system (ref. 2-40).

Immediately following the impact of the pulse-unit debris, the pusher plate would move toward the vehicle and its energy would be gradually distributed between the vehicle (as kinetic energy) and the shock absorbers (as potential energy). After the relative motion between the pusher plate and the vehicle had been arrested, the motion would reverse and the potential energy stored in the shock absorbers would be transfered to the vehicle proper. The pusher plate should arrive at its starting point with its initial velocity reversed (no damping), at which time the next detonation occurs, reverses the pusher-plate velocity, and repeats the cycle. Damping of the pusher-plate motion appears to be impractical, due to large amounts of energy which would have to be dissipated in the dampers, so a simple harmonic system was chosen. It would appear to be advantageous to have special "undersized" pulse units available to start and stop each propulsion interval without overstressing the shock-absorber units. Details of the shock-absorber analysis can be found in reference 2-40.

The vehicle is sized by the characteristics of nuclear charges. The smaller an efficient nuclear charge could be built, the smaller the vehicle could become. Atomic weapon technology in 1965 limited the Orion vehicles to charges equivalent to about 100 tons of TNT if efficient use of plutonium was desired. Today's technology is able to produce much smaller, efficient nuclear charges and this could have very beneficial effects on vehicle size and on perceived nuclear contamination. Unfortunately, data required to assess the effects of current weapon technology on Orion-type vehicles are classified putting it beyond the scope of this study.

The performance available with an Orion-type vehicle far exceeds that of any other concept using near-term technology. Unfortunately, however, the

same grounds used in 1965 to terminate the original Orion project are still valid today. For instance:

a. The large size and power of the vehicle made full-scale tests difficult and very expensive (final testing in space required).

b. The 1963 nuclear-test-ban treaty specifically excluded nuclear explosions in the atmosphere or in space.

c. No specific mission existed which demanded such a large, high-performance system.

In addition, discussions with some of the principals involved in the 1965 studies (F. Dyson and C. Schwenk) indicate several questions remained open at the conclusion of these studies. Specifically, questions remained about the lifetime of the pusher-plate surface since it (in ground tests) had never been exposed to debris from a nuclear explosion, only chemical explosions; and there remained serious reservations about the effect this vehicle would have when it injected large masses of ionized material into the ionosphere/magnetosphere.

For these reasons the pulsed nuclear rocket was not carried any further in this study. However, it is recommended that in the near future another study be funded which would specifically address the issues of high-energy nuclear propulsion, including the nuclear (fission) pulse rocket. The potential advancement in propulsion capability at the high-energy levels available is too great to ignore.

2.4 Fusion Rockets

Background. The recent signing of the fusion research bill has committed about $20 billion to the research and development of ground-based fusion power through the year 2000. In fact, the plan is to have a commercial-sized fusion test reactor in operation by that year. A large portion of these funds will be spent on developing components and technologies also applicable to fusion rockets. Without this large national effort on ground-based fusion, there

would be little hope for a working fusion rocket in the foreseeable future. This would be unfortunate because all analyses indicate that only fusion rockets (or pulsed fission rockets) can operate at the power levels necessary to perform reasonable-length manned missions to the outer solar system (beyond Mars).

Description. A fusion reactor must keep its fuel plasma in a limited volume to achieve reasonable fuel burnup. This is known as the confinement problem. The two accepted solutions are magnetic confinement and inertial confinement.

Magnetic confinement uses magnetic fields to control and compress the plasma fuel and to divert hot, burned fuel into a magnetic nozzle where it can be diluted with a propellant gas and expelled to produce thrust.

Inertial confinement is based on compressing a solid fuel pellet so rapidly that shock heating at the center initiates a fusion reaction which runs to completion before the outer layers of the pellet can be blown out of the way. This is done by hitting a spherical target with a precise high-energy "driver" pulse of light or charged particles. The outer shell of the target is vaporized and as it rushes outward (ablation), the remainder of the target is compressed inwards (implosion). Within nanoseconds, the imploding target is compressed and heated to fusion ignition temperatures. Fusion goes rapidly toward completion, and the target explodes like a miniature hydrogen bomb. A series of explosions can drive a space vehicle forward by the pusher-plate/momentum conditioner method described in section 2.3.

The other fusion problem to be addressed is the choice of fuel. There are four fusion reactions within the capability of near-term fusion reactor technology. They are:

a. $D + T \rightarrow He^4 + n + 17.59$ MeV

b. $D + D \rightarrow T + p + 4.03$ MeV

c. $D + D \rightarrow He^3 + n + 3.27$ MeV

d. $D + He^3 \rightarrow He^4 + p + 18.35$ MeV

The probability of any of these reactions occurring inside the reactor is determined by the fusion cross-section measured in barns (10^{-24} cm^2). The fusion cross-section as a function of particle energy for these reactions (and one of the more interesting less likely ones) is shown in Figure 2.4-1. As can be seen, the reaction which is by far the easiest to

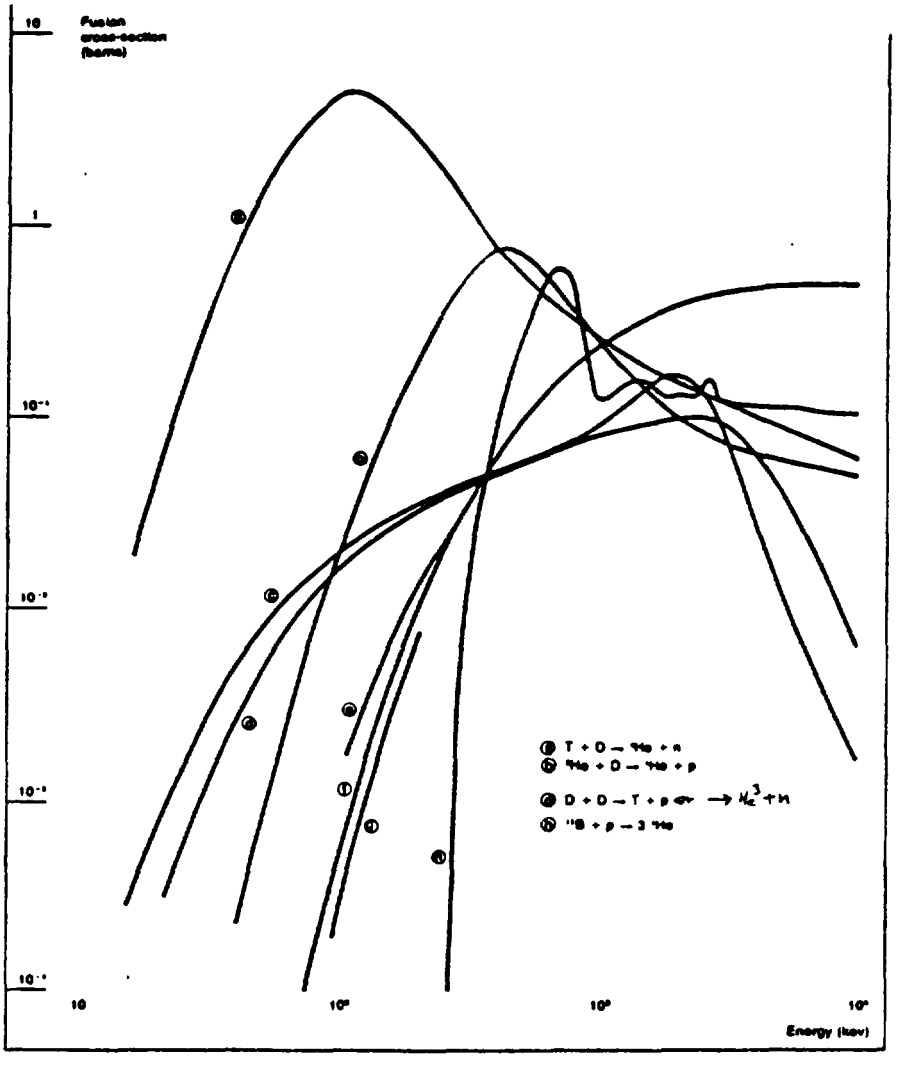

Figure 2.4-1: Important Fusion Cross-Sections

ignite (low energy at peak cross-section) and contain (large cross-section requires lower number density) is reaction a, deuterium plus tritium. Unfortunately, while deuterium is readily available and reasonably cheap, tritium does not occur in nature, is extremely radioactive with a half-life of 12 years, and, as such, cannot be stored for long periods. In addition, every D + T reaction results in a 14 MeV neutron which carries off 80% of the

available energy and deposits it in the worst possible places (e.g., magnet windings, payload, nearby manned habitats, etc.). Since 4π shielding with its required radiators would be prohibitively heavy, it appears that the deuterium-tritium reaction is not well suited to fusion rockets and may not be feasible at all for magnetically confined rocket concepts. Because a D + T reaction produces 3.52 MeV in charged particles for every neutron produced, an unshielded D + T fusion rocket with 200 MW of jet power could not regularly operate within 16,800 km of a manned space facility without exceeding the radiologically safe dose for continous exposure to MeV neutrons (10 neutrons/cm^2/sec).

If fusion reactor technology is sufficiently advanced to operate at higher temperatures (40 to 100 keV), reactions b, c, and d become usable. Use of the deuterium-deuterium reactions (b and c) does not markedly reduce the neutron flux problem (4.86 MeV in charged particles per neutron at 40 keV, where the D + He^3 reaction will not take place, and 12.96 MeV per neutron at 100 keV, where it will). The corresponding radiologically safe distances for the examples above decrease to 14,300 km and 8760 km, respectively. The principal advantage of deuterium fuel is that it is cheap and readily available.

The deuterium-helium 3 reaction results in better than two orders of magnitude reduction in neutron production (732 MeV in charged particles for each neutron) and drops the radiologically safe distance to 1160 km. Unfortunately, helium 3 is a very rare isotope, with a natural abundance of 1 part in 100,000; although it can be produced by bombarding lithium 6 with neutrons from an Earth-based fusion reactor. Deuterium-helium 3 would be the obvious fuel if performance was the sole criterion, but cost and availability may force the fusion rocket designer to select D + D.

The large radiologically safe distances involved indicate that fusion rockets might never be allowed to operate from low Earth orbit, which limits their usefulness in the current study mission model. The most practical appication of fusion rockets might be to base them at a GEO base (well above the Van Allen belts which would trap their charged particle exhaust) and use them for round-trip deep-space manned and unmanned missions.

2.4.1 Magnetic Confinement Concepts

Background. Since the beginning of fusion reasearch, the main approach has

been the use of intense magnetic fields to confine the fusion plasma in a closed magnetic bottle. Mirror bottles are like tubes that are partially open at both ends to allow some particles to leak out. To operate as a reactor, either: (1) the tube must be 1 km long (for high-density pulsed reactor conditions) or 100 km long (for steady state), (2) the plasma flow must be restrained along the tube axis with magnetic constrictions (mirrors) at the ends, or (3) the tube must be bent into a donut shape (torus) with no open ends. No justification appears in the literature to reject option (1) out of hand; but there appears to be no advantage in considering very long fusion rockets, especially in terms of the minimum weight for required structures. Option (2) is the mirror machine concept discussed in the next subsection; option (3) is the mainstream of ground-based fusion reactor design, leading to experimental devices including astrons, multipoles, stellarators, and tokamaks.

Mirror Fusion Machines. Magnetic-mirror systems are open at both ends but most escaping particles are reflected from field constriction plugs located at the ends. Because some particles are always escaping, more particles must be injected into the plasma to maintain steady state. Neutral beam injection appears optimal, but cold injection with microwave heating is possible. Additional magnetic fields (at the expense of greater weight) may provide magnetic wells where the plasma is confined.

In 1967, Kelley proposed (ref. 2-41) that the plug at each end be itself a mirror machine. In this tandem-mirror concept, constant potential is maintained between magnetic-mirror machines, reducing loss to the center machine. However, a practical tandem-mirror reactor is a great deal more complex than the original magnetic-bottle concept (see Figure 2.4-2).

R. F. Post proposed in 1970 to convert the leaking fusion energy directly into electrical current (refs. 2-42 and 2-43). Ions and electrons diffusing through the mirrors would enter a large fan-shaped region called the "expander" (see Figure 2.4-3). Particles would be guided by magnetic fields that taper from roughly 1.5×10^5G at the center to 5×10^2G at the periphery. Plasma density would fall by a factor of 10^9, such that electrons and ions would be separated from each other and collected with almost all their kinetic energy converted into electrical current. This current would drive ion engines for thrust or feed back through neutral beams to heat the fusing

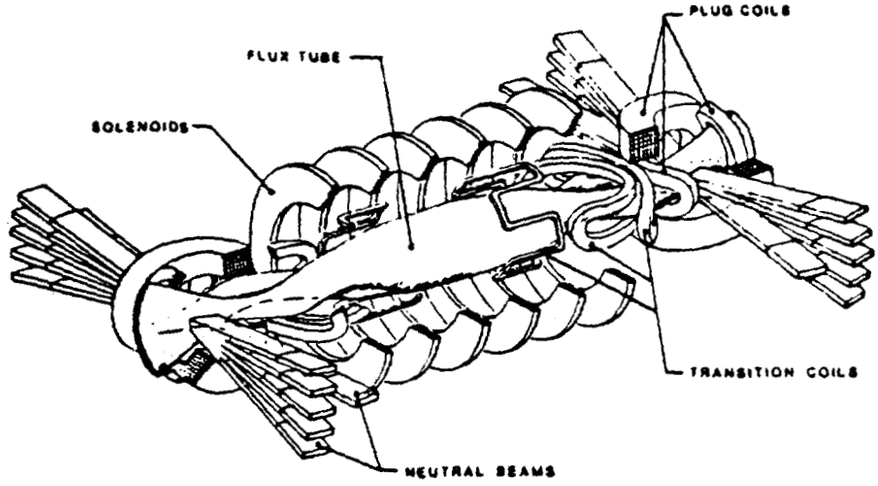

FEATURES

- ISP = 2,500 - 200,000 SECS (CONTROLLED BY H_2 PROPELLANT FLOW)
- INITIAL T/W = 10^{-4} - 10^{-5}
- UNDER DEVELOPMENT FOR GROUND-BASED POWER PLANTS (MFTF - B COMPLETE 1982)

RISK/FEASIBILITY ISSUES

- WEIGHT OF DIRECT CONVERTER & SUBSYSTEMS
- D - He_3 AVAILABILITY
- WEIGHT OF SUPERCONDUCTING MAGNETS

Figure 2.4-2: Tandem-Mirror Conceptual Configuration (TMX 1976)

plasma. Post's direct electrostatic approach might improve D-He^3 fusion cycle confinement by a factor of 2 to 3 (almost all reaction products are charged particles) giving an overall system generation efficiency of ~ 60% and making D-He^3 magnetic mirrors competitive with mainstream D-T mirrors.

A practical mirror-machine rocket would probably consist of a single or tandem-mirror reactor with a direct convertor at one end and a magnetic nozzle with propellant injectors at the other. Propellant injectors would be required because the plasma exiting the reactor would have a specific impulse in the range of 200,000 sec, far beyond the optimum value for planetary applications. By throttling the hydrogen propellant flow, the specific impulse of the fusion rocket could be varied from 2000 to 200,000 sec.

Toroidal Fusion Machines. It is likely that most torus mainstream designs would be rejected as fusion rockets on the basis of their heavy secondary magnets used to bend the plasma tubes to stabilize them, but there are a few concepts which might be competitive with mirror machines.

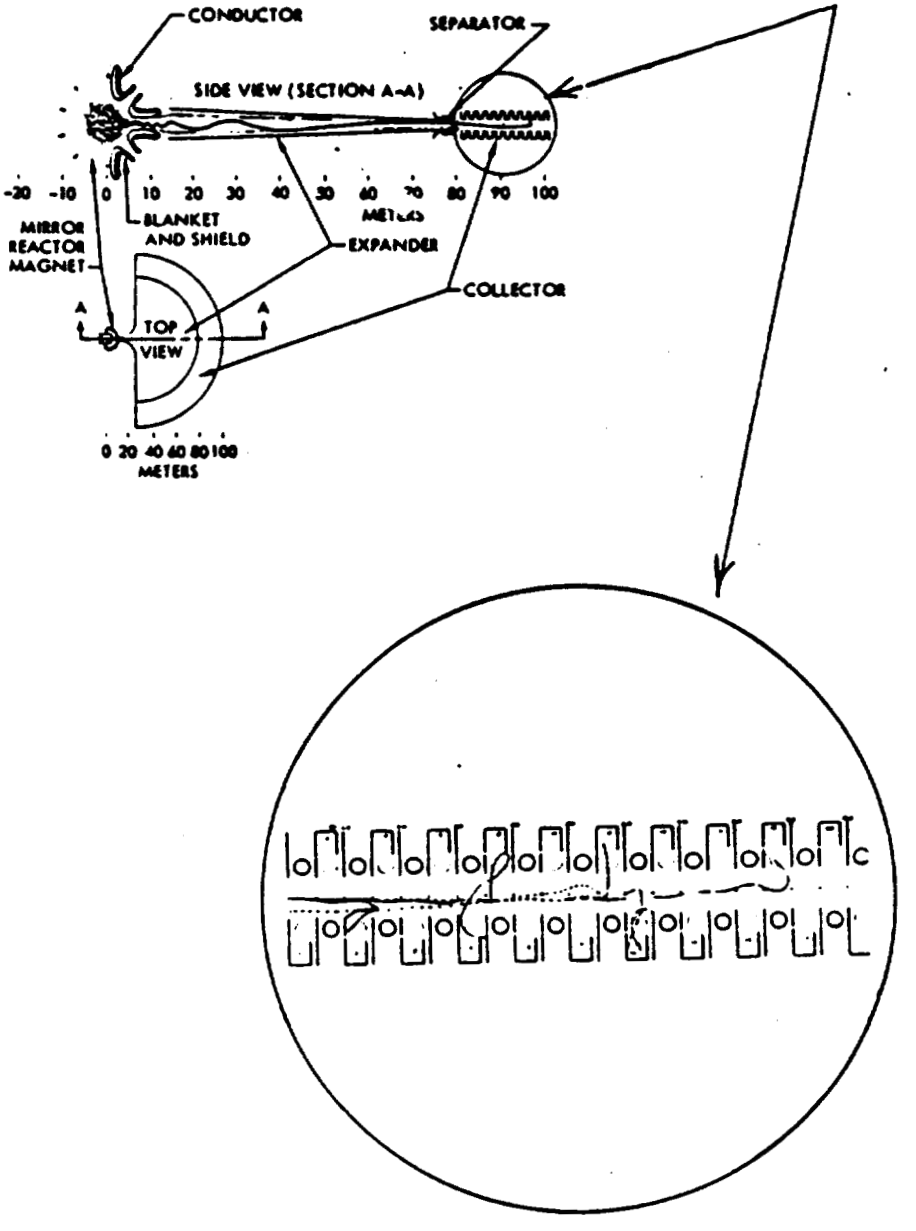

Figure 2.4-3: Schematic of Direct Converter for Mirror Reactor

Stellarator Concept: T. K. Chu of Princeton claims that, "The stellarator is unique among magnetic-confinement concepts. It is the only scheme yet suggested...that promises a fusion reactor that would require no power input after it reaches ignition. Once the deuterium-tritium plasma starts to burn, the neutral-beam injection could be shut off. (One does of course have to maintain steady confining currents in the external windings.)" (ref. 2-44). For fusion rockets of all other designs, there must be an

ignition/reignition/power-storage subsystem which is a significant fraction of total vehicle mass. The stellarator concept was virtually abandoned in the 1970's, 20 years after its Princeton invention, but was convincingly demonstrated in 1980 by Grieger, Renner, et al. of the Max Planck Institute for Plasma Physics in Garching, Germany (ref. 2-45).

Riggatron Concept: The Riggatron, or throwaway tokamak, is a device being developed by International Nuclear Energy Systems Co. (Inesco). Invented by nuclear engine designer Robert W. Bussard and by MIT professor of physics Bruno Coppi, the Riggatron's main advantage over other fusion devices for space vehicles is its estimated small size and weight (about 4 metric tons according to ref. 2-46). The Riggatron differs from the mainstream tokamak fusion reactors like the Princeton tokamak fusion test reaction (TFTR) in that it would (1) operate at much higher magnetic field strengths and hence plasma densities, (2) be driven to ignition by ohmic heating alone (no expensive neutral beam injectors), (3) raise its power level to 50 times the ignition level with "bootstrapping" (i.e., injecting fuel at proper rates and recycling excess fusion energy, (4) use highly stressed water-cooled copper magnet coils which are much reduced in size because they are designed to operate inside, instead of outside, the neutron shield, and (5) be designed for a limited lifetime (approximately 1 month) and then be recycled as scrap or thrown away.

A privately funded, ($100 million, 5-year development program is currently underway to build and test five slightly different Riggatron devices with a goal of 200 MW_{th} power output by 1984-85. Advanced versions of this device have been analyzed for use of the D-D reaction, and the resultant D-D machines would be roughly 3m (120 in) in diameter and weigh approximately 30,000 kg (66,000 lb). If shown feasible for ground-based use, Riggatrons should excel in space applications because most other magnetic confinement fusion designs require large cryogenic cooling systems with their massive waste-heat radiators. A proposed Riggatron D-T ground-based fusion reactor shown in Figure 2.4-4 would have the following characteristics:

Power: 300 to 1000 MW_{th}
Plasma radius: 50 to 70 cm
Toroidal field strength: 1.8×10^5 G
Coil material: AMAX-M2C copper alloy, or 30% W/Cu composite

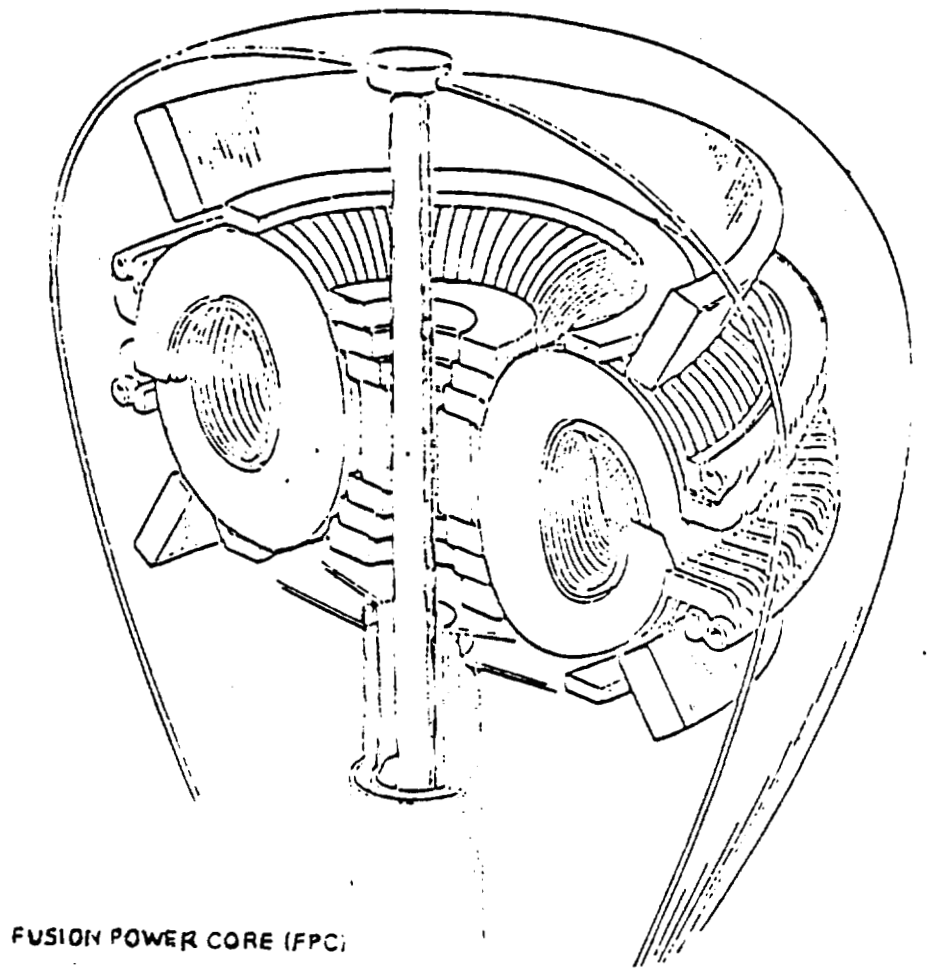

Figure 2.4-4: Artist's Concept of D-T Fueled Riggatron

Yield stress: 1.4 to 1.8 x 10^5 lb/in^2
Fatigue life: 2 x 10^4 cycles
Plasma current: 3 to 4 x 10^6A
Weight: 4 x 10^3 kg

Converting a ground-based toroidal fusion reactor into a fusion rocket requires the addition of a magnetic nozzle with suitable propellant injectors and an auxiliary power supply capable of maintaining the magnetic fields and providing the energy required for ignition. An example of a fusion rocket based on a toroidal reactor design is shown in Figure 2.4-5. The magnetic nozzle design is based on the partial divertor presently being tested in the TFTR.

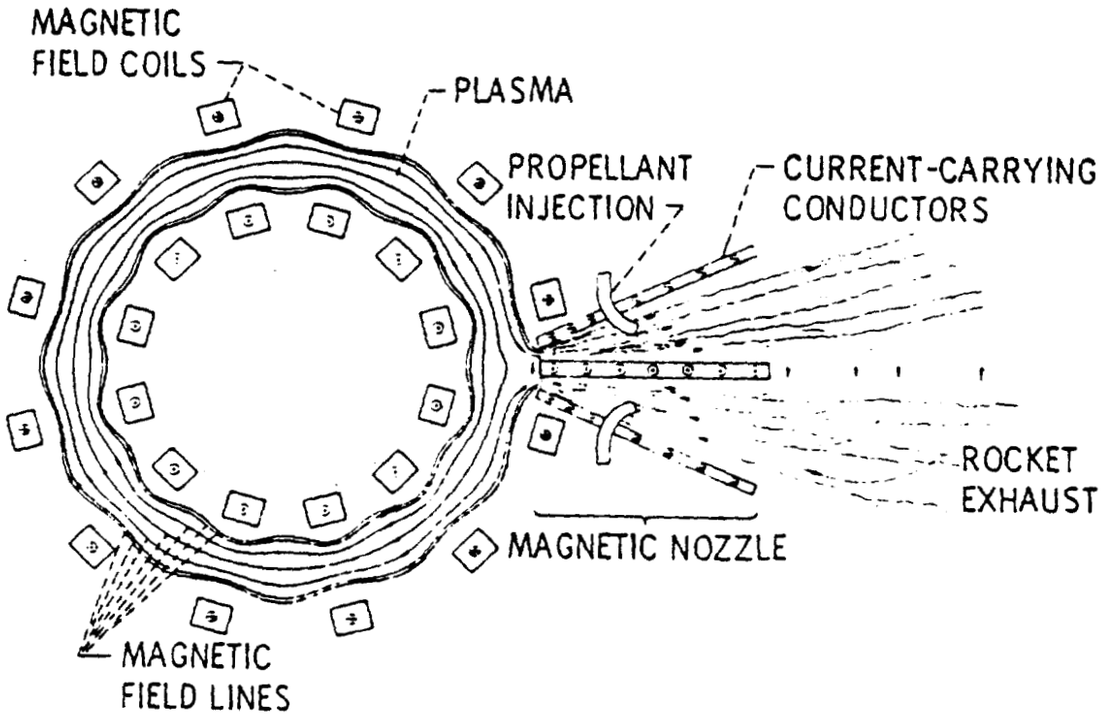

Figure 2.4-5: Direct Fusion Rocket Based on Toroidal Fusion Reactor

2.4.2 Inertial Confinement Concepts

Background. Inertial confinement fusion goes back to the hydrogen bomb. The pulsed fusion rocket concepts discussed here in effect use miniature hydrogen bombs as a source of energy and momentum. Pulsed fusion rockets were the obvious follow-on to the pulse fission rocket after project Orion was cancelled. Whereas a fission pulse unit has definite minimum critical mass to attain an efficient reaction, a fusion pulse unit has no lower limit and could theoretically be as small as a few thousand atoms. This means that fusion pulse rockets could be built in any size and power range to meet specific mission requirements.

Inertial confinement research for other than bombs started much later than magnetic confinement and is currently far behind in technology development. The basic remaining problem is the need to couple more energy in less time and more efficiently to the fuel pellet. With this in mind, recent work has begun on the use of light-ion (H+) beams instead of laser beams as drivers for inertial confinement fusion. Light ions couple more efficiently into the implosion process because they do not create hot electrons which can preheat the fuel in the center of the pellet before the shock wave arrives to

initiate fusion. In addition, the overall efficiency of light-ion beams is predicted to be 30% to 40% compared to 5% to 20% for lasers. Light ions, however, are more difficult to focus on the target pellet.

Fusion pulse propulsion technology is obviously less well developed then ground-based inertial confinement fusion technology and so it is doubtful that a pulsed fusion rocket could be made operational in less than 15 to 20 years. However, the potential of such a vehicle is so enormous that a number of studies have examined hypothetical pulsed fusion concepts; results are summarized below.

Pulsed Fusion Rockets. A nuclear pulse rocket using fusion microbombs is shown in Figure 2.4-6. The concept is identical to the pulsed fission rocket discussed in section 2.3 except a laser or particle-beam system is required to

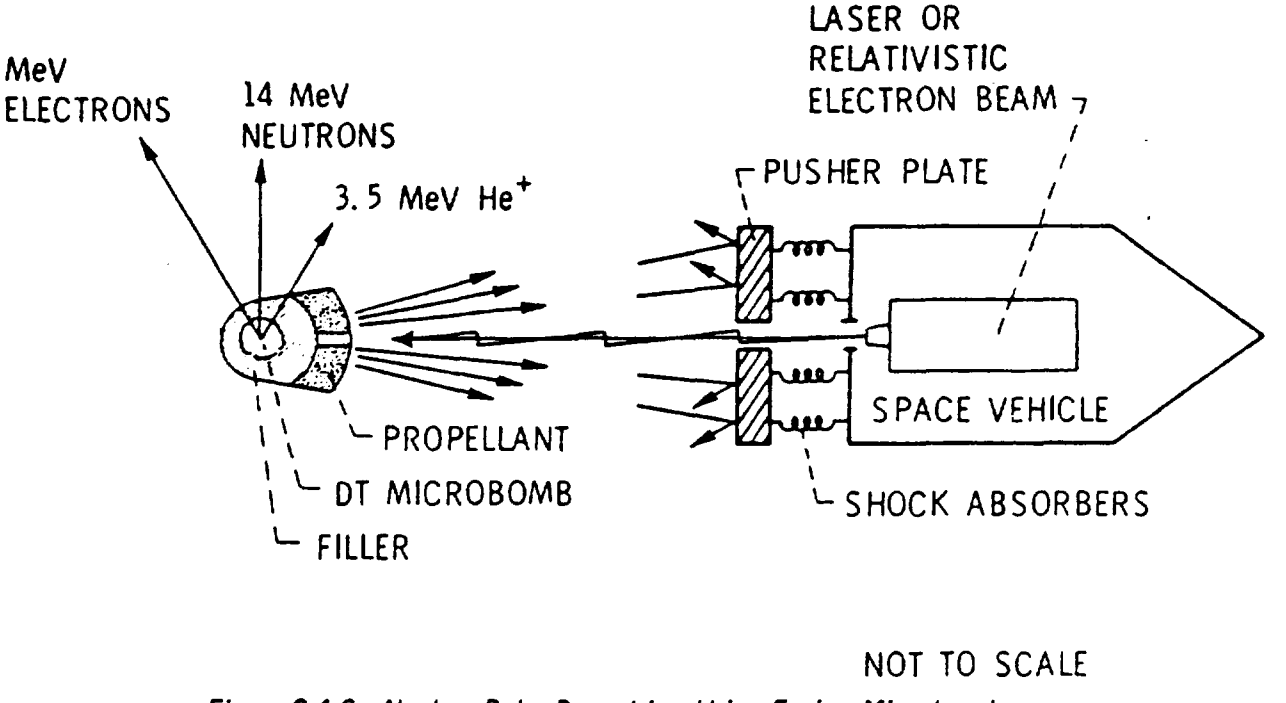

Figure 2.4-6: Nuclear Pulse Propulsion Using Fusion Microbombs

supply the ignition pulse to trigger the microbombs. The propellant located on each bomblet serves as a conical radiation shield to absorb most of the fusion neutrons which would otherwise impact the vehicle and cause excess heating. After serving this function, the shield is vaporized in the ensuing explosion and becomes reaction mass to impact the pusher plate. According to reference 2-47, beryllium appears to be an excellent propellant/shield for this application.

One key to improving fusion pulse propulsion design is to reduce the power requirements of the ignition subsystem. With a laser-induced fusion rocket system such as the Blascon, Sirius, or Hyde-Wood-Nuckolls fusion rocket concepts (refs. 2-47, 2-48, and 2-49), the weight of the laser was critical. This same problem applied to charged-particle-beam drivers. Recent results of F. Winterberg show how to reduce ignition power requirements for fusion microexplosions by a factor of 100 (ref. 2-50). Charged-particle beams or hypervelocity projectiles could be used in a two-stage process to initiate the fusion pulses which drive the space vehicle. In the first stage, the initial driver (reduced in power from $\sim 10^{14}$W to $\sim 10^{12}$W) causes ablative implosion of a spherical target (see Figure 2.4-7). A thin but high-atomic-number gas

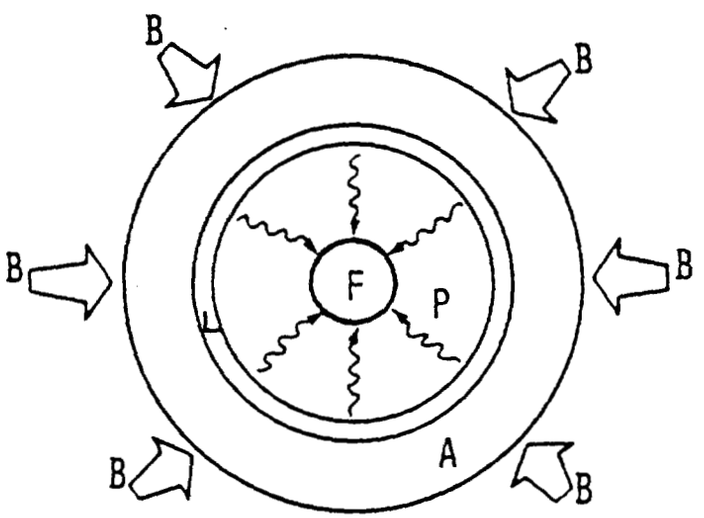

A: ABLATIVE LAYER
L: DENSE LINING OF ABLATOR (U)
P: PHOTON BLACKBODY IMPOSION
F: FUSION PELLET (DT, He^3D, p"B...)
B: BEAMS OF IONS OR RELATIVISTIC ELECTRONS FROM DRIVER

Figure 2.4-7: Pulsed Fusion Rocket Using Two-Stage Ignition Process

inside the target (krypton, UF_6) converts the implosion shock wave into an intense blackbody radiation (mostly soft X-rays). In effect, the radiation is compressed and amplified by the implosion. These X-rays strike the fusion pellet and ignite the propulsive thermonuclear micorexplosion. Because power is amplified by compression and delivered at peak power, a smaller and lighter initial driver system can trigger the final fusion output. This two-stage

process requires material in the target besides the fusion explosive, which increases thrust but lowers specific impulse; consequently, Winterberg's concept, as used here, would be more applicable for interplanetary rather than interstellar travel. Note that the X-ray photon compression stage is a temperature-heightening process. This might make the low-cost, very clean, proton-boron fusion reaction attainable for space propulsion.

Another approach for reducing the size of the fusion driver subsystem is to bunch or overlap multiple charged-particle beams onto centimeter-sized hydrogen targets. Several beams can be transported to a single target by passage along plasma discharge channels in a background gas. The channels carry current (from capacitor banks) and are initiated by lasers. The multiple beams can deliver 10 times as much beam current density to the target as a single beam. This approach is being investigated experimentally at Sandia National Laboratories. There are a number of problems in applying this to fusion pulse propulsion. The greatest difficulty is the complexity of combining capacitor, laser, charged-particle-beam accelerator, and background gas subsystems in a low-weight, high-reliability system for initiating inertial confinement fusion.

Magnetic fields can be used to replace or shield the pusher plate from high-energy plasma damage (refs. 2-49 and 2-51). Now a standard option in speculative designs, the magnetic field protects the pusher plate from ablation and spallation. This adds weight and power requirements but allows higher velocity plasma to impinge on a pusher plate of given tensile strength. Specific impulse should be improved by this approach, but no thorough mathematical analysis is currently available. Martin and Bond (ref. 2-52) claim that magnetic systems allow specific impulses greater than 10^6 sec.

The specific impulse of fusion pulse propulsion can be optimized for specific missions in a manner similar to the magnetic confinement fusion rockets. Fusion pulse rockets with specific impulses of 3300 sec have been compared to chemical and fission rockets in reference 2-47, with fusion pulse giving best results. Livermore studies (ref. 2-49) considered external magnetic fusion pulse rockets with specific impulses of 5.5×10^5 sec, which could reach any destination in the solar system in under 1 year, with round trips under 2 years.

2.5 Laser Powered Rockets

Of all applications proposed for high-powered lasers, none challenges every aspect of laser technology as thoroughly as the concept of using lasers to transmit the power thrust to a free-flying rocket thousands of kilometers away. This concept of a laser-powered rocket could revolutionize space transportation technology, but it is also fraught with many feasibility issues and operational concerns. The primary concerns to be addressed here are the problems of collecting the laser beam and transfering its energy to the rocket propellant.

Recent studies of laser rockets have taken two different approaches: those using pulsed lasers for ground-launched operations and those using continous wave lasers for space-launched operations. Both options will be summarized here for the sake of completeness.

2.5.1 Pulsed-Laser Concepts

There were two ground-launched, pulsed-laser rocket concepts recently under study. The concept proposed by Physical Sciences, Inc. (PSI), is shown in Figure 2.5-1. In this concept a high-powered pulsed laser is directed into

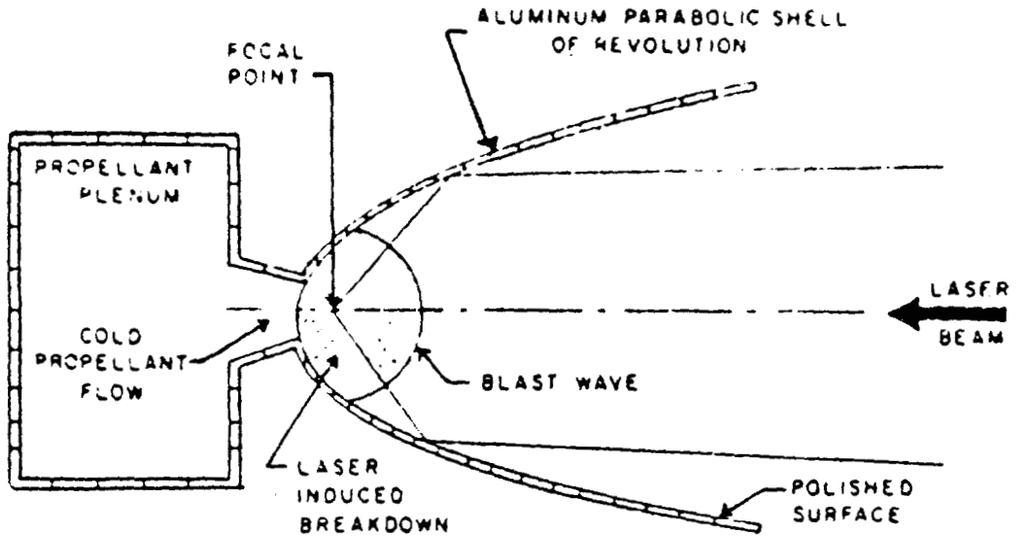

Figure 2.5-1: Acoustically Valved Ground-Launched Laser Rocket

the nozzle where it is focused to a high intensity in a cloud of propellant gas. This initiates a high-temperature, high-pressure plasma in the form of a blast wave which propagates up the laser beam. Provided the pulse is sufficiently short so the high-pressure gas remains in the vicinity of the nozzle wall, this concept provides an efficient propulsion device. The strength of the laser-induced blast waves and laser repetition rate specifies the propellant mass flow. This is because the laser-induced blast waves stop the propellant flow through the throat whenever the pressure in the nozzle is greater than the pressure in the plenum chamber. This process is called acoustic valving. Tests of this concept reported in ref. 2-53 indicate a maximum specific impulse of 900 ± 400 sec at 1 atm and 1000 ± 100 sec at 10^{-4} atm using hydrogen propellant. The reported energy conversion efficiency (exhaust energy/laser energy) was about 50%.

Feasibility issues of this concept concerned the ability to preserve the structural integrity and optical reflecting quality of the nozzle, and at what weight penalty. Peak gas temperatures at the nozzle wall will approach 10,000°K and the 2m-diameter nozzle must be rugged enough to withstand strong impulsive hoop stresses.

The second ground-launch laser-rocket concept is proposed by AVCO and called the laser-sustained detonation wave rocket. The principle behind this concept is shown in Figure 2.5-2. It is somewhat similar to the PSI pulsed rocket except the laser beam is not concentrated by the nozzle bell and the amount of propellant used for each pulse is determined by a preliminary pulse which ablates a measured amount of solid or liquid propellant off a flat surface. A second high-flux pulse then ignites a laser-sustained detonation wave which shields the surface from further radiation. The detonation wave propagates back towards the laser, heating the propellant gas to approximately 20,000°K and generating a large pressure pulse on the propellant surface and expansion skirt. Reference 2-54 quotes a specific impulse of 800 sec for a 2 x 10^7 W/cm^2 laser pulse of 10 μs duration resulting in an impulse load of approximately 30 atm on the base.

In this AVCO design, the two weak points of the PSI design are not present because (1) the hot propellant gas is in contact with the vehicle for a much smaller fraction of the duty cycle and (2) the exposed surface is mainly a flat plate which does not need to withstand hoop stresses or be of optical quality. This design does have some unique problems of its own,

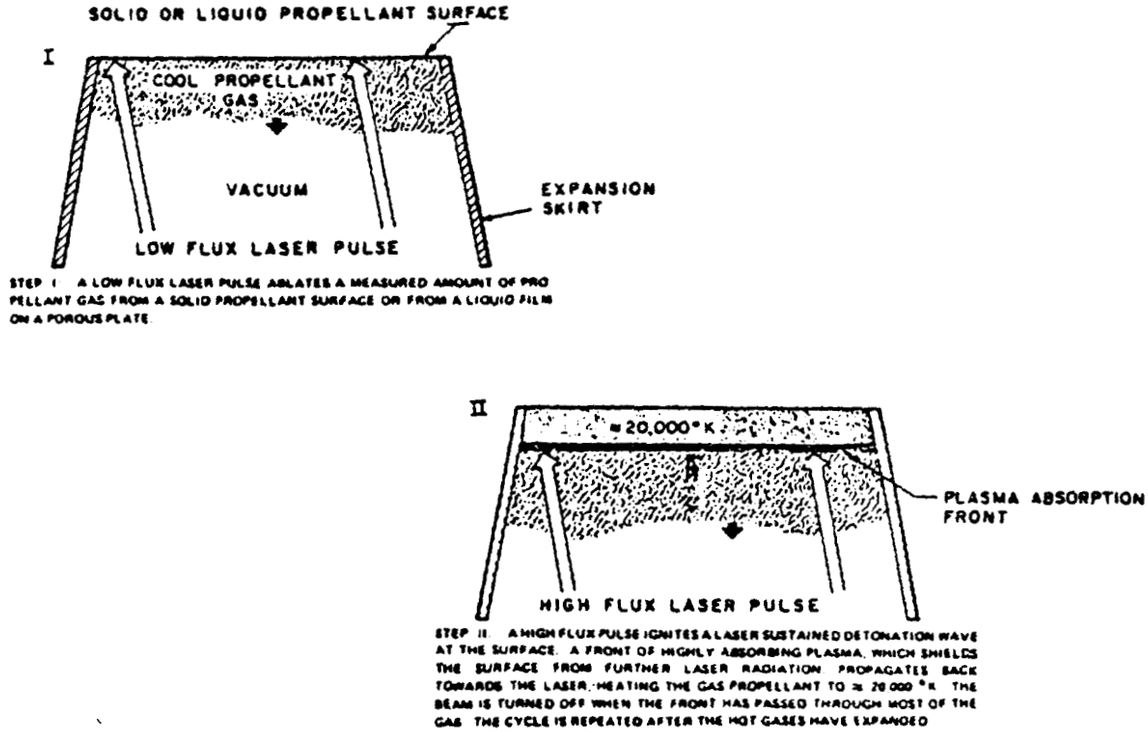

Figure 2.5-2: Laser-Sustained Detonation Wave Rocket Engine

however: (1) How is the propellant fed onto the flat surface? (2) If by transpiration, is there sufficient specific heat to cool the surface and how is the flow rate controlled? (3) If the surface is a solid ablator, how is the surface flatness controlled and how are the expansion skirts moved as the surface recedes? Also, if the laser pulse arrives off center or uneven, the vehicle will experience a large impulsive torque which could set the vehicle tumbling in a fraction of a second. These are unresolved feasibility issues for the AVCO design to address.

2.5.2 Continuous-Wave Laser Concepts

There are several space-launched, continuous-wave, laser-rocket concepts under study. They all involve collecting a laser beam transmitted over considerable distances, concentrating that beam, and directing it into a thrust chamber where it is used to heat a gaseous propellant (hydrogen). The propellant is allowed to expand through a conventional rocket nozzle and produce thrust. Hydrogen has been the propellant selected in every previous study because its low molecular weight results in the best specific impulse, as discussed previously. The primary issues with respect to the

continous-wave laser rocket are the choice of coupling mechanism used to transfer the photon energy of the laser to the hydrogen propellant and related problems of wavelength and laser location.

The simplest way conceptually of using the laser energy is to introduce the beam directly into the thrust chamber through a window and thermalize the propellant. This method places an additional constraint on the working fluid because it must be made opaque to the laser beam. Several ways are available to accomplish this, and the major characteristics of proposed coupling techniques are discussed below.

Inverse Bremsstrahlung. A leading candidate among possible coupling mechanisms is inverse Bremsstrahlung which is applicable for any wavelength laser and working fluids hot enough for significant ionization. The free electrons in a partially ionized gas can be made to oscillate in the varying electric field caused by the transmitted electromagnetic beam. This oscillation in itself is a conservative process for an isolated electron and results in no energy transfer. However, in the relatively dense gas in the thrust chamber, the electrons undergo inelastic collisions with atoms, molecules, and ions which tends to transfer energy from the beam to the gas and results in even more free electrons. The result is that once the laser flux exceeds a certain threshold level (and provided sufficient free electrons are available), the gas will become highly absorptive to the radiation. One of the attractive features of the inverse Bremsstrahlung mechanism is its relative insensitivity to wavelength; therefore it can be used with most lasers, although there is a drop in absorption coefficient at shorter wavelengths (below 3 μm). This absorption mechanism also has no inherent high-temperature limit which makes it unique among laser coupling techniques; however, this same high-temperature characteristic could also be its downfall, as is discussed below.

A schematic of the inverse Bremsstrahlung coupled-laser rocket is shown in Figure 2.5-3 from reference 2-55. In this case the laser beam has been collected and focused into the chamber close to the throat of a supersonic nozzle. A laser-supported combustion (LSC) wave is ignited at the focus through use of an electrical arc (or microwave discharge, etc.) which initiates the ionization process. Working fluid (propellant) is introduced at a rate which just balances the propagation rate of the LSC wave, resulting in

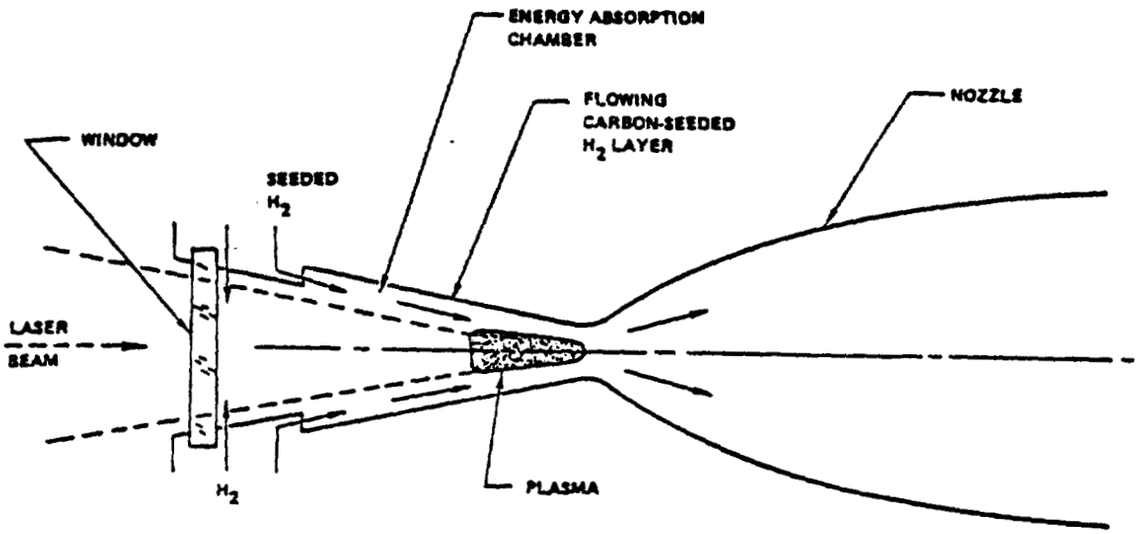

Figure 2.5-3: Inverse Bremsstrahlung Coupled-Laser Rocket

a stationary plasma source. Because of the high radiation flux from this plasma, it is necessary to shield the chamber walls. This is done by introducing a buffer layer of hydrogen seeded with submicrometer-sized carbon particles, which provides a radiation absorption layer to aid in the cooling of the chamber wall. As a specific example, the 5-MW laser rocket designed in reference 2-55 assumed an average plasma temperature of 12,000°K with a resultant heat flux of 6400 W/cm^2. The thrust chamber is regeneratively cooled and the mass of propellant passing through the 2-cm throat is only capable of absorbing a combined heat flux (convective plus radiation) of around 1500 W/cm^2. Hence, about 90% of the radiant heat flux from the plasma must be absorbed by the working fluid via some mechanism yet to be determined. Experiments being conducted at NASA MSFC are exploring this critical area.

Later analyses of this same engine (ref. 2-56) showed the maximum temperature in the plasma to be much higher than the temperature assumed in reference 2-55 (19,000°K rather than 15,000°K) and the average temperature to be 17,000°K instead of 12,000°K. Because the radiated heat flux varies as the 4th power of temperature, this results in a revised heat flux of approximately 25 kW/cm^2 which requires either 99% radiation absorption of the carbon particles or a greatly increased mass flow of hydrogen for regenerative cooling. This increased mass flow would reduce the engine specific impulse to well below 1000 sec and make it noncompetitive.

Additional studies and testing of inverse Bremsstrahlung coupling are proposed or currently underway to determine (1) the average LSC wave plasma temperatures in hydrogen at typical engine operating conditions and (2) the absorption characteristics of submicrometer-sized carbon seed under the same conditions. These are viewed as basic feasibility tests with respect to this coupling concept. Another feasibility issue to be addressed during these tests is the problem of vaporized seed material condensing on the cooled window surface. A very small amount of seed material condensing on the window surface will increase its absorption and destroy the window.

Molecular Resonance Absorption. Radiation can also be absorbed by seeding the propellant with molecules which undergo transitions from a ground state to a higher vibrational-rotational energy state by absorbing a photon of the appropriate wavelength. If the absorption cross-section is large, the absorber gas may form a small percentage of the gas molecules in the combustion chamber and not significantly degrade the specific impulse relative to a pure hydrogen propellant. If the absorption is from the ground state of a molecule, the process can be started in a cold gas which would eliminate the need for a separate starting system and greatly simplify engine operation.

There are several limitations on molecular resonance absorption. First, the absorbing molecules exhibit large absorption cross-sections over very limited wavelength ranges, thus requiring accurately matched laser wavelengths. Second, thermal saturation decreases the absorption coefficient with increasing temperature as the absorbing molecules at the upper energy levels begin to predominate the mixture. Short relaxation times and absorption at energy levels above ground state tend to counter thermal saturation problems. The maximum temperature at which molecular absorption can operate is determined by dissociation of the absorber gas. Dissociation will deplete absorbing molecules and reduce the absorption coefficient. In addition, the resulting constituents may chemically react with the propellant and/or engine walls before they are able to recombine.

A recent study (ref. 2-57) investigated the feasibility of using molecular resonance absorption to couple CO and CO_2 laser radiation to hydrogen propellant at rocket chamber conditions. Of the candidate molecules for coupling to CO laser radiation, the CO molecule performed the best, exhibiting an absorption per centimeter of 10^{-2} at temperatures as low as $300^{\circ}K$ and a chemical stability which permits this absorption level to be

maintained to temperatures in excess of 6000°K. The molecule H_2O was found to couple effectively at both CO and CO_2 wavelengths. Its calculated absorption per centimeter exceeded 10^{-2} over a temperature range of 400°K to 3800°K for CO wavelengths and 1300°K to 4800°K for CO_2 wavelengths. The equilibrium chemistry of CO and H_2O in H_2 is shown in Figures 2.5-4 and -5 from reference 2-57, and the measured absorption per centimeter as a function of temperature is shown in Figures 2.5-6 and -7 from the same reference. The measured

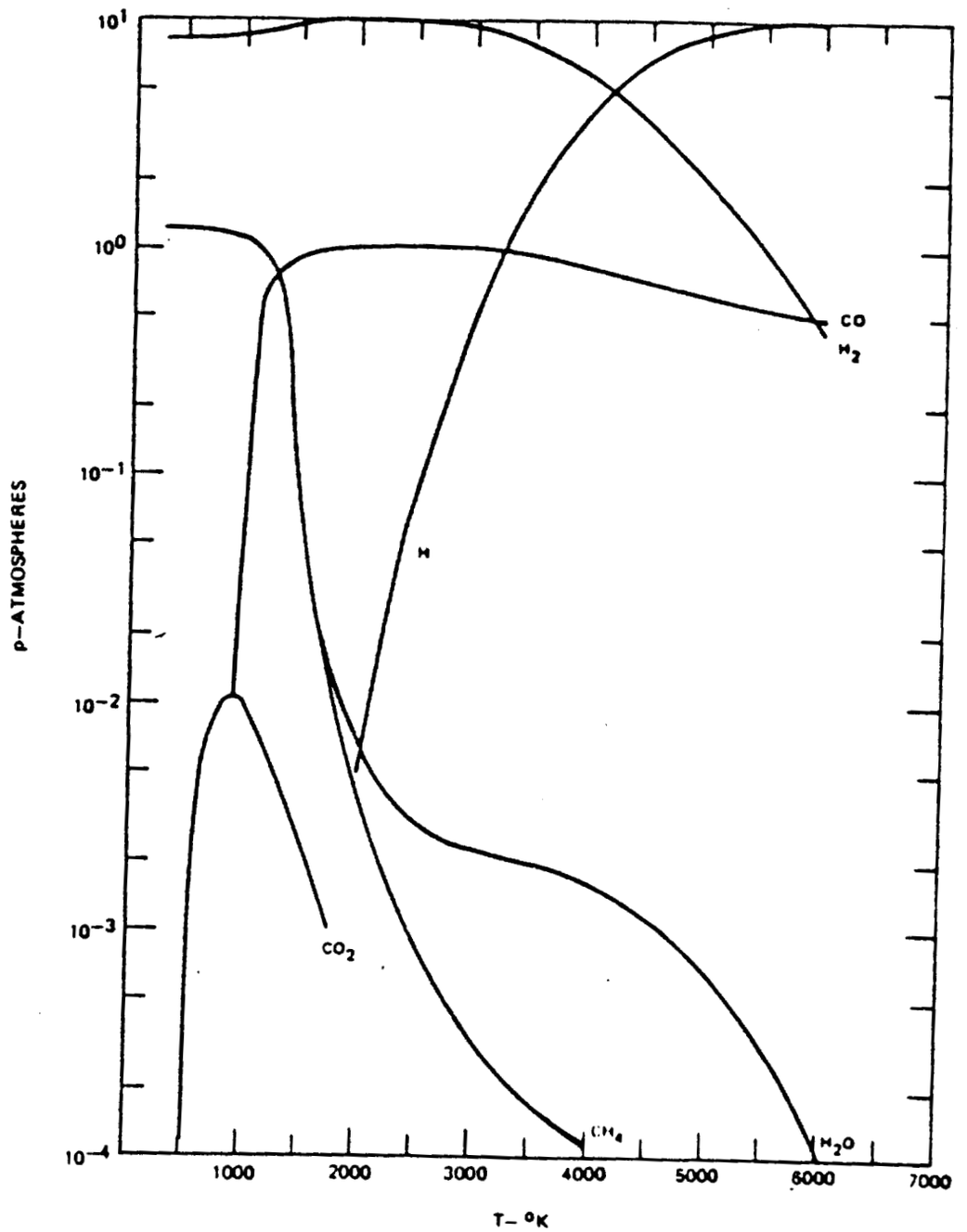

Figure 2.5-4: Equilibrium Chemistry of 10-H_2 and 1-CO versus Temperature

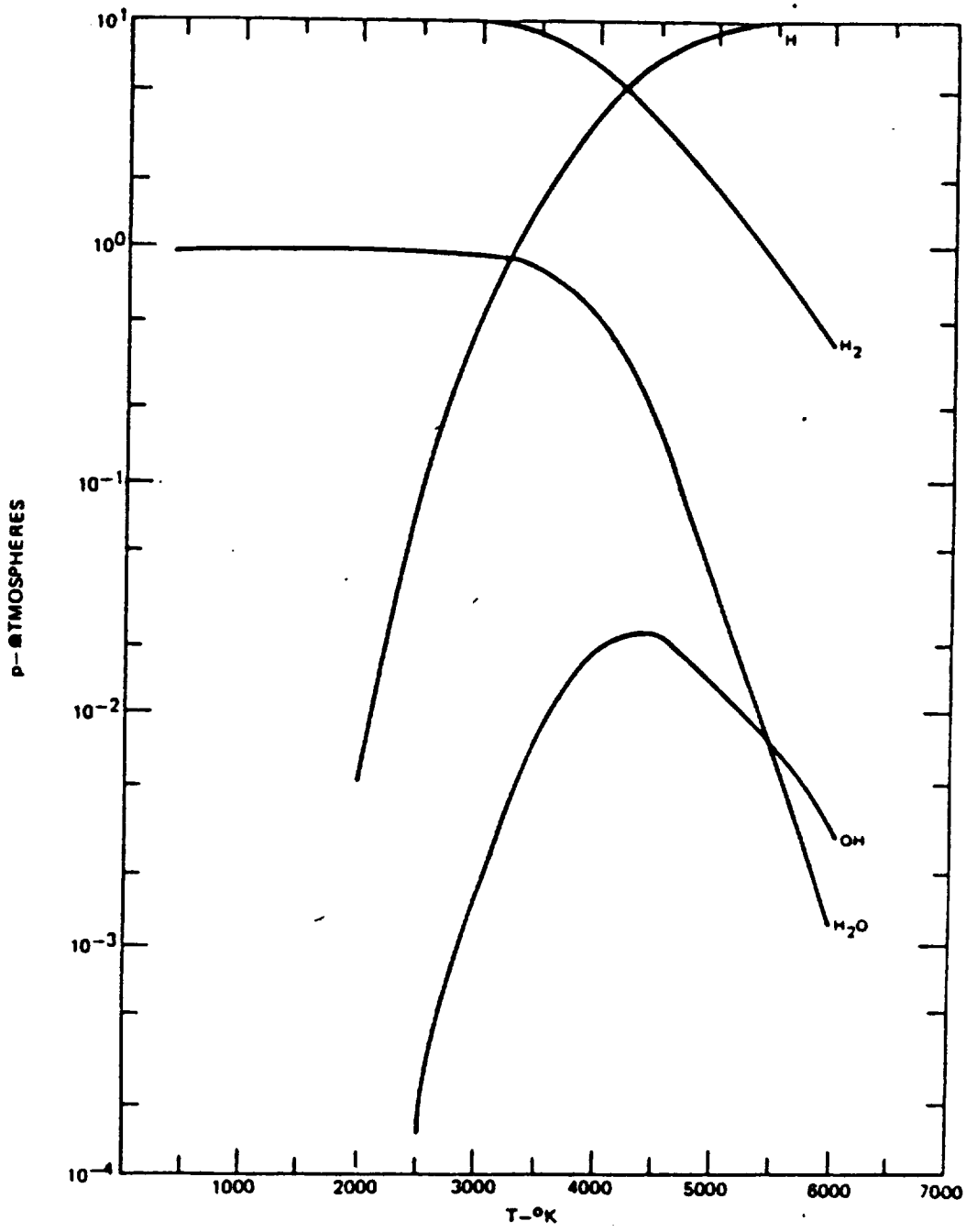

Figure 2.5-5: Equilibrium Chemistry of 10 atm-H_2 and 1 atm-H_2O versus Temperature

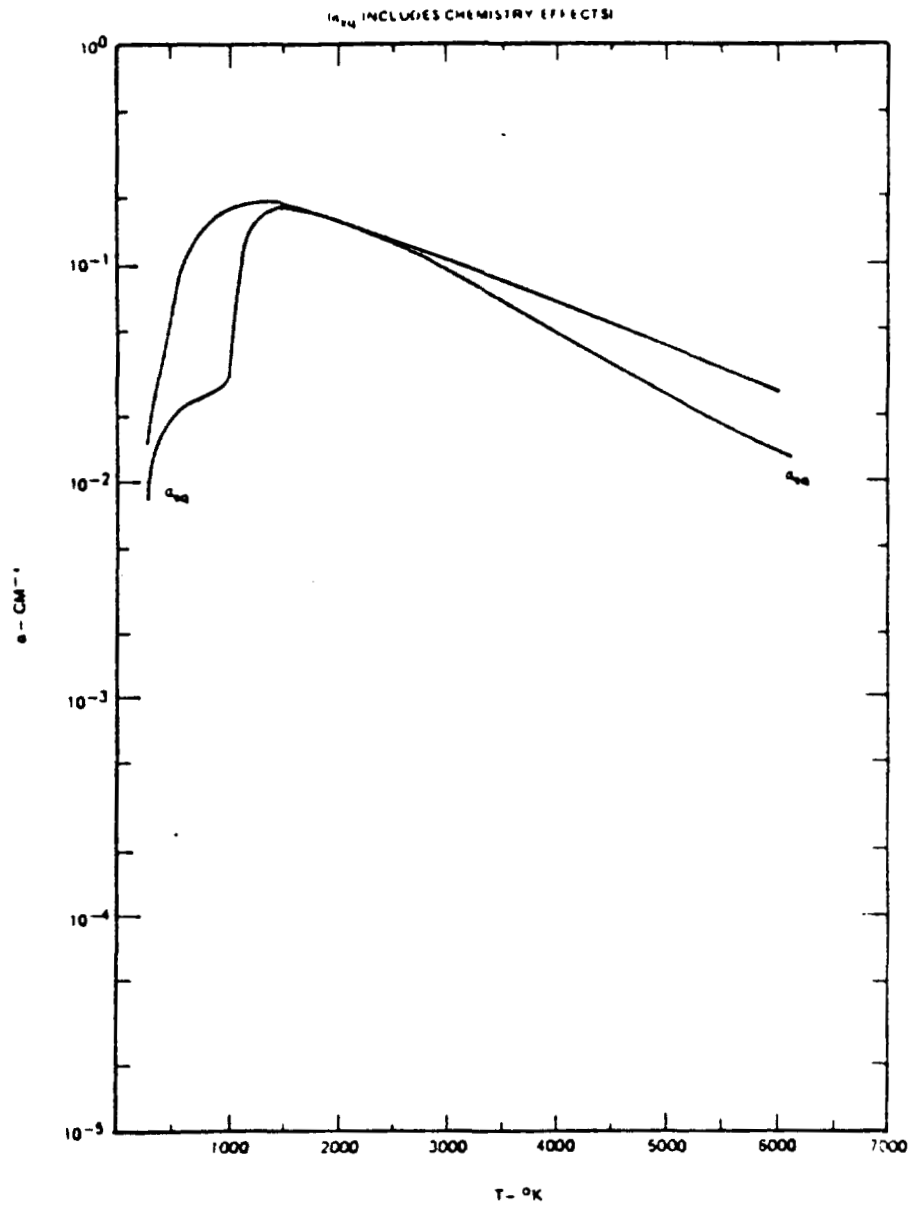

Figure 2.5-6: Absorption per CM versus Temperature, 1-atm CO in 10-atm H_2

absorption of the water molecules exceeded the analytically predicted values by one order of magnitude and another study is underway to verify those results.

These preliminary data indicate that molecular resonance absorption has definite potential as a direct coupling method for laser-rocket applications. Further work is required to verify the H_2O coupling results and an investigation of the coupling characteristics of the HF molecule is highly

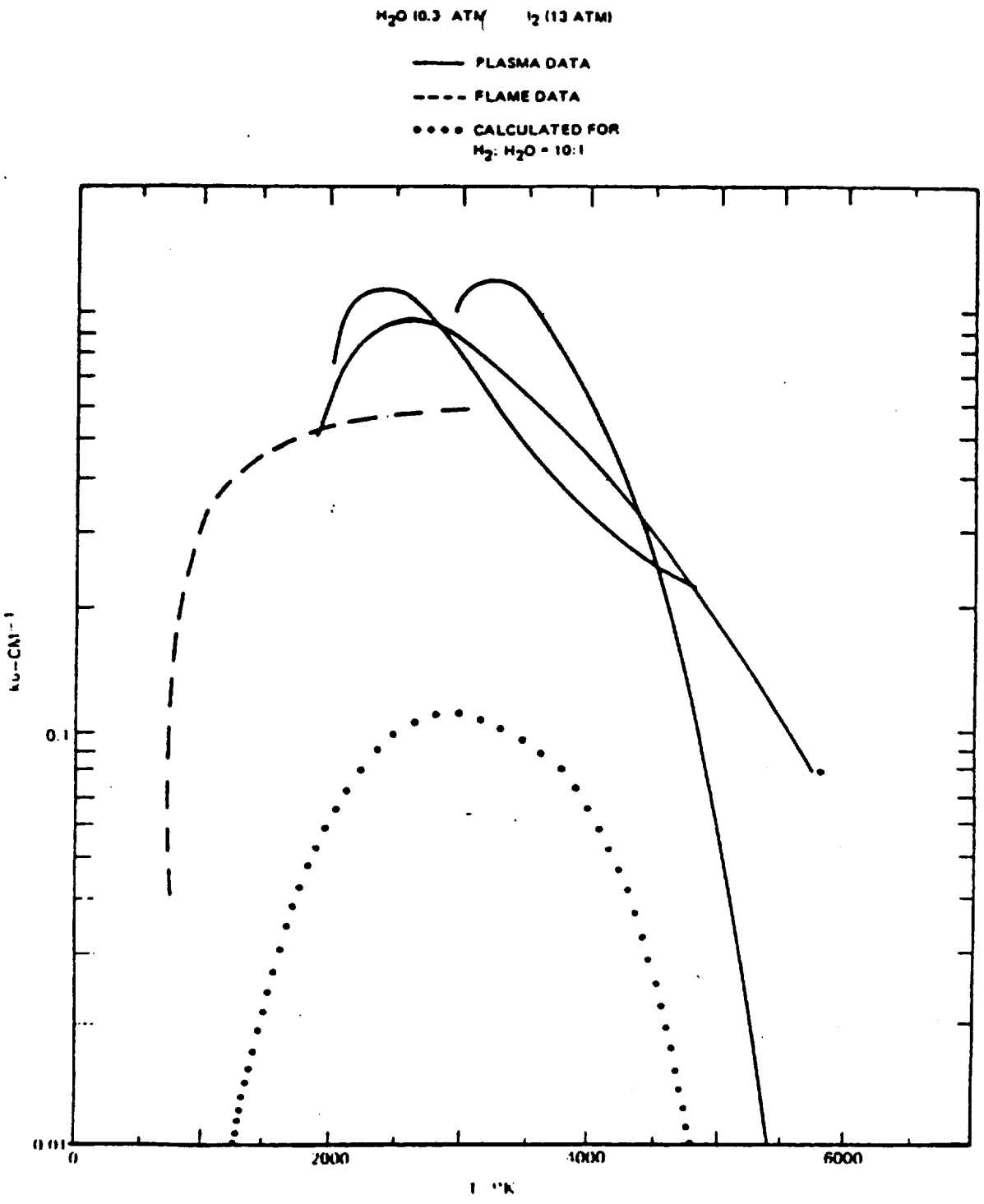

Figure 2.5-7: Measured Absorption Coefficient (Ku) versus Temperature (T) for H_2O (0-3 atm) in H_2O (3 atm)

desirable. Not as stable as CO, HF is still very stable and its high temperature dissociation would be suppressed by the high concentration of hydrogen present. Usable concentrations should be available up to 5000°K.

Particulate Absorption. Laser energy may also be coupled to the propellant by seeding it with highly absorbent particulate matter. The particles absorb the laser light, are heated to temperatures above the surrounding gas, and thermally conduct the energy to the working fluid. This process is identical to the heat-transfer method discussed for the nuclear gas-core reactor rockets and a large data base is available from that source. Ideally, the particulate matter would be retained in the engine by use of a vortex centrifugal separator because it might be a high-density material such as tungsten that could significantly degrade engine specific impulse.

Experimental data on the bulk exit temperatures available with particulate absorption of radiant energy from a dc arc (simulating a gas-core reactor) are shown in Figures 2.5-8 and -9. Figure 2.5-8 from reference 2-58 shows bulk exit temperature versus the incident radiation flux for argon seeded with micrometer-sized carbon particles to simulate hydrogen propellant. The maximum temperature reached in experiment (3860°K) was limited by vaporization of the carbon seeds, so a second experiment was run using tungsten seeds which do not vaporize until 5900°K. Results of this second experiment are shown in Figure 2.5-9 from reference 2-59. The maximum bulk exit temperature reached in this experiment (4515°K) was limited by the amount of radiation incident on the test section which was determined by the arc power supply and mirror cooling limits. The apparatus used for these experiments is shown in Figure 2.5-10. As expected, the tungsten seed benefited from higher melting and boiling points and higher opacity in the vapor state; but for peak performance, the mass flow of tungsten seed was three times the mass flow of argon working fluid. This condition would result in prohibitive specific impulse losses in a rocket engine; hence the interest in containing the seed through use of centrifugal forces such as proposed for the colloid core or dust-bed nuclear rocket.

The use of carbon seed would limit the bulk exit temperature to approximately 3800°K (specific impulse of approximately 1200 sec), which is not really competitive with the coupling methods discussed previously. The use of tungsten seed would allow the bulk temperature to increase to almost 5900°K, which could result in specific impulses up to 1600 sec. However, use of tungsten requires further investigation of seed containment techniques, and gas temperatures approaching 6000°K require greatly enhanced nozzle cooling techniques.

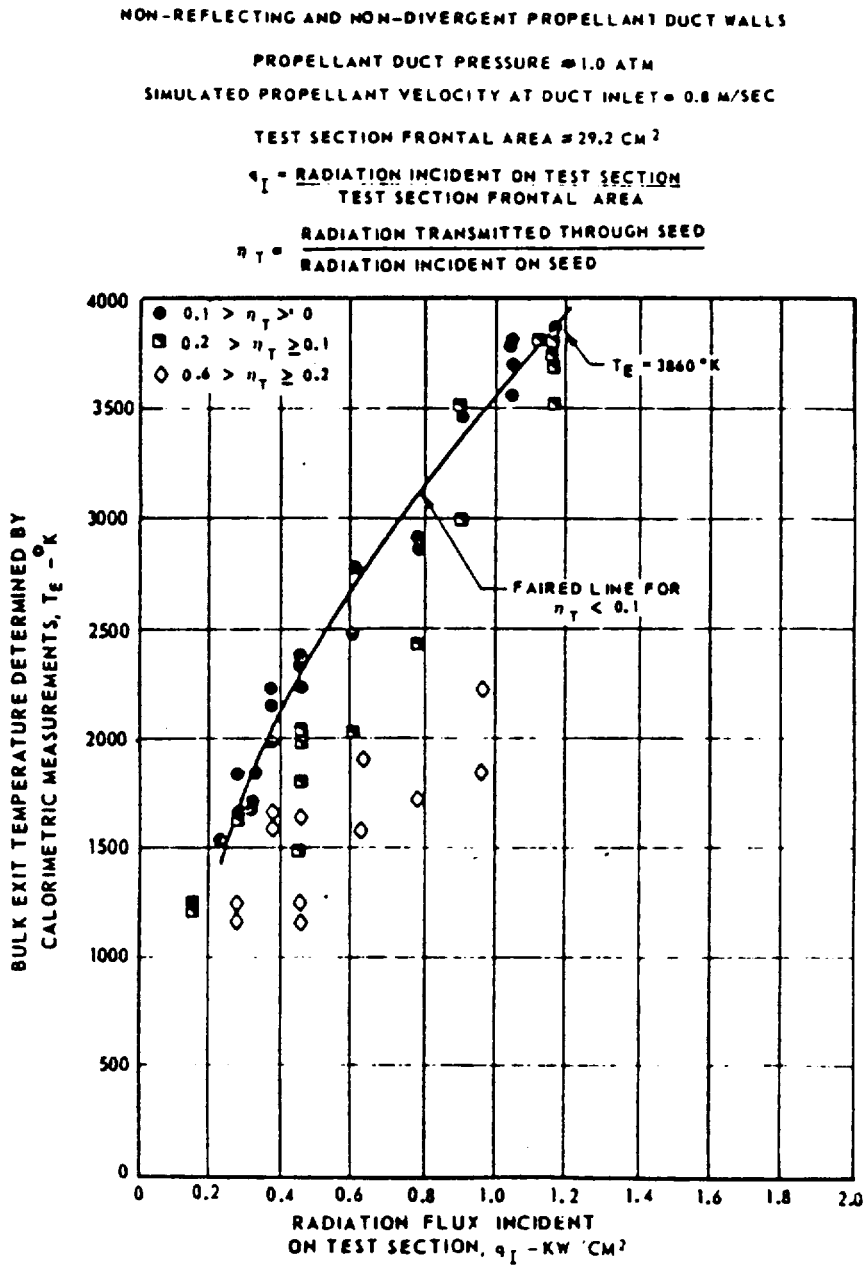

Figure 2.5-8: Results of Simulated Propellant Heating Tests using Carbon Seed Material

REFLECTOR AT OUTER WALL OF PROPELLANT DUCT

SYMBOL	ARGON WEIGHT FLOW, W_A - G/SEC	TUNGSTEN WEIGHT FLOW, W_W - G/SEC
○	2.2	7.0
◑	4.4	7.0
●	8.8	7.0
□	8.8	5.0 AND 5.5

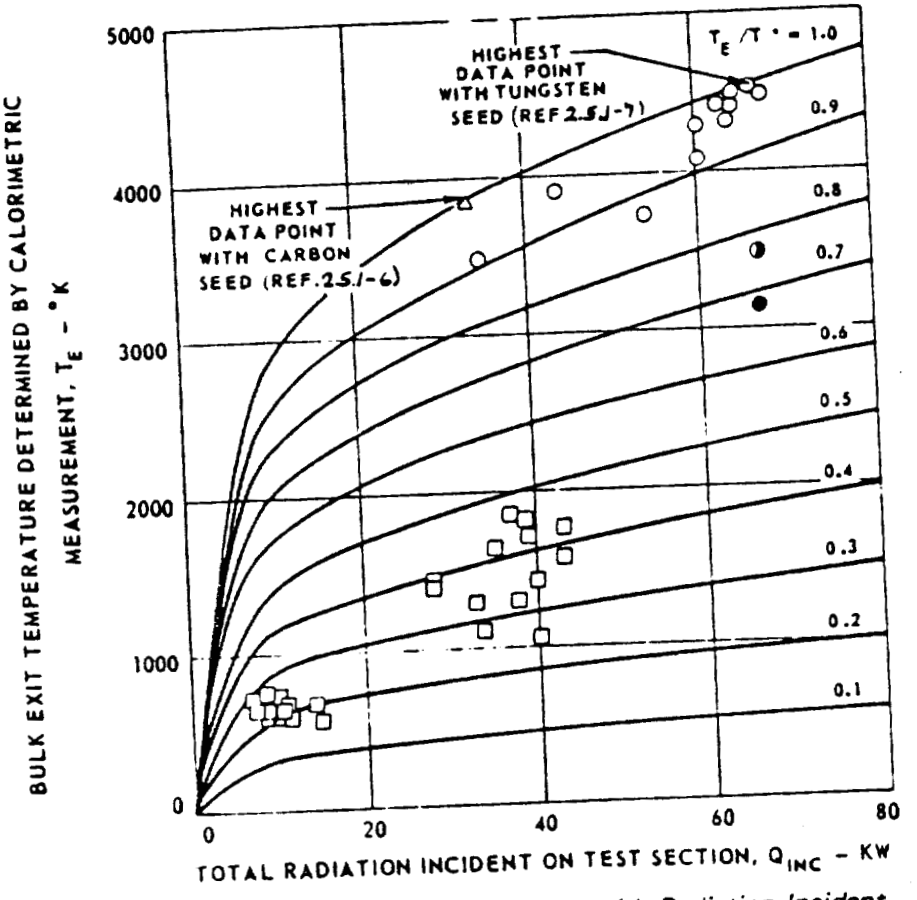

Figure 2.5-9: Variation of Bulk Exit Temperature with Radiation Incident on Test Section for Propellant Heating Tests

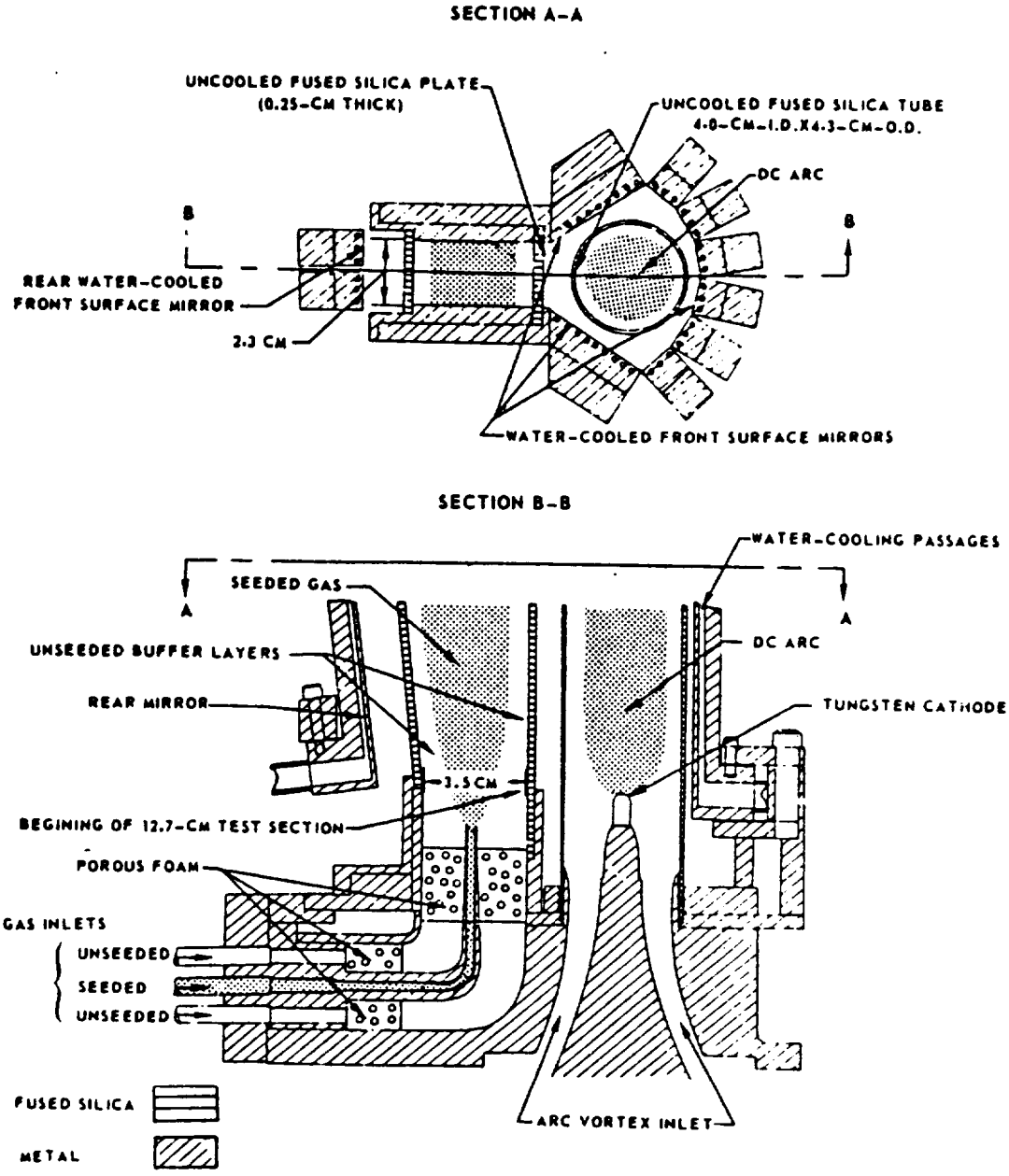

Figure 2.5-10: Propellant Heating Test Configuration

The use of either solid seeding material presents the possibility of contaminating the window and/or the beam collector with a resultant loss of optical efficiency and, in the case of the window, with a possibility of catastrophic failure. Overcoming the condensation of vaporized seed materials on the cool window will require careful design and much testing, but this problem is not thought to be a showstopper at this time.

Solid Heat Exchanger. The laser beam can also be focused onto a solid surface which heats up and conducts to the propellant. This energy coupling concept is well outlined in reference 2-60 and will not be covered in depth here. The solid heat exchanger concept is thought to be capable of temperatures to 3300°K which would deliver specific impulses of 900 to 1000 sec. Specific impulses this high can be achieved with solar or nuclear rockets, which do not require a relatively inefficient laser in the system, and would undoubtedly prove superior. Consequently, there does not appear to be reason to pursue solid heat exchangers to couple laser beams to the rocket propellant.

Laser-Coupling Summary. There appears to be insufficient data available to select the best laser-coupling method. Inverse Bremsstrahlung, molecular resonance, and particulate absorption all seem capable of achieving 1500 to 1600 sec of specific impulse, which happens to be near the limit for regenerative cooling of the engine nozzle at low mass flow rates. Until additional analytical or test results are available, 1500-sec specific impulse should be assumed, and no laser-coupling mechanism should be specified in characterizing laser rocket vehicles.

2.6 Solar Thermal Rocket

Background. The solar thermal rocket concept consists of an optical sunlight concentrator which collects solar energy and focuses it into some form of thermal engine which uses it to pressurize and heat hydrogen propellant/working fluid. The hydrogen working fluid (now quite hot) is then expanded in a conventional rocket nozzle to produce thrust. In various forms and sizes, this concept appears to offer a delivered specific impulse of 800 to 1500 sec. A schematic of the basic solar rocket concept as proposed in reference 2-61 is shown in Figure 2.6-1. This configuration uses two collector "wings" to power one or more thruster units mounted in the conventional thruster location aft of the propellant tankage and payload. In this configuration, thrust and collector pointing are accomplished by rotating the vehicle around the thrust axis to place the mirror axis perpendicular to the Sun's rays and rotating the mirrors about the mirror axis to acquire and track the Sun. Vehicle thrust to weight is a function of the size and specific mass of solar collectors deployed. Reference 2-61 investigated

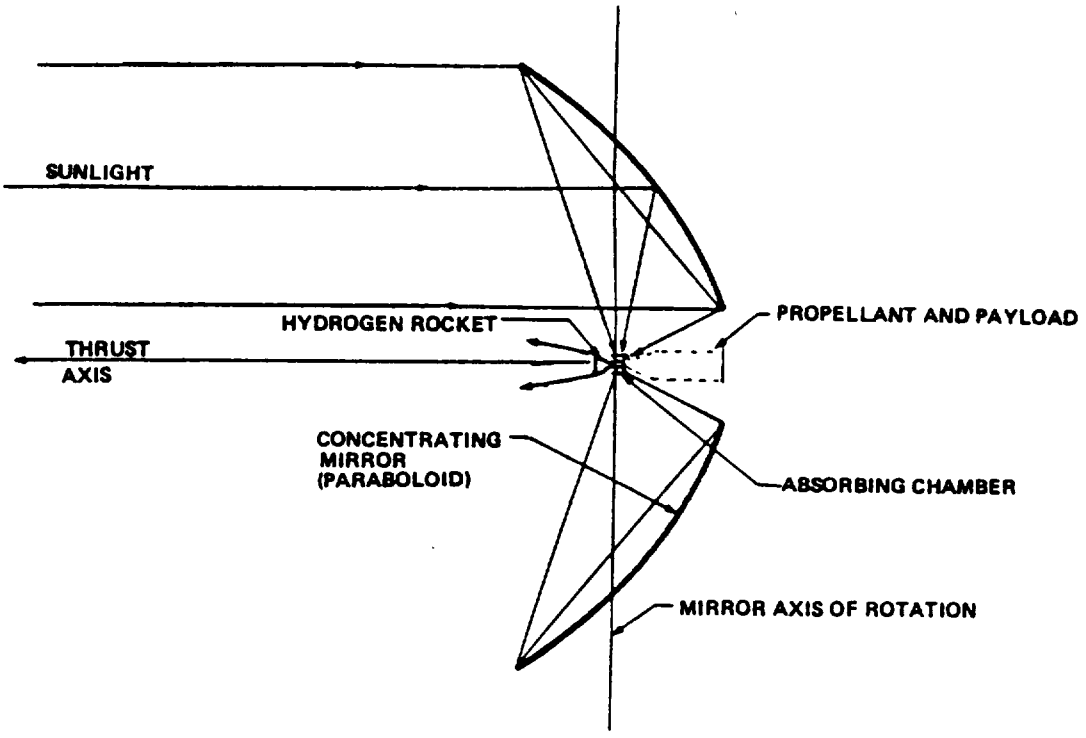

NOTE: THRUST POINTING IS BY COMBINED ROTATION OF MIRRORS ABOUT THE MIRROR AXIS WITH HYDROGEN ROCKET ROTATION ABOUT THE THRUST

Figure 2.6-1: Principal Solar Thermal Rocket Elements

several types of collectors for solar rocket application and selected the nonrigidized, inflatable, off-axis concentrator configuration shown in Figure 2.6-2.

The solar thermodynamic rocket is similar in many ways to the laser thermodynamic rocket characterized in the last section. The principal difference between concepts is the lack of an obvious method to directly couple the Sun's radiant energy to the hydrogen propellant/working fluid. Neither inverse Bremsstrahlung nor molecular resonance appear feasible for coupling solar energy (the former because solar light is not coherent and the latter because it has a broad range of wavelengths). With no apparent means for direct coupling, some form of particulate absorber or solid heat exchanger is necessary, presenting several unique problems that could be avoided in the laser rocket.

The use of a particulate seed absorbent presents a very real possibility of contaminating the optical window and/or the solar collector with a resultant loss of optical efficiency or, in the case of the window, with a

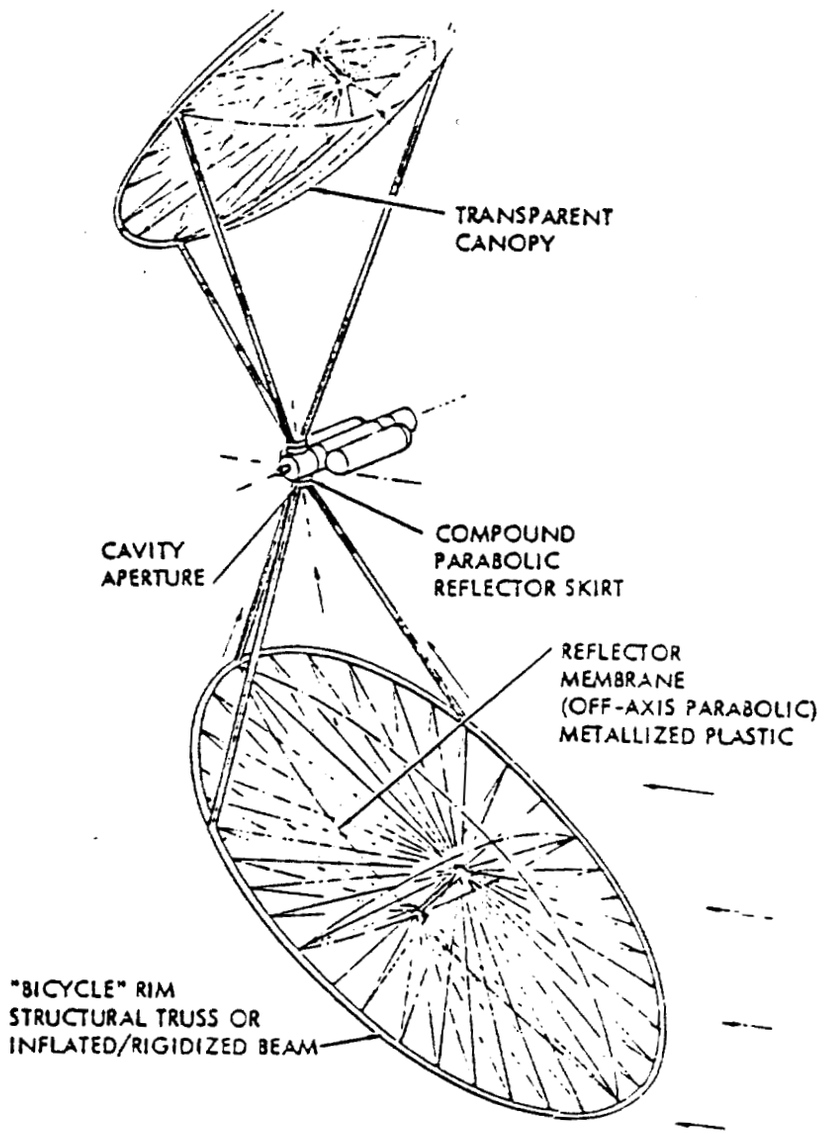

Figure 2.6-2: Non-Rigidized, Inflatable, Off-Axis Concentrator Configuration

possibility of a catastrophic failure. The use of a solid heat exchanger reduces the possibility of condensing vaporized solids on the cooled window surface but also limits the propellant temperature to well below the melting point of the heat exchanger materials.

Absorber Concepts. Five different concepts for transfering energy from the focused solar radiation to the hydrogen propellant are under investigation (ref. 2-62). The most straightforward concept, currently under construction and scheduled for testing next year, is the windowless heat exchanger cavity

shown schematically in Figure 2.6-3. This concept uses a cavity absorber lined with small-diameter coolant tubes which absorb the Sun's energy and transfer it to the hydrogen propellant. Because the tubes must contain the entire working pressure of the engine, they experience considerable stress, which limits their operating temperature. This concept avoids the complication of a cooled window but is limited to chamber temperatures of 2730oK (4910°R) by material limits, giving a delivered specific impulse of about 900 sec.

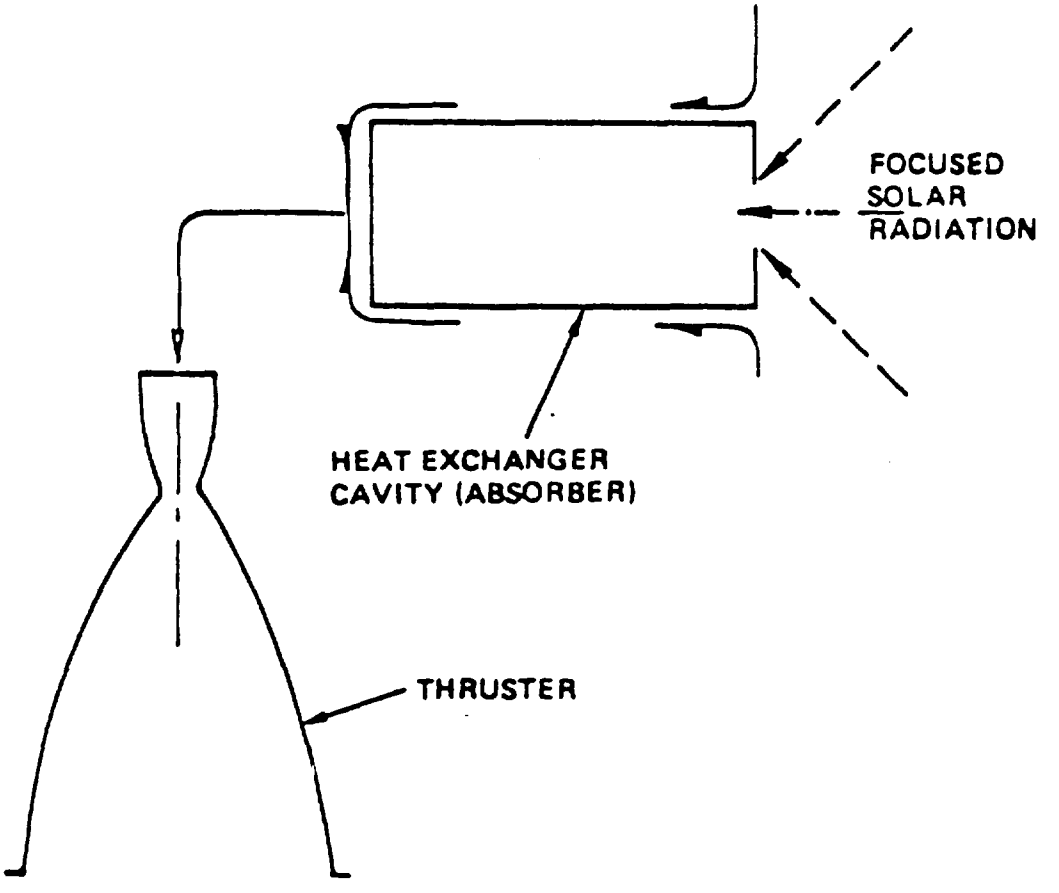

Figure 2.6-3: Windowless Heat Exchanger Cavity

The transpiration cooled liner concept, shown in Figure 2.6-4, adds a solid window to allow the heat exchanger to operate with only thermal loads (which are significant, especially at ignition). This allows a chamber temperature increase to 3780°K (6800°R) for a specific impulse of about 1060 sec.

Further increases in temperature require a absorbent to be subdivided into particulate form to withstand the thermal stresses involved and allow

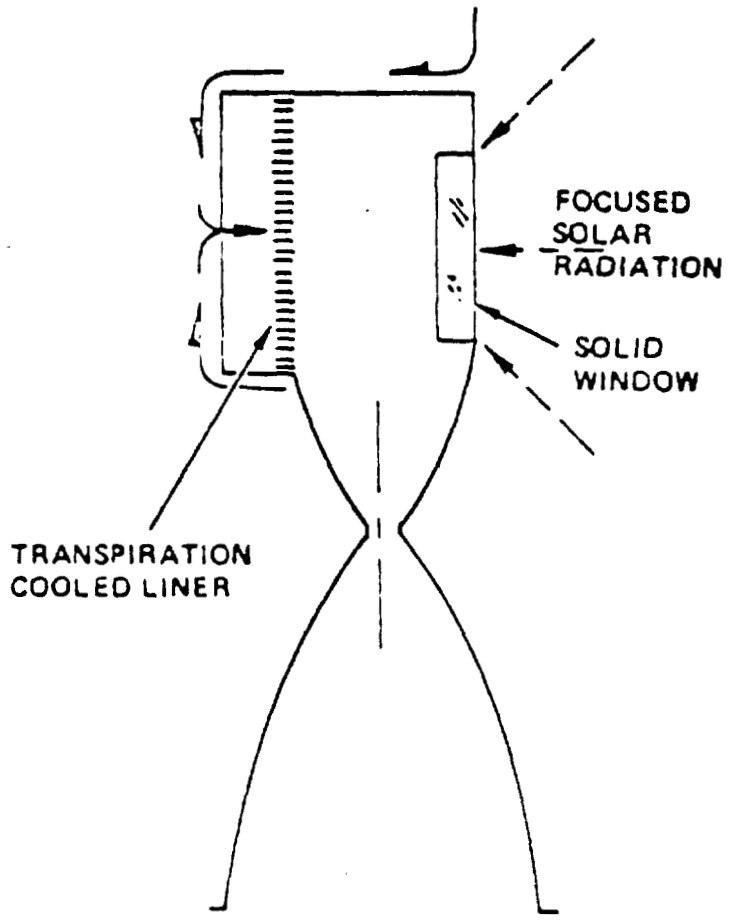

Figure 2.6-4: Windowed Heat Exchanger Cavity

replenishment as the particulates sublime. The simplest direct solar absorption concept is shown in Figure 2.6-5. In this concept the particulate seed is mixed with the hydrogen gas and both are discharged through the nozzle. A gas temperature of 3900°K (7000°R) can be achieved using carbon seed, but the high fraction of carbon by weight in the exhaust products limits the specific impulse to 100 sec or less (Figure 2.6-6).

Two methods of retaining the absorbent seed and thereby increasing the specific impusle have been proposed. The first method, shown in Figure 2.6-7, uses the centrifugal (cyclone) separator principle to retain the seed along the walls of the absorption chamber. Tests of this concept for the colloid-core nuclear reactor (ref. 2-19) showed good seed retention but highlighted problems with window contamination during startup and shutdown sequences. It is highly likely that some form of mechanical shutter would have to be deployed to protect the window from contamination during startup

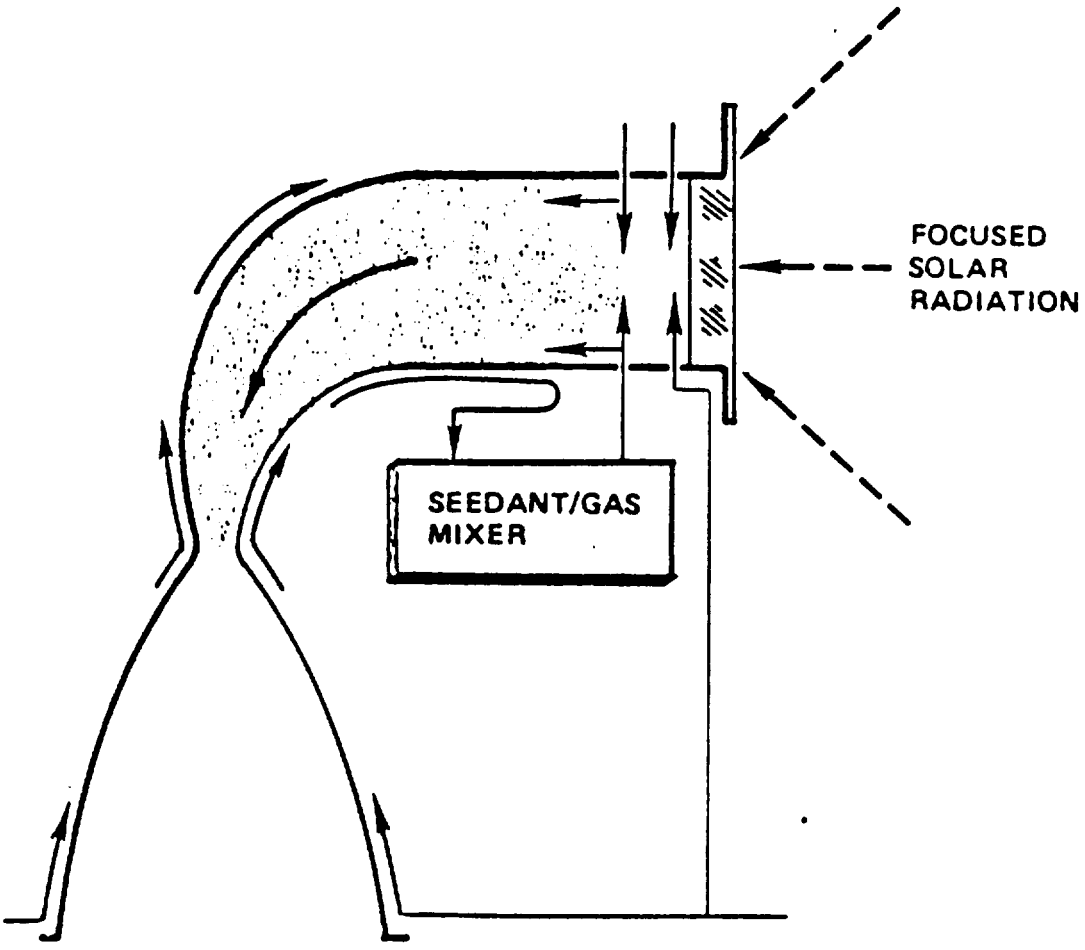

Figure 2.6-5: Windowed Molecular or Particulate Direct-Solar Absorption Concept (Discharged Seed)

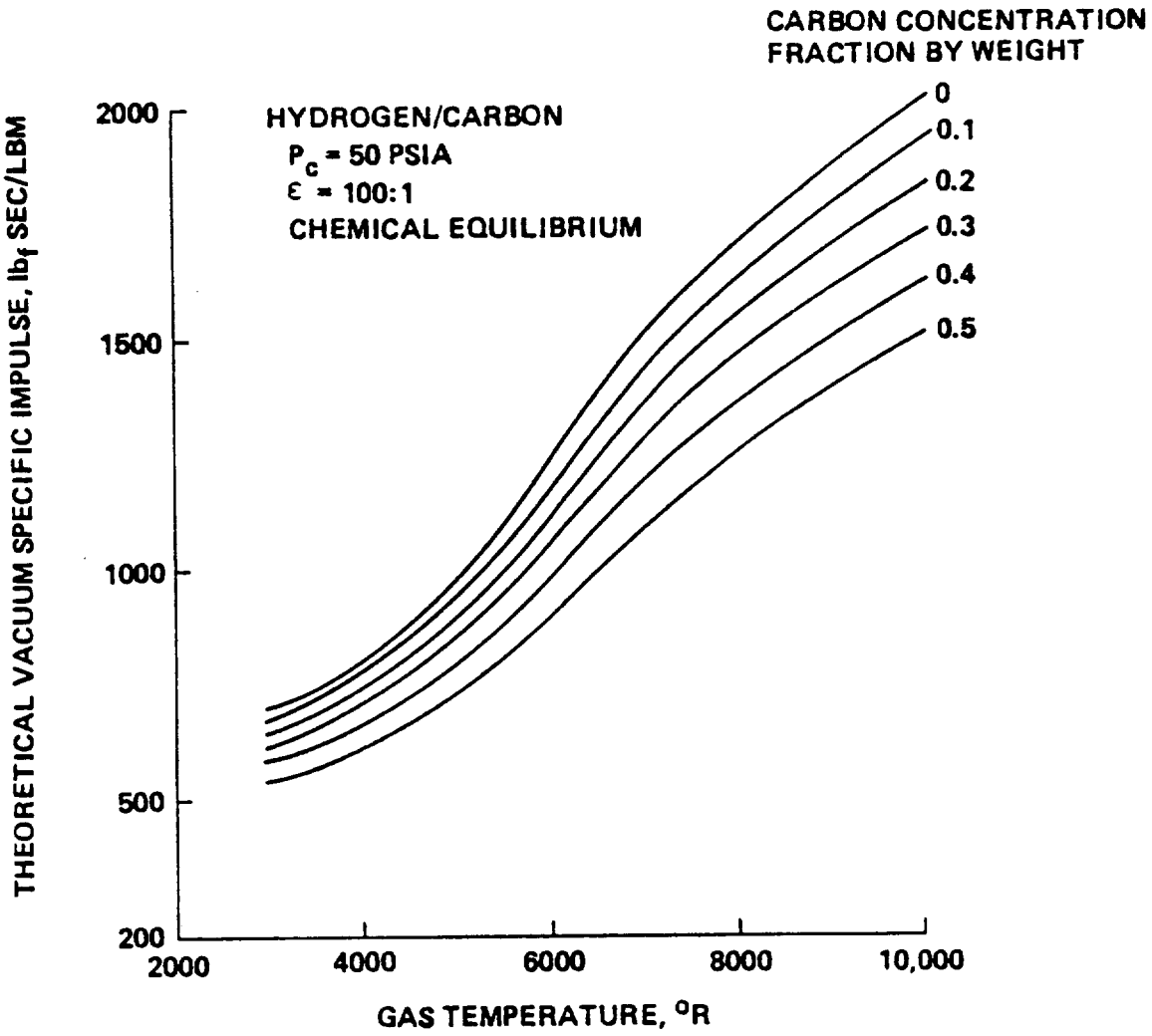

Figure 2.6-6: Theoretical Vacuum Specific Impulse Variation with Carbon Concentration and Gas Hydrogen/Carbon

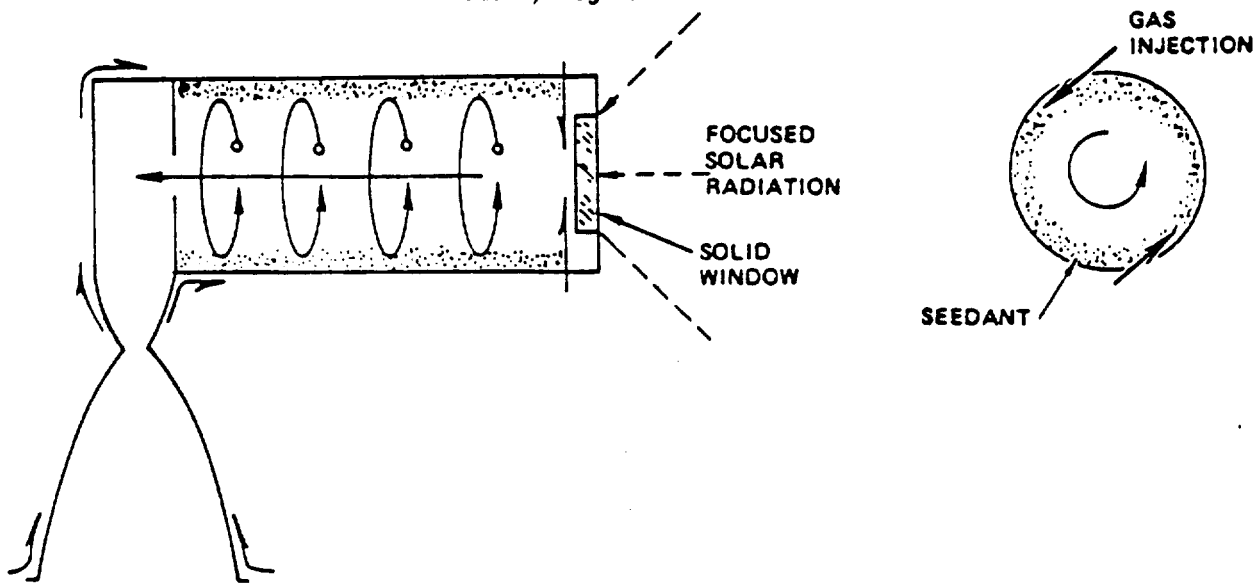

Figure 2.6-7: Windowed Vortex Flow Direct-Solar-Absorption Concept (Retained Seed)

and shutdown. The second method, of retaining the absorbent seed shown in Figure 2.6-8, uses a rotating-bed concept similar to the rotating-bed reactor concept discussed in section 2.2.2. The absorbent seed, in the form of 100 μm

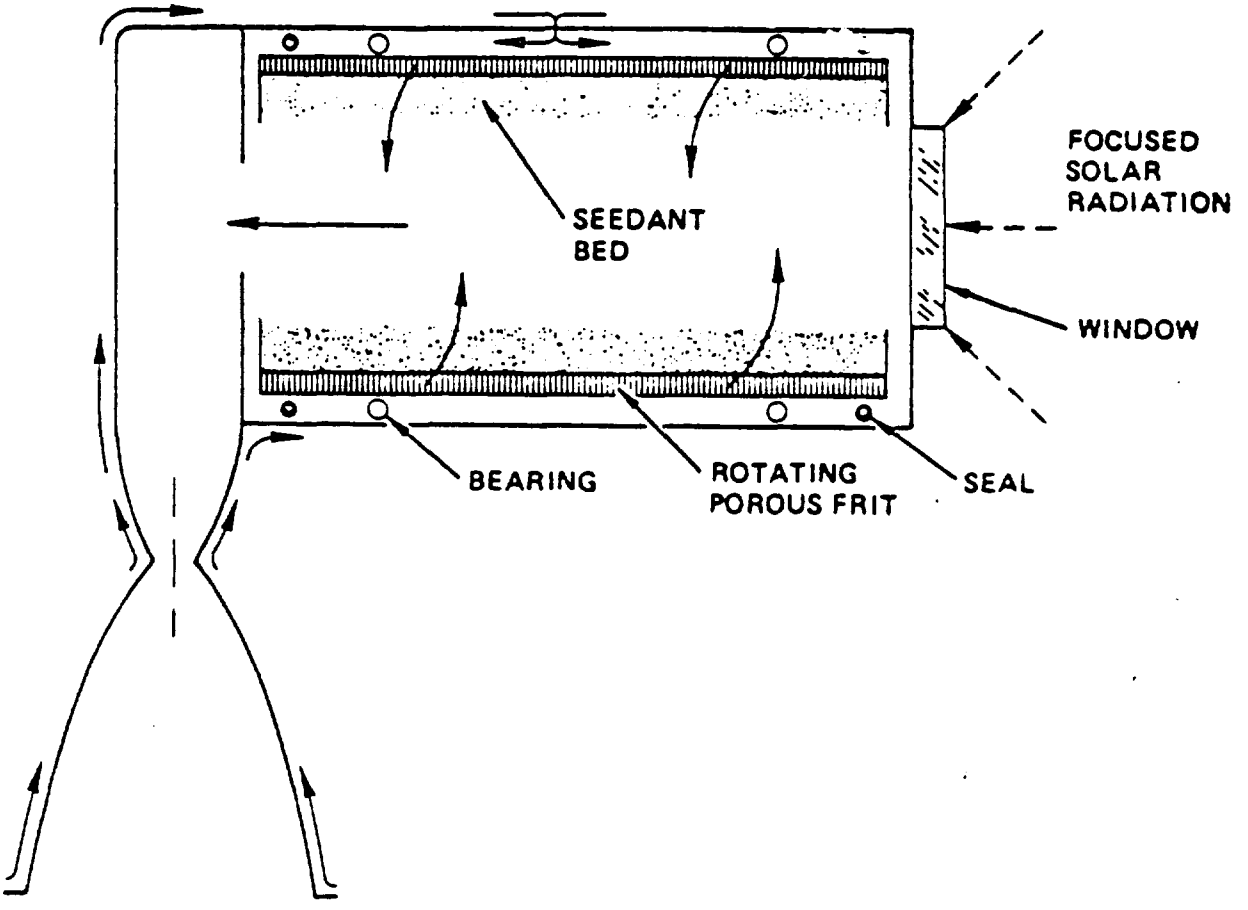

Figure 2.6-8: Rotating Bed Direct-Solar-Absorption Concept (Retained Seed)

particles of tantalum carbide, is retained by centrifugal force in a rotating cylinder to form an annular absorption cavity. The cylinder is made of a porous material backed up by a high-temperature squirrel-cage-type support structure known as a frit. The hydrogen propellant regeneratively cools the rocket nozzle then enters the core chamber where it flows radially inward through the frit at a velocity sufficient to fluidize the bed. The weight of the bed can be adjusted to match any flow rate by varying the r/min of the frit. Finally, the superheated gas flows through the nozzle generating the desired thrust. The rotating-bed concept has also been tested as a possible nuclear rocket core (refs. 2-15 through 2-18), shows excellent particle containment characteristics, and does not suffer from window contamination problems (if the bed is continously kept rotating).

The rotating-bed configuration appears to be the more desirable of the retained absorbent seed concepts. A gas temperature approaching 4000°K (7200°R) should be possible with tantalum carbide seed, which would deliver a specific impulse of around 1100 sec. The primary advantage of retained particulate seed concepts over transpiration cooled liner concepts is the avoidance of hotspots. Imperfections in the concentrator surface would result in an uneven Gaussian distribution of power at the focal plane. This distribution would vary with time and vehicle attitude and would result in local hotspots within the absorption cavity. The constant movement of individual particles in the fluidized rotating bed distributes the energy absorbed throughout the bed and automatically adjusts for uneven power distributions. The transpiration cooled liner, on the other hand, would be designed to operate below its ultimate temperature potential to prevent an occasional hotspot from destroying the porous liner.

Propulsion System Characteristics. Important design criteria used in characterizing solar thermal propulsion systems are:

a. Concentration ratios achievable with a lightweight concentrator configuration

b. Optical, thermal, and structural characteristics of the absorber windows (or choice of windowless designs)

c. Thruster size effects on energy balance and boundary layer losses

d. Nozzle efficiencies (kinetic and frozen flow losses)

The collector concentration ratio is an important design criterion because it determines the absorber adiabatic wall temperature which, in turn, determines the cavity efficiency. The absorber adiabatic wall temperature can be approximated by the relationship:

$$T_{wall} = T_{sun} \times (2.2 \times 10^{-5} \times \gamma_{conc} \times cr)^{1/4}$$

where T_{sun} = 6000°K (Sun's surface temperature)

cr = concentration ratio

η_{conc} = concentrator efficiency

Emissivity assumed = 1.0.

The cavity absorber efficiency can then be approximated by:

$$\eta_{cavity} = 1 - \left(\frac{T_{H2}}{T_{WALL}}\right)^4$$

where T_{H2} = chamber working temperature

T_{wall} = adiabatic wall temperature

The achievable concentration ratio with the nonrigidized, inflatable, off-axis concentrator analyzed in reference 2-61 is 14,328 as shown below.

Collector assumptions:

- Rim angle = ± 45 degree
- Surface error = 1/8 deg standard deviation
- Concentrator efficiency = 0.80
- Reflector cone concentration (theoretical) = 2:1
- Off-axis correction factor = 0.95
- Pointing error correction factor = 0.95
- Window transmission factor = 0.90
- Reflector cone reflective efficiency = 0.90.

Average concentration ratio at inlet to reflector cone = 9800; average concentration ratio at exit of reflector cone = 14,328.

This collector would have a theoretical adiabatic wall temperature of 4250°K and provide a cavity absorber efficiency of 21.5% for a cavity working temperature of 4000°K. The above calculations assume a windowless absorber

design; the relatively inefficient absorption process results when almost 80% of the collected energy is reradiated from the absorption cavity.

Introduction of a well-designed optical window and redesign of the absorption chamber can appreciable increase the cavity efficiency. The transmission and reflection characteristics of a coated quartz window are shown in Figures 2.6-9 and 2.6-10 from reference 2-62. Note, that a properly

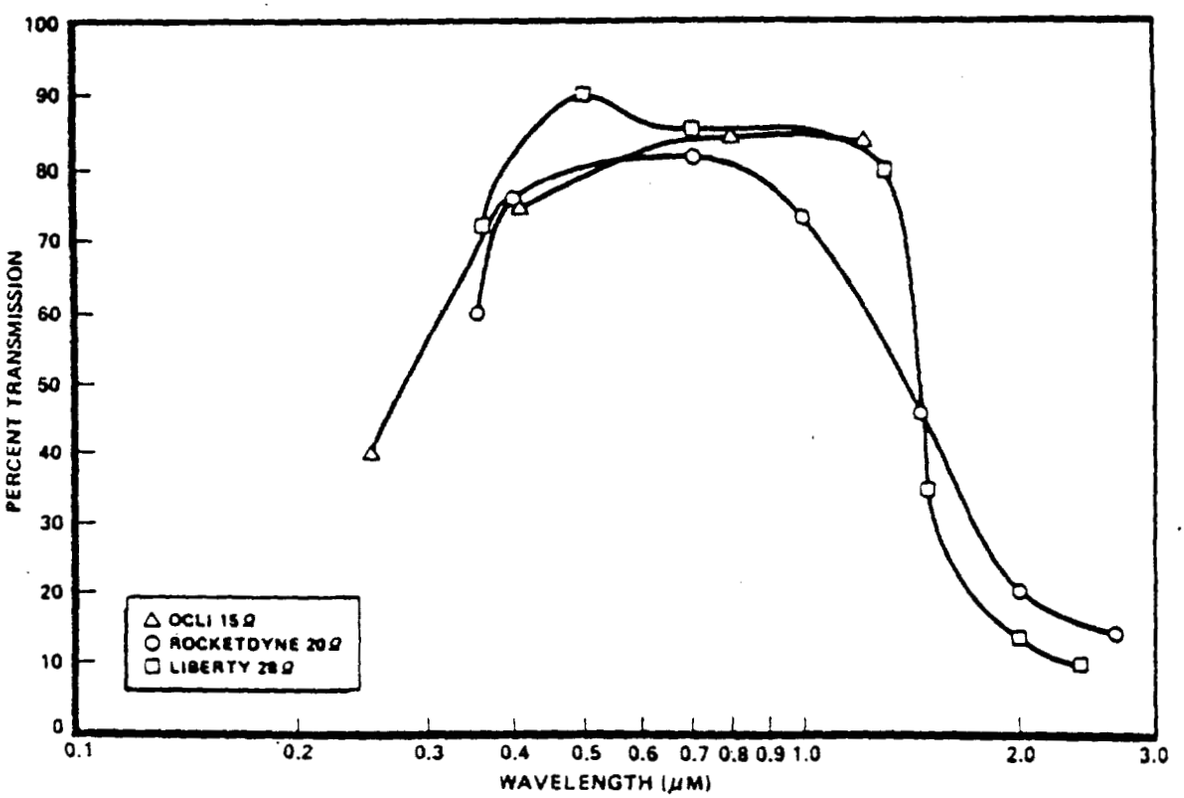

Figure 2.6-9: Solar Rocket Coated-Window Transmission Properties

coated window can transmit 85% to 90% of the solar spectrum and at the same time reflect over 50% of the longwave infrared being reradiated by the cavity. If the window can be adequately cooled (it absorbs almost half of the infrared energy being reradiated), it should then be possible to operate at cavity efficiencies of 60% to 80%, even at temperatures as high as 4000°K. If the cavity is designed with a cooled reflective duct such as shown in Figure 2.6-11, the infrared radiation absorbed by the window can be substantially reduced through increasing the reradiated wavelength, which increases the fraction of energy reflected by the window. This would allow a further increase in propellant temperature and/or less window cooling flow.

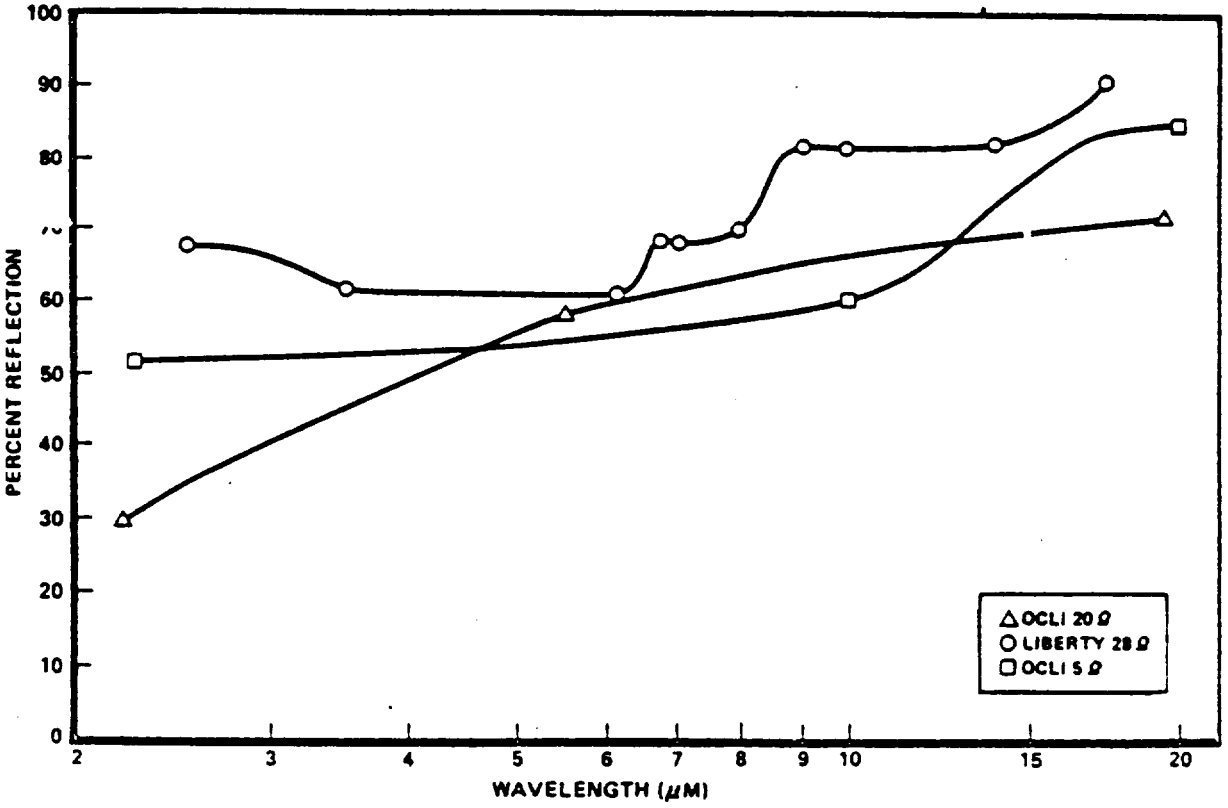

Figure 2.6-10: Solar Rocket Coated-Window Reflection Properties

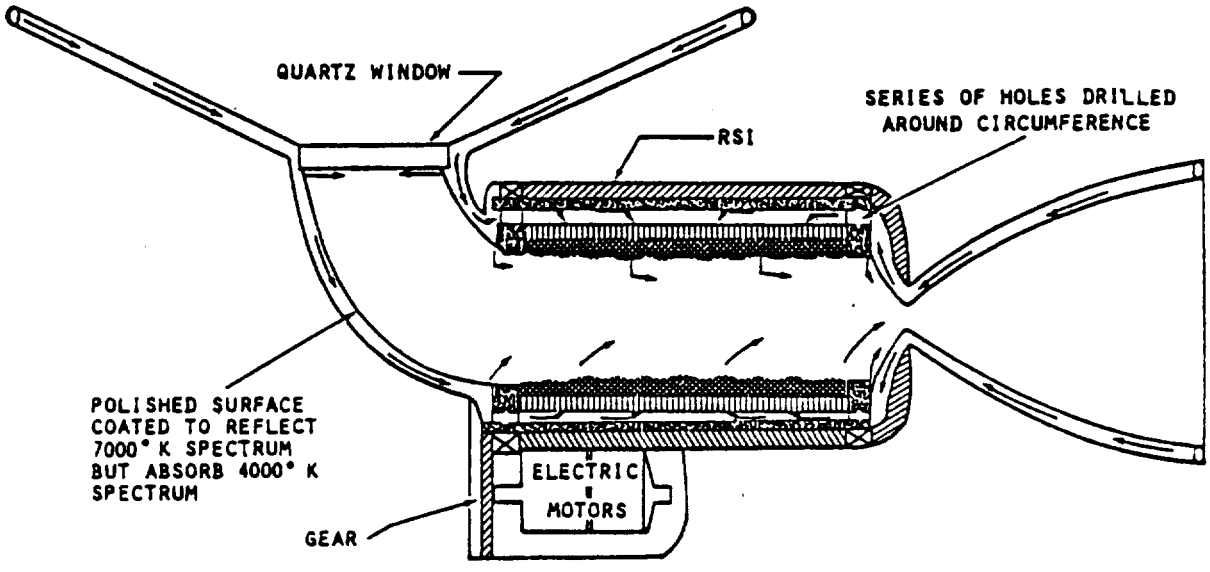

Figure 2.6-11: Rotating-Bed Absorber Solar Rocket

There are three different effects of varying thrust levels. First, for a fixed specific impulse (operating temperature) the diameter of the collector, the window, and the absorber vary with the square root of thrust. Hence, above a certain thrust level, the diameter grows to where it is no longer possible to use a single pane of quartz to contain the chamber pressure. The maximum diameter for a single pane to contain 3 atm is thought to be about 50 cm (20 in), which would limit the maximum collector diameter to around 50m. Multiple pane window designs are certainly practicable, but have more complex structural and cooling characteristics.

Second, the thrust chamber walls must be cooled. Regenerative cooling by the propellant, radiation cooling, or cooling via an auxiliary thermal control system would be required. The mass of an auxiliary thermal control system would be virtually prohibitive; therefore, regenerative cooling would be desirable. Because propellant mass flow varies directly with thrust level while the area to be regeneratively cooled varies as the square root of thrust, cooling problems can be alleviated by increasing the design thrust level and providing more mass flow per unit area.

Finally, there is the effect of boundary layer losses and frozen flow. Increasing the thrust level tends to increase the amount of mass flow outside the boundary layer and improves the overall efficiency. Chamber temperatures as high as 4000°K result in substantial molecular dissociation and the energy involved can be frozen into the flow if rapid expansion in the nozzle does not allow time for recombination and release of the energy of dissociation. This process is somewhat size dependent because a larger nozzle results in slow rates of expansion and more time for recombination. As a result, an optimum solar rocket would tend to be a compromise between various design criteria with the tendency being to make it as large as practicable.

3.0 ELECTRIC ROCKET CONCEPTS

Electrically powered rockets are power limited and not energy limited like the thermodynamic rockets discussed in the last section. Electric rockets use sunlight, nuclear reactors, or power beams as power sources and use electromagnetic forces to accelerate charged propellant molecules to much higher velocities than can be attained with most thermal processes (fusion being a possible exception). However, thruster concepts using electrostatic or electromagnetic forces instead of fluid dynamic forces must operate at extremely low densities to enable the electric forces to predominate, and this implies very low thrust densities and commensurate low thrust levels relative to the thermodydnamic rockets.

Electric rockets consist of a power source, often a power processor which converts raw power into the form required by the thruster, and a thruster which electrically accelerates the propellant. A listing of possible electric-powered rocket concepts is shown in Figure 3.0-1. The possible power sources and thruster types are addressed separately along with the subsection in which they are discussed.

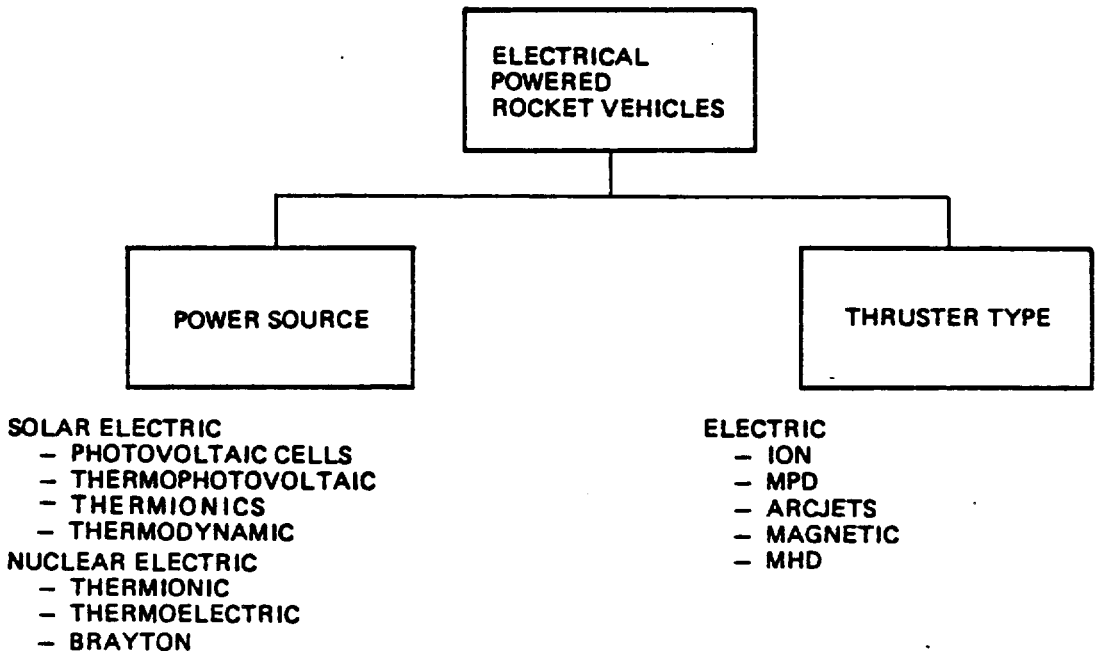

Figure 3.0-1: Morphology of Electric-Powered Rocket Concepts

Basic functional concepts, technology status, characterization data, and recommendations for further analyses are developed in the following discussions of each propulsion system option. The first two subsections discuss power sources and the remaining subsections discuss thruster types.

3.1 Solar Electric Power Sources

3.1.1 Solar Photovoltaic (SPV) Powerplant

Background. Electrical power can be obtained by solar illumination of solar cells. The power conversion efficiency is generally low (10% to 15%), but the cells annd their supporting structure can be made thin, lightweight, and deployable in large areas to obtain the desired power. Contemporary technology is represented by NASA-inspired designs for SEPS: Beginning-of-life (BOL) power is 32 kW, mass is 420 kg, and area is 180 m^2 (values approximate). Being solid-state electronic devices, the efficiency of solar cells will be degraded by any transit of the radiation belts; typically 50% for LEO to GEO electric propulsion missions.

The SEPS technology uses 8-mil cells with 4-mil coverslips (required for thermal control and radiation protection). The obvious approach to improve technology is to reduce the thicknesses of cells, coverslips, and supporting substrates and to develop higher efficiency cells.

Because 2-mil silicon solar cells are presently being developed, we believe their use in lightweight array technology can be established by 1990 at present activity levels. A specific weight characterization for this technology is shown in Figure 3.1-1, which also indicates the expected improvement with respect to SEPS technology. The ultimate specific weight of a 2-mil cell array is about 2.6 kg/kW but requires on-orbit assembly with very light structure. These levels of performance are minimum risk and are recommended for use in the remainder of this study.

Issues. The central issues for solar electric propulsion are the demonstrations of a radiation-resistant 2-mil solar cell array and a prototype lightweight PPU for Earth orbit applications. Predicted specific weights are not essential to SEP utility, but increases in propulsion mass directly detract from payload performance. A more important issue is degradation of

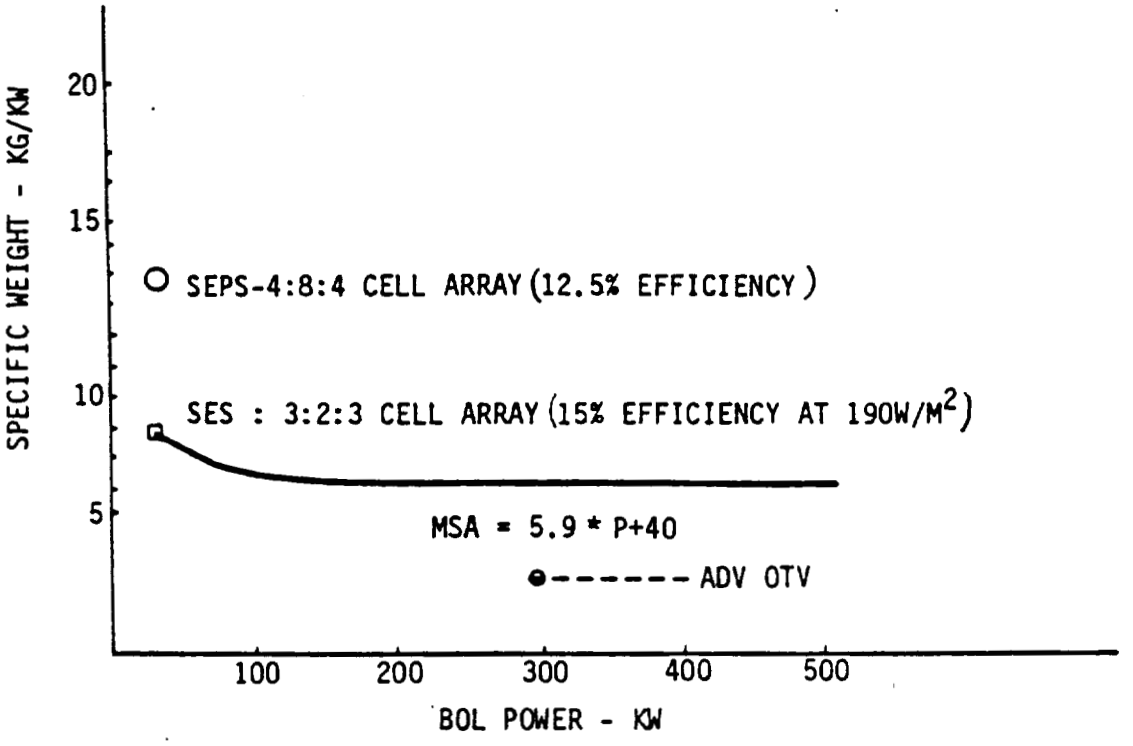

Figure 3.1-1: Solar Array Specific Mass

the solar array caused by high radiation levels in the Van Allen belts. This issue is presently under intensive study.

Recommendation. Because of the advanced state of technology of SEP components, the solar electric ion rocket should be the benchmark against which all electric advanced concepts are compared.

3.1.2 Solar Thermophotovoltaic (TPV) Powerplant

The solar thermophotovoltaic powerplant is similar to the baseline solar photovoltaic concept except that a highly concentrating optical system is used to focus the Sun's energy into an absorption cavity/reradiator which then illuminates a small area of solar cells. This system provides several advantages over the conventional solar photovoltaic array. First, by carefully sizing the optics and the cavity, the reradiator can be designed to operate at temperatures of 2000°K to 2500°K, which provides a blackbody spectrum matched to the peak absorption wavelength of silicon solar cells (see Figure 3.1-2. In addition, by using edge junction silicon cells over a highly reflective substrate, the cells can be made to reflect back into the

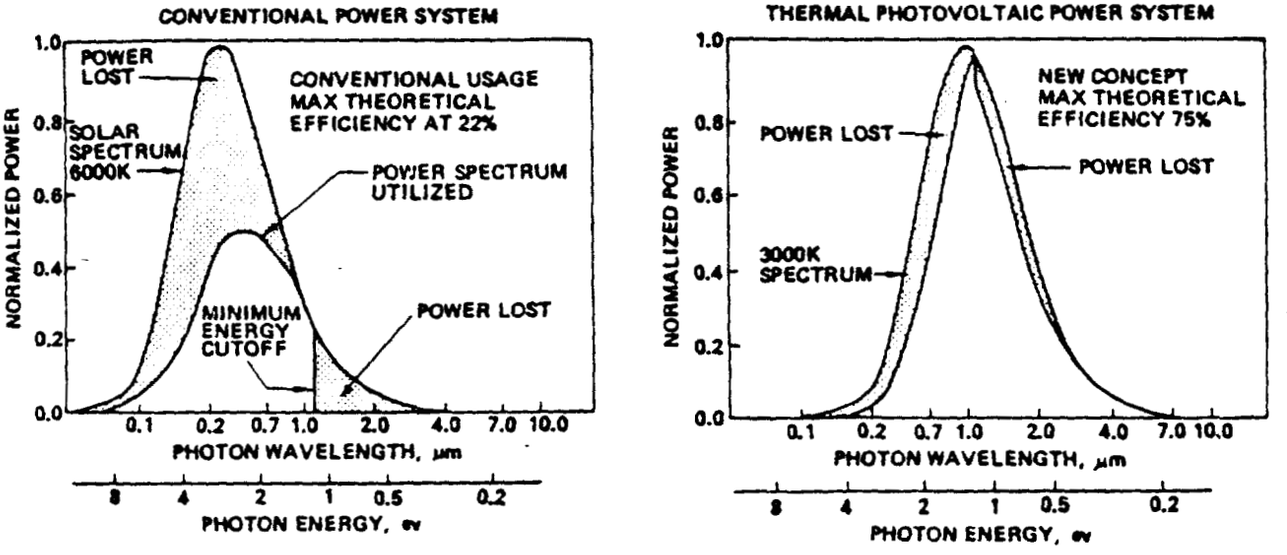

- NEW TPV CONCEPT TRIPLES MAX THEORETICAL EFFICIENCY

Figure 3.1-2: Spectral Matching with TPV Silicon Cells

reradiator most of those photons with insufficient energy to generate an electron. This concept has about triple the maximum theoretical efficiency relative to a conventional solar cell array and in preliminary testing has achieved efficiencies on the order to 40%.

Further advantages of TPV over conventional solar arrays are reduced cost and lack of radiation degradation. TPV operates at very high concentration ratios which reduce the amount of very expensive solar cells to a few square meters. Basically TPV reduces cost by using a large area of cheap radiators instead of a large area of expensive solar cells. Because the solar cells are enclosed within a matrix of heat pipes and radiators, they are protected from radiation effects and do not degrade during transits of the Van Allen belt like a conventional solar array. A schematic of the TPV concept is shown in Figure 3.1-3.

Issues. The foreseeable issues that may influence the practicality of the TPV rocket concepts are:

a. Efficiency attainable with mass production solar cells

b. Powerplant specific mass, kg/kW

c. Degradation of the transmissivity and/or optical reflectivity of the structural films comprising the pressurized optics due to contamination by thruster effluents (principally Mo from the ion thruster grids), space radiation, or natural aging

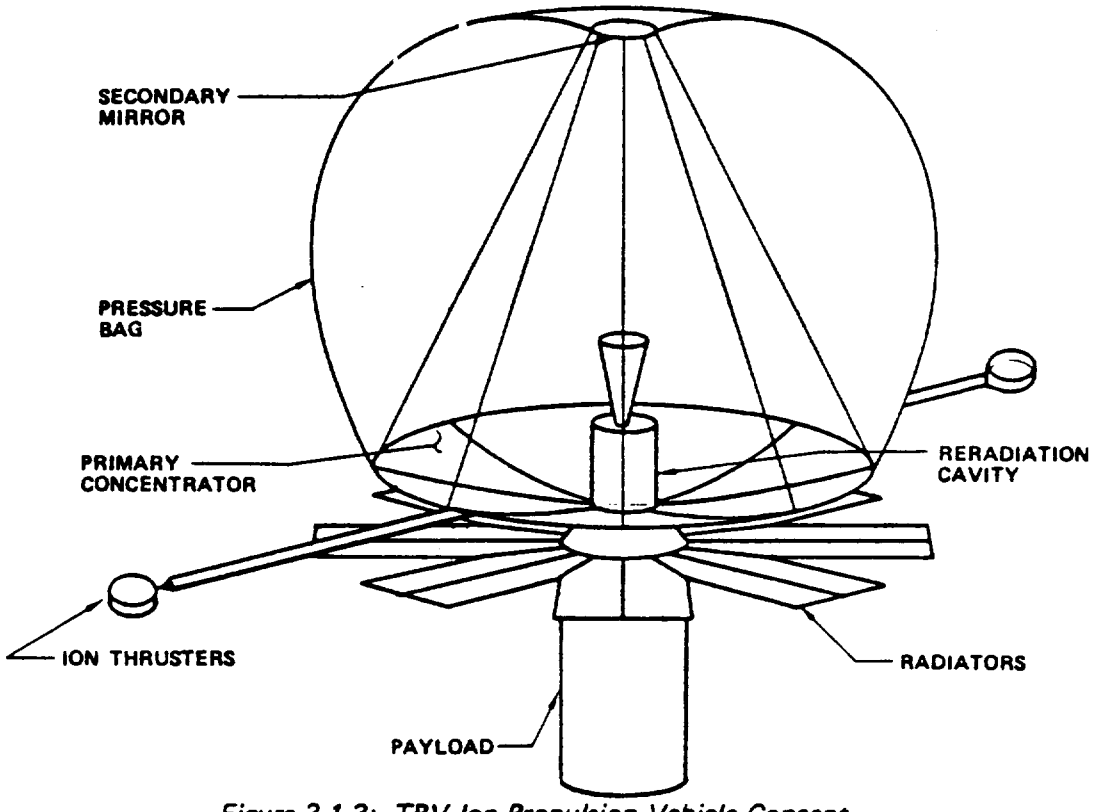

Figure 3.1-3: TPV-Ion Propulsion Vehicle Concept

d. Attitude control: center-of-gravity control, nonpropulsive (off-Sun) operations, TVC precision

e. STS packaging, deployment and checkout of pressure-stabilized optics, radiators, and propulsion units

f. Thermal control: optimized radiator/coolant system, off-Sun structural heating, cavity optimization

g. Refurbishment intrinsic life of powerplant cavity

The main concentrating surface is conceived to be "silvered" plastic film, pressure stabilized in the desired curvature by a transparent plastic bag. This technology has been demonstrated (ref. 2-61).

An overall configuration option is shown in Figure 3.1-4. Although no system level characterization data have been developed (including a structural concept suitable for propulsion and STS storage), preliminary studies of pressure-stabilized optical concentrators indicate a 100-kW TPS may have a specific weight as low as 5 to 15 kg/kW. Considering that, in this concept, the solar cells are almost immune to space radiation, it may be highly competitive with conventional solar cell arrays.

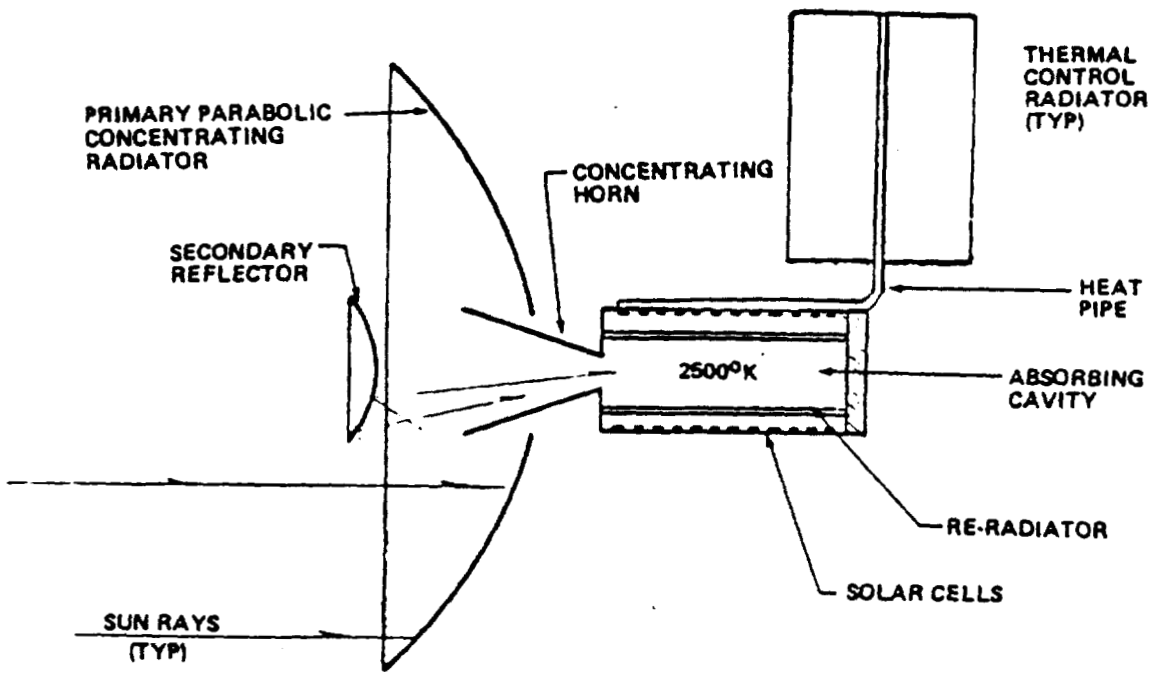

Figure 3.1-4: Key Elements of the Thermo Photovoltaic Concentrator

Recommendation. The technology for concentrators, photocell components, and other system elements appears to be sufficiently well defined to allow an engineering design synthesis.

3.1.3 Solar Thermoionic (STI) Powerplant

A solar thermoionic power system combine the lightweight inflatable solar concentrator discussed in section 3.1.2 with the theoretically lightweight and long-lived thermoionic converters discussed below.

In a thermionic diode, electrons are produced at the emitter (cathode) due to its elevated temperature, and travel to the lower temperature collector (anode). The circuit is completed through the load. Several processes within

the emitter-collector gap tend to reduce the efficiency of power generation from the applied thermal energy. For example, the electrons in the gap tend to repel those being produced at the emitter.

The diodes are mounted in the wall of the solar cavity absorber; the emitters are heated by the concentrated solar energy. By allowing the collectors to dissipate waste heat to space, the temperature differential required for operation is produced. Fins are added to the collectors to improve cooling. This concept, however, was not pursued because it does not appear to be competitive with the TPV power system.

3.2 Nuclear Electric Power Systems (NEPS)

Nuclear electric power systems use nuclear reactors for power sources, changing thermal energy to electrical energy by direct thermionic conversion or by a thermodynamic conversion method such as the Brayton cycle. A typical vehicle concept is shown in Figure 3.2-1 from reference 3-1. Its characteristic features are the elongated configuration to minimize nuclear shielding and the large cylindrical radiator required to reject waste heat. It can be sized to be shuttle compatible, especially if the payload will fit inside the heat exchanger body.

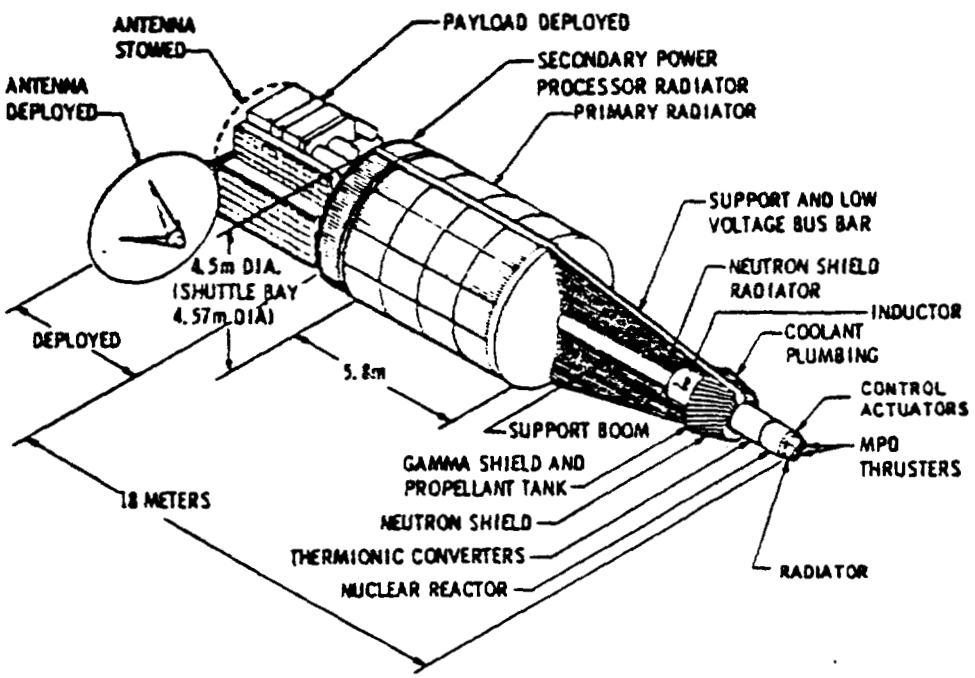

Figure 3.2-1: Nep Spacecraft MPD Thrusters (Deployed Configuration)

3.2.1 Nuclear Thermionic (NTI) Power Sources

This concept consists of a fission reactor, cooled by heat pipes which convect the fission energy to the hot junction of an out-of-core cesium thermionic power converter. The cold junction is also cooled by heat pipes, the waste heat being rejected by a space radiator. Contemporary technology for each of these elements appears adequate for useful conversion efficiency but the material limitations have delayed development of this concept.

Typically, an emitter temperature of 1650°K (2510°F) and a collector temperature of 900°K (1160°F) are required to achieve a specific weight of 16.05 kg/kW at 400 kW_e (JPL 715-40, March 15, 1980). JPL has had this concept under detailed study for over 5 years, including design and test of high-temperature heat pipes and thermionic converters. The JPL thermionic converter design is shown in Figure 3.2-2. It is conceptually a simple, passive structure; however, it has been unable to withstand the severe temperature changes during startup and shutdown and the significant thermal gradients during nominal operation--not a simple design problem.

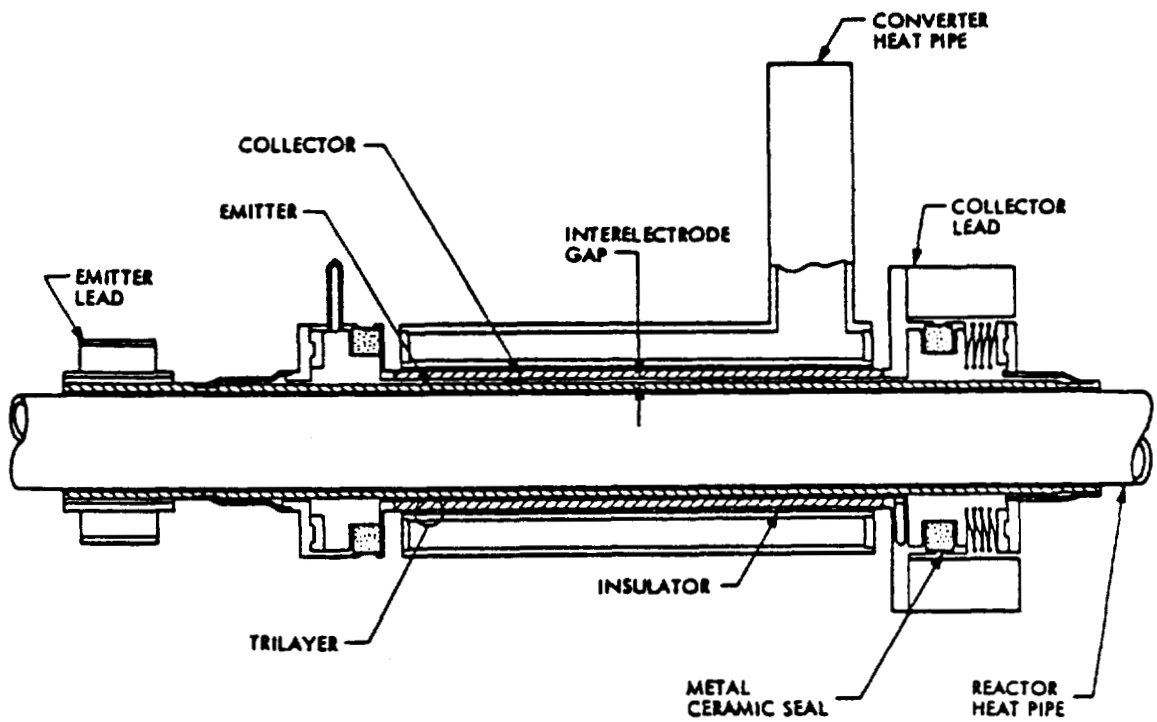

Figure 3.2-2: Thermionic Converter Concept

The thermal system for the nuclear thermionic concept is also conceptually simple, as shown in Figure 3.2-3, particularly in comparison with the Brayton cycle (see section 3.2.3). A warmup heater system (not shown) will be required to melt the lithium working fluid prior to system startup.

Issues. Foreseeable issues with respect to the achievable performance of this concept are:

a. Specific weight and lifetime of the nuclear thermionic power source

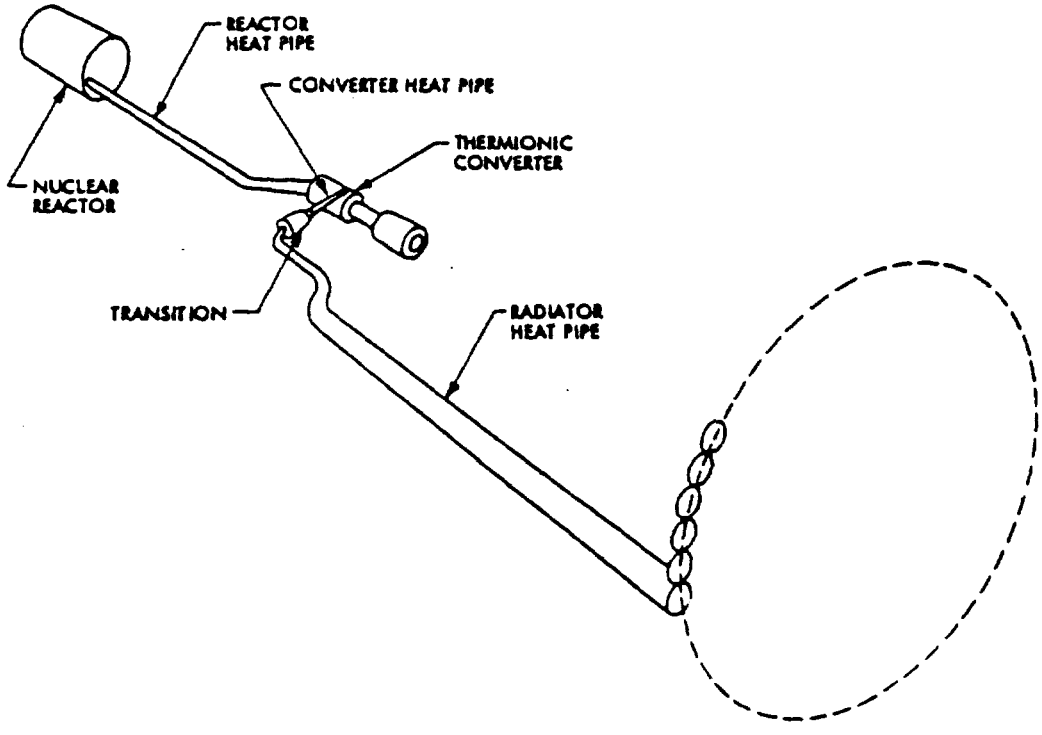

Figure 3.2-3: Thermionic System Heat-Rejection Concept

b. Applicability to Earth-orbit missions and space-based operations

3.2.2 Nuclear Thermoelectric (NTE) Power Sources

Background. Extensive studies of NTE power sources are currently being conducted under the auspices of the space reactor (SPAR) Electric Power Supply Program by the Los Alamos Scientific Laboratory for the Department of Energy and other agencies.

The current program is aimed at NTE power sources of 10 to 100 kW_e (electrical) with specific masses of 16 to 17 kg/kW at 100 kW_e. The current funding level is approximately $2M per year at Los Alamos with some additional monies going to General Electric Valley Forge for thermoelectric converter technology development.

System Description. The NTE concept is quite similar to the NTI powerplant discussed in a previous section. The NTE power source consists of a heat-pipe-cooled fast-spectrum reactor with a thermoelectric power conversion system. The general features of this system are identical to those discussed

in Figure 3.2-1. The reactor design features a beryllium reflector and a laminated core configuration with sheets of molybdenum (Mo) interspersed between layers of uranium dioxide (UO_2). Reactor heat is transfered by the molybdenum sheets from the UO_2 to an array of Mo/Na heat pipes. The heat is then transported by the heat pipes around a lithium hydride (LiH) neutron shield to a ring of high power density thermoelectric converters constructed of modified silicon-germanium (SiGe) alloys. Conversion takes place over a temperature difference from 1375K to 775K with a projected efficiency of 8.5% to 9%. Residual heat (90%) is rejected by a network of radiators constructed using titanium heat pipes.

The key element which differentiates the NTE power source from the NTI power source discussed in the previous section is the thermoelectric conversion elements. These elements are built into cylindrical modules surrounding the core heat pipes as shown in Figure 3.2-4. In this unit, six

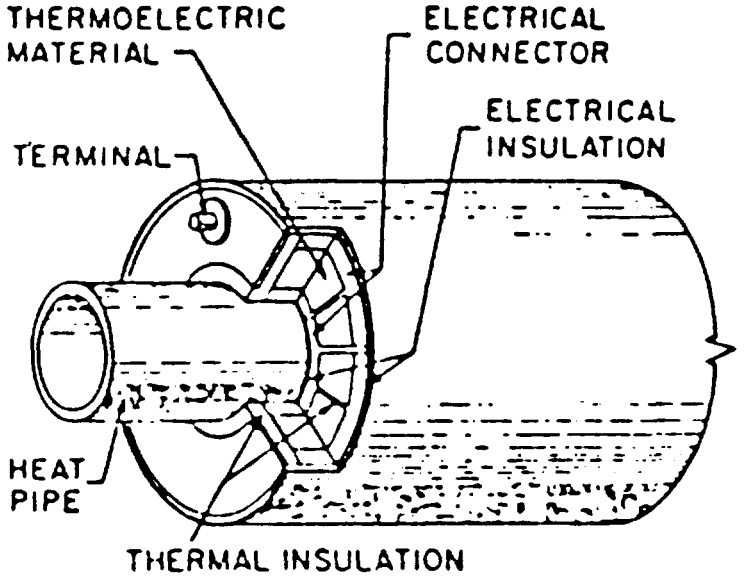

Figure 3.2-4: High-Power-Density Thermoelectric Module

SiGe n-p couples are positioned circumferentially around the core heat pipe in a series configuration that yields approximately 1V output under normal operating conditions. A power module is formed by placing these ring units adjacent to each other along the pipe, the number of units being determined by the output voltage required. For power levels of 100 kW_e, a voltage of 100V to 150V dc is desirable to minimize transmission losses.

Not shown in Figure 3.2-4 is the system to remove waste heat from the thermoelectric modules. In the SPAR program this is done by an annular heat pipe which encloses the entire module, as shown in Figure 3.2-5. The coupling heat pipes serve to change the geometry from cylindrical to square in order to couple better thermally with the radiator stringer pipes. The radiator stringers are arranged so that several cool each thermoelectric module.

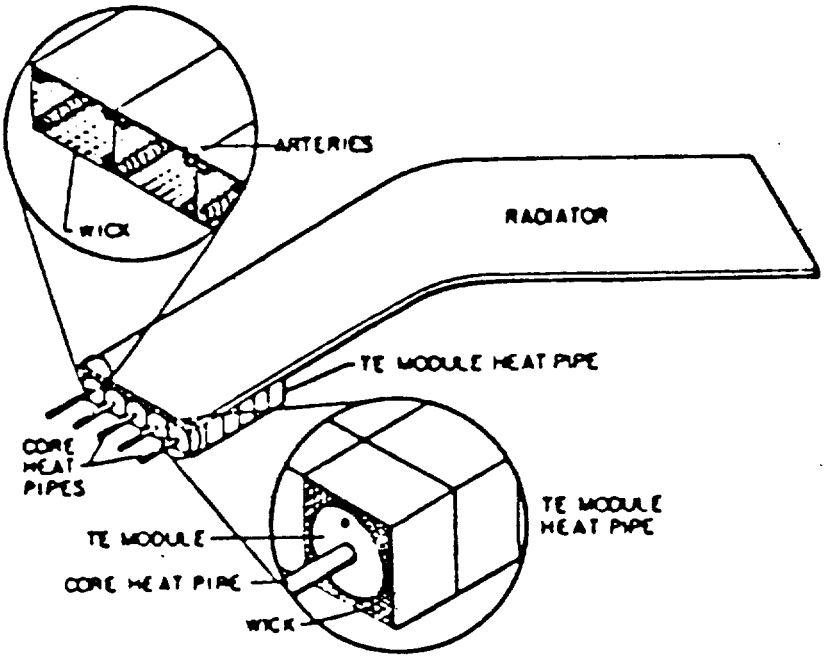

Figure 3.2-5: Radiator Segments

The proposed radiator design shown in Figure 3.2-5 has five thermoelectric modules grouped together to form a basic panel segment. The coupling heat pipes of adjacent thermoelectric modules are thermally connected so that if one of the radiator stringer heat pipes fails, its heat load will be shared by nearby stringers. The stringer heat pipes will be made of titanium to take advantage of its relatively low density combined with its high temperature capability.

Issues. The NTE power source is currently the furthest developed of the three competing NEPS units. At the time this is written (1981), it probably has the best chance of attaining hardware status. The principal issue remaining with respect to attaining satisfactory performance is the inservice lifetimes of the thermoelectric units, especially the lifetimes of dissimilar material junctions.

3.2.3 Nuclear Brayton Cycle (NBC)

Background. This concept uses a nuclear reactor to provide source energy for a helium Brayton cycle which, in turn, drives a generator to produce electrical power. The nuclear Brayton power cycle is shown considerably simplified in Figure 3.2-6 (from ref. 3-2). Control circuits and instrumentation, valves and expansion joints, fluid storage, and thermal control radiators for lubricants, the alternator, avionics, and electrical actuators have been omitted. This concept has all the complexity of a commercial nuclear power plant. Its principal attraction appears to be that, except for thhe limits to turbine inlet temperature (TIT), a complete design technology exists. Because TIT has a major influence on efficiency and specific weight, any uncertainty in it raises a risk issue, and an all-up system demonstration (including lifetime testing) will be required to reduce this risk. Predicted specific weights for the power system are shown in Figure 3.2-7. Existing technology for TIT is 1325°K (1925°F), giving a specific mass of 35 kg/kW$_e$ (100 kW$_e$), according to a contemporary design analysis. SNAP experience suggests that a large growth allowance be considered to assess risk.

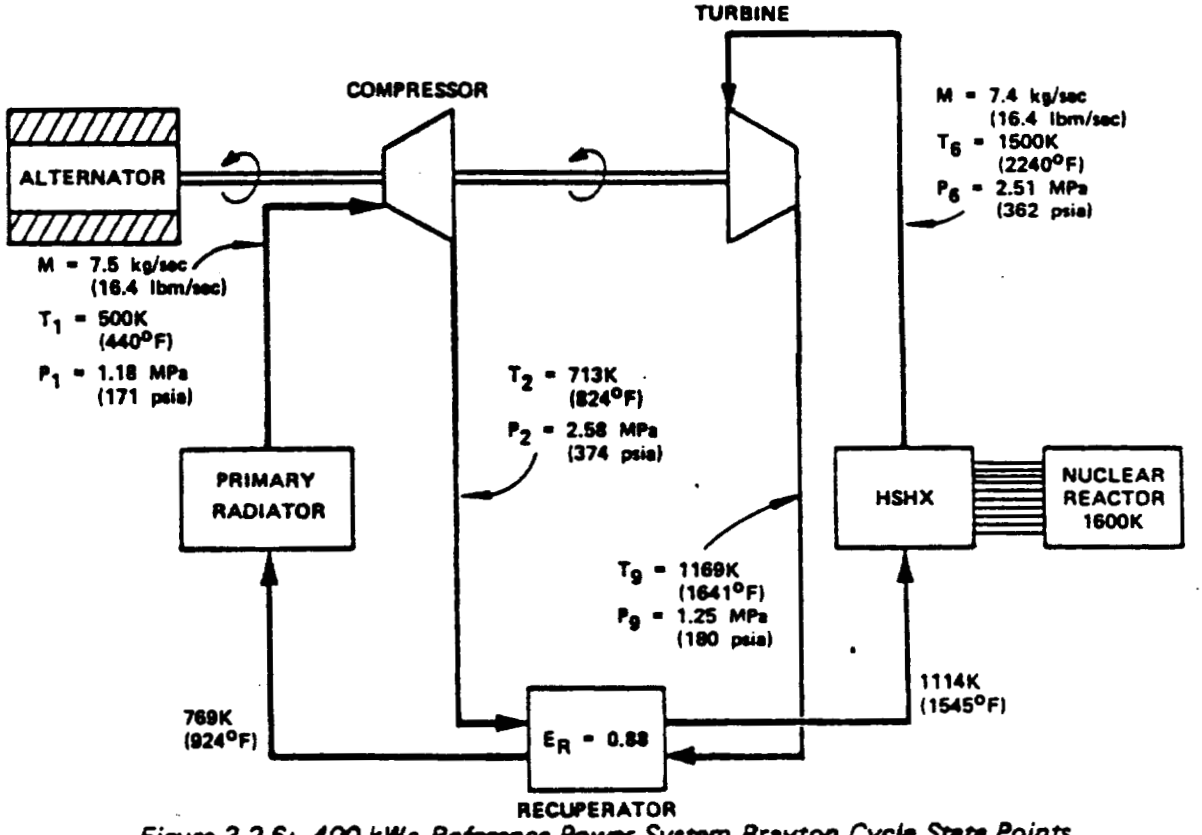

Figure 3.2-6: 400-kWe Reference Power System Brayton Cycle State Points

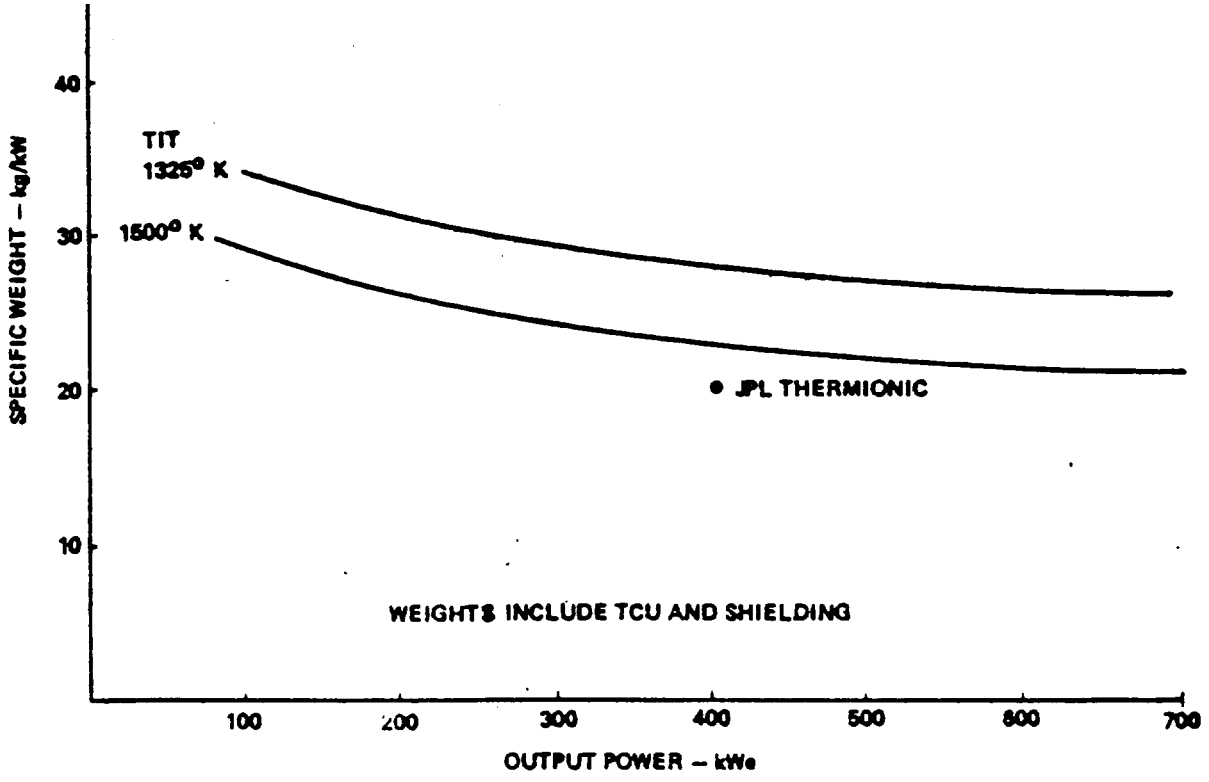

Figure 3.2-7: Predicted Specific Weight for Nuclear Brayton Cycle Power Systems

Issues. Foreseeable issues that may influence the practicality of the nuclear Brayton cycle power sources are:

a. Turbine inlet temperature limit: achievable lifetime, efficiency, and specific weight versus TIT

b. Life cycle performance demonstration: test scale (full size or subscale), orbital or ground, test evaluation of radioactive hardware

c. Interaction of propellant plume with neutron and gamma radiation from unshielded areas of the reactor

d. Component level design feasibility in adverse thermal and nuclear radiation environments

e. Flight safety: STS abort, ground handling requirements, deployment and checkout, on-orbit aborts and rescue.

3.3 Electrostatic Ion Thrusters

Ion thrusters produce thrust by electrostatic acceleration of ions extracted from an electron bombardment ionization chamber. They have been under experimental development for over 20 years: within the last 3, a nearly complete design theory has matured.

3.3.1 Advanced Ion Thruster

For the purposes of this study, a 50-cm argon ion thruster is developed to illustrate this maturity of technology and theory. The 50-cm size is arbitrary but has been chosen by NASA LeRC for technology development by Hughes Research Lab (HRL) and Xerox Electrical Optical Systems (XEOS). For thrusters larger than the 30-cm SEP type (which uses a divergent magnetic field for preliminary electron confinement), a multipole containment field is required to improve beam uniformity (flatness) and to maintain primary electron confinement in the larger plasma volume. Both the HRL and XEOS concepts feature multiple magnetic poles. A Boeing multipole concept is shown in Figure 3.3-1 (some components have been omitted for clarity).

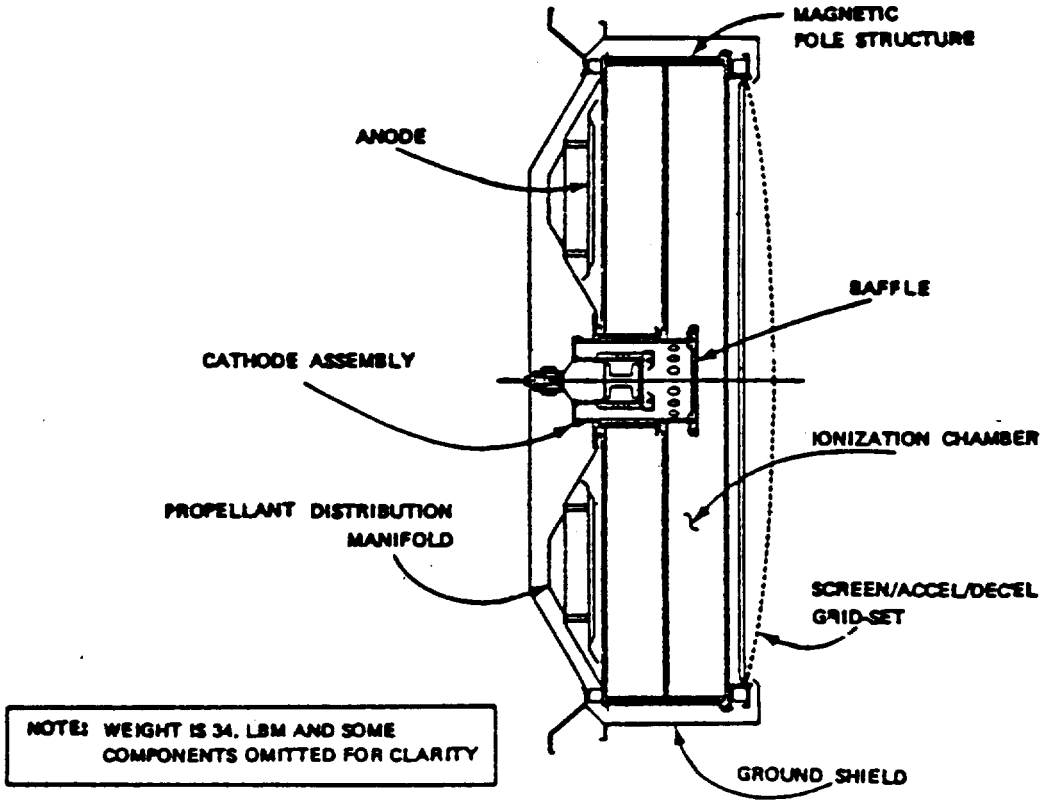

Figure 3.3-1: 50 cm Ion Thruster

Its design features are:

a. Dished screen and accelerator grids for thermoelastic stability
b. Single cathode - SEPS technology
c. Upstream anode
d. Quick disconnects for easy refurbishment
e. Low energy recombination surfaces isolated by magnetic fields (multipoles)

Thruster characterization requires an analytical description of each phenomenon which comprises the overall behavior. Collectively, these descriptions (equations) become a mathematical model to determine thrust (F), specific impulse (I_s), efficiency (η_T), lifetime (L), and power (P_t). This had been accomplished for the following:

a. Production of singly charged ions (discharged process)
b. Production of doubly charged ions
c. Efflux of uncharged propellant atoms
d. Ion extraction including optical transmissivity
e. Ion interception by the screen grid
f. Ion acceleration

Predictions of beam divergence and optical transmissivity depend on empirical data as does the sputtering yield for molybdenum (required for screen grid erosion calculations).

The process of theoretical characterization is shown in Figure 3.3-2. Its unique features include a first-order theory relating emission current (J_e) with the optical transmissivity (X) of the grids, the discharge voltage (V_d), the neutral mass efflux (Mo), and the beam current (J_b). This relationship is shown below. Except for variations in the optical transmissivity, the discharge process is independent of the process of ion acceleration, a circumstance which admits a simple characterization model.

$$J_e = Cn * (1/X) * (1/(V_d - V_r)) * (1/\dot{N}_o) * J_b$$

Where C_n is a constant and $\dot{N}_o$ the neutral efflux. If experimental data exist, the constant C_n can be determined, If J_e is prespecified by some

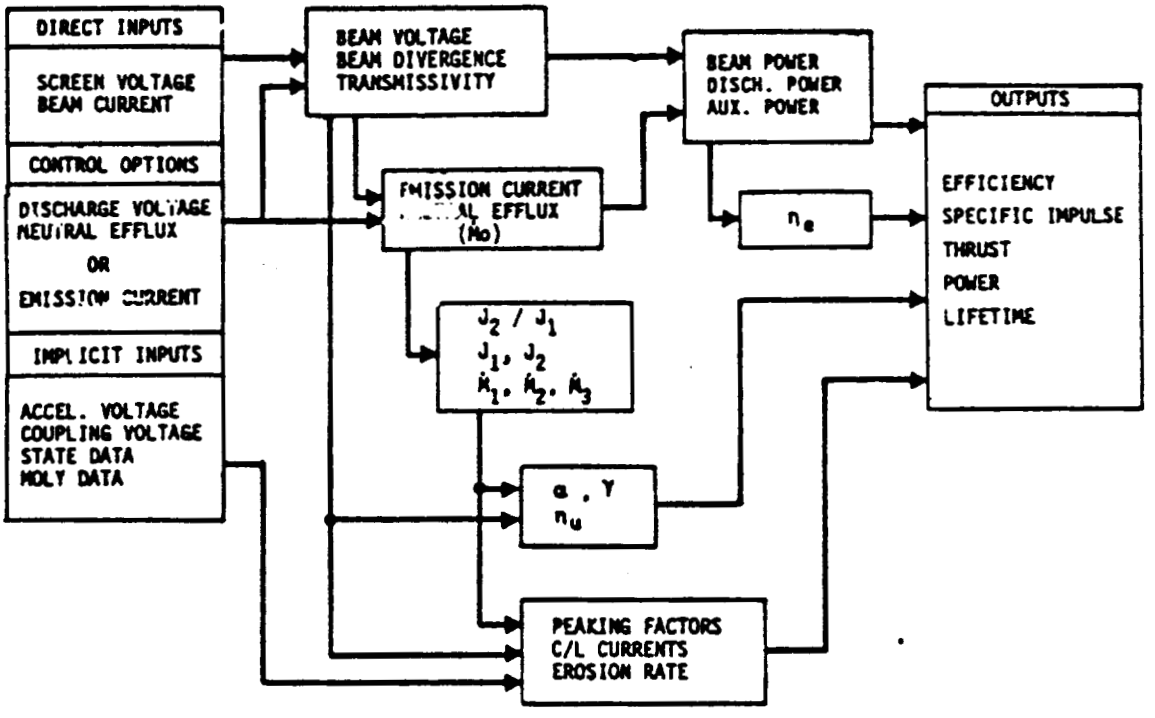

Figure 3.3-2: J-Thruster Characterization Program Block Diagram

control algorithm, the discharge law can be solved for the required neutral efflux.

The first step in thruster characterization is to establish a reasonable discharge control option by calculating thruster efficiency as a function of neutral efflux (proportional to ionization chamber pressure). These data are shown in Figure 3.3-3 and illustrate discharge optimization via trading utilization efficiency against electrical efficiency. The dashed line is the optimum control path but control by constant neutral efflux is simpler and practically as efficient. It is used for subsequent data.

Because changing the screen voltage (to change I_{sp}) changes the electrical efficiency, the optimum neutral efflux should also change, as shown in Figure 3.3-4. This is not a straightforward option: reducing neutral efflux tends to shorten thruster lifetime as indicated in Figure 3.3-5.

Having picked a control scheme, a thruster operating map can be determined as shown in Figure 3.3-6. Operation below about 1000V will require triple-grid optics. These data illustrate that a given size ion thruster can operate over a wide range of power and I_{sp}.

Note the above data are based on J-type thruster optics which are nonoptimum for argon. Optimized optics for argon should have either an

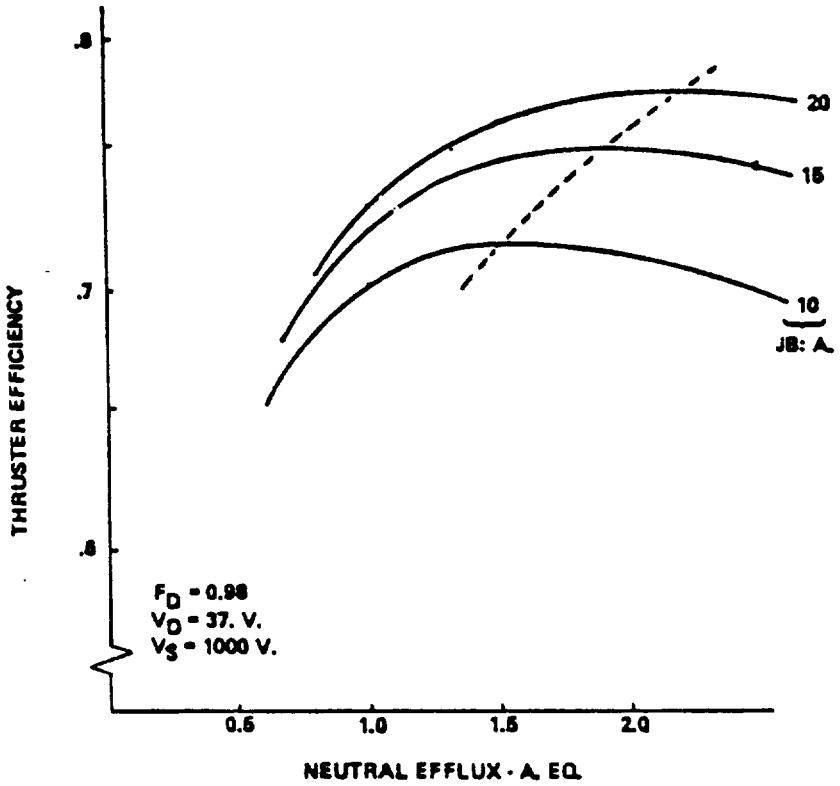

Figure 3.3-3: Discharge Control Optimization 50-cm Argon Ion Thruster

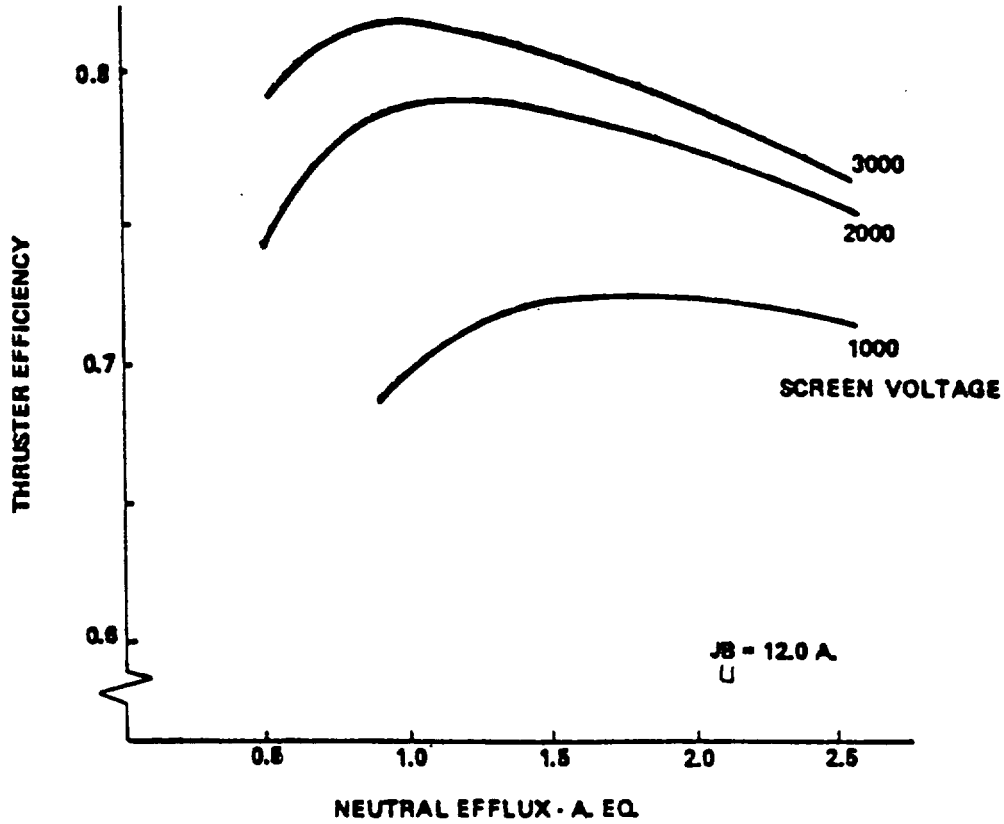

Figure 3.3-4: Discharge Optimization = 50-cm Argon Ion Thruster

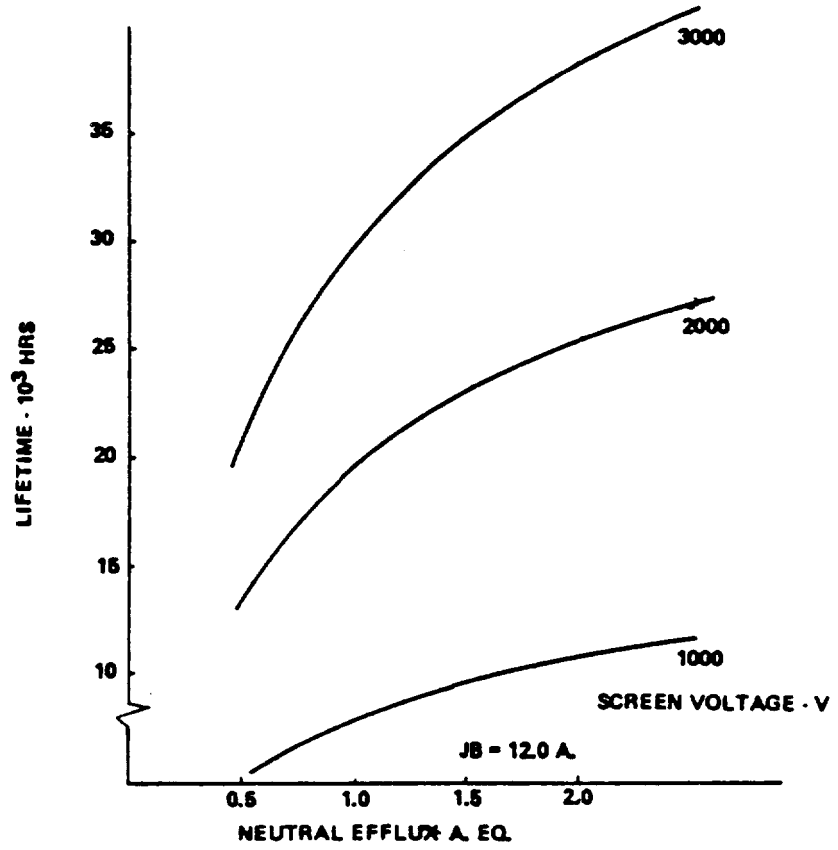

Figure 3.3-5: Life Trends for a 50-cm Argon Thruster

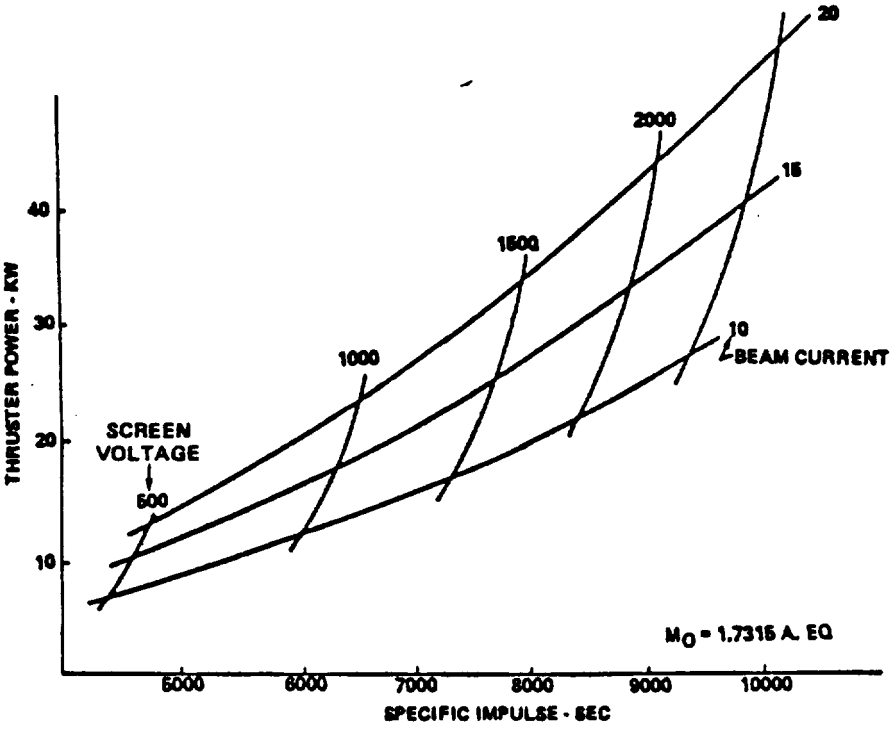

Figure 3.3-6: 50-cm Argon Ion Thruster Power Requirement

increased grid gap (reducing beam divergence and neutral efflux) or reduced size accelerator grid holes (increasing transmissivity and also reducing neutral efflux), or some best combination of these. This analysis is straightforward but infringes on the practicalities of thermoelastic structural design, which is a separate subject.

The operating map data also include efficiency and thrust, shown separately in Figure 3.3-7 for clarity.

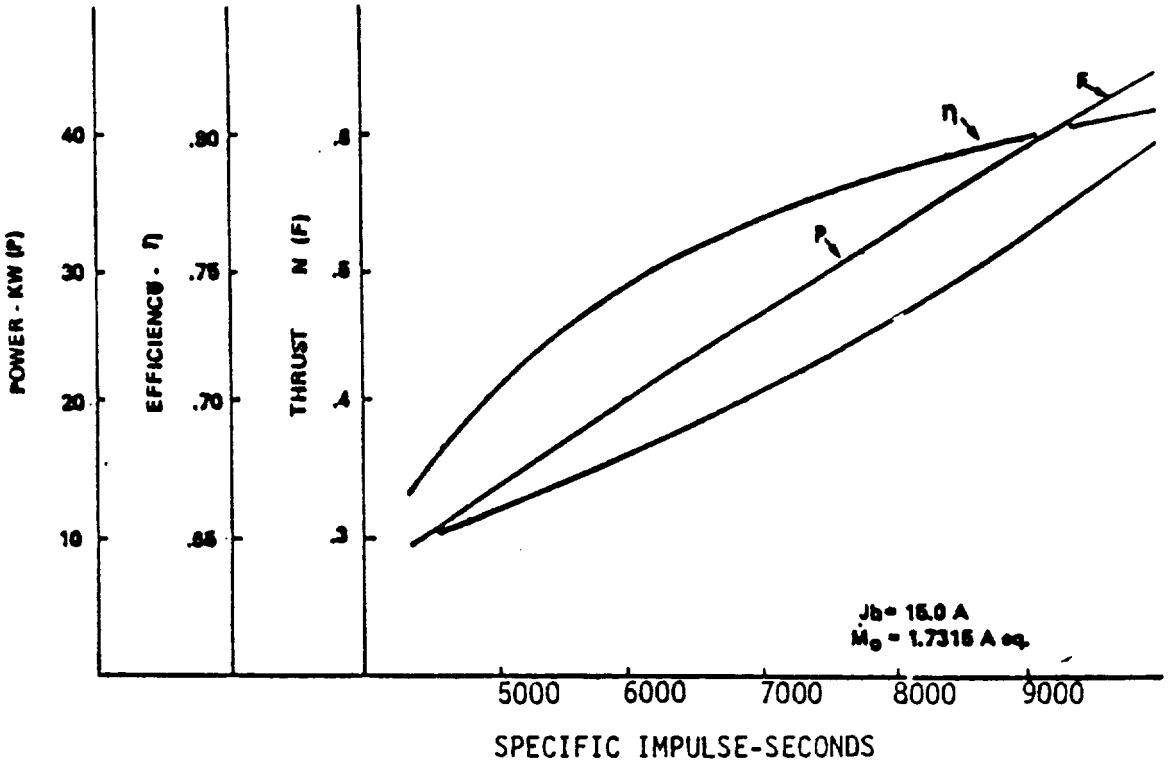

Figure 3.3-7: 50-cm Argon Ion Thruster Performance Characterization

Because the optical transmissvity is a function of beam current (Jb) and screen voltage (Vs), the interception of ions by the screen grid is also dependent on Jb and Vs, which implies a similar dependence for thruster lifetime. Based on this phenomena, predictions of life trends are shown in Figure 3.3-8. These data show that the electric propulsion system designer must consider beam-current limitations which are dependent on specific impulse as well as mission duration.

Ion Thruster Power Processing. Contemporary (SEPS technology) power processing units (PPU) for the 30-cm J-type thruster weigh 70 to 80 lb for a

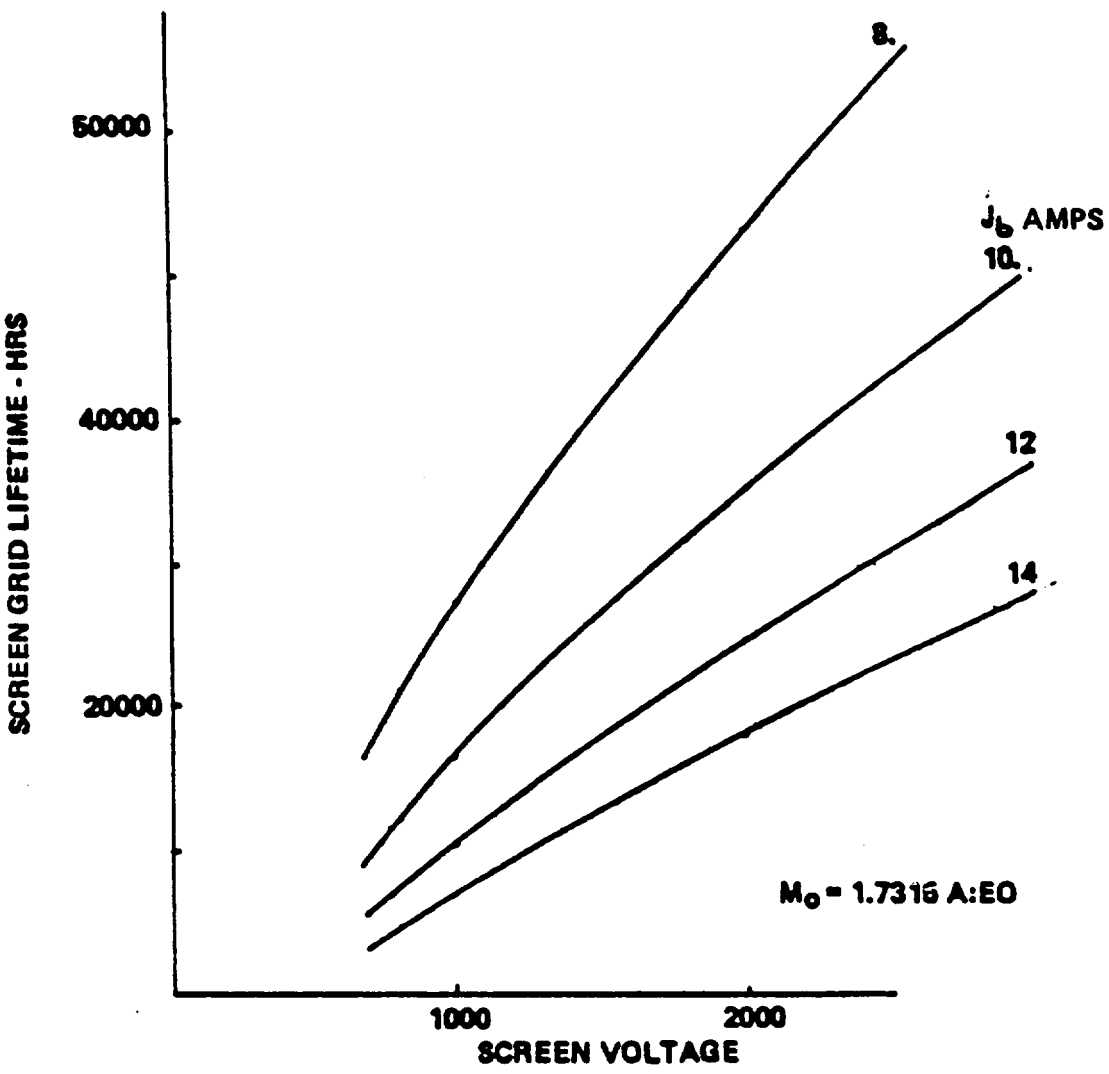

Figure 3.3-8: 50-cm Argon Ion Thruster Life Trends

3-kW, 1100V rating. These PPU's have 10 to 12 separate power supplies (each thruster requirement treated independently), a microprocessor for control, and input filters and isolation switches for EMC. They are intended for scientific payloads sensitive to EMI and are designed to control I_{sp} in interplanetary space with naturally varying solar array voltage (100V to 200V). (Actually, controlled I_{sp} is mainly a convenience for the interplanetary mission designer--there is no essential requirement for it). For Earth orbital missions, there is no requirement whatever for voltage (I_{sp}) control, and payloads for mass transit are comparatively insensitive to EMI. Therefore the PPU can be much simplier. Furthermore, combined function power supplies can be used to reduce the required number to as few as three for argon and five for mercury (demonstrated in 1977 at LeRC).

For a 12A, 50-cm argon thruster, the PPU specific weight (P_{mmu}/P_{ppu}) and efficiency are as shown in Figure 3.3-9. The improvement with respect to SEPS technology is notable and accrues directly because of the reduction in number of supplies (5 instead of 12), removal of screen voltage regulation, and concentration of power in the screen supply, which has a component specific weight of only 0.5 kg/kW.

These data can be used in vehicle sizing studies. The methodology can be used to characterize larger thrusters and/or alternative propellants as required.

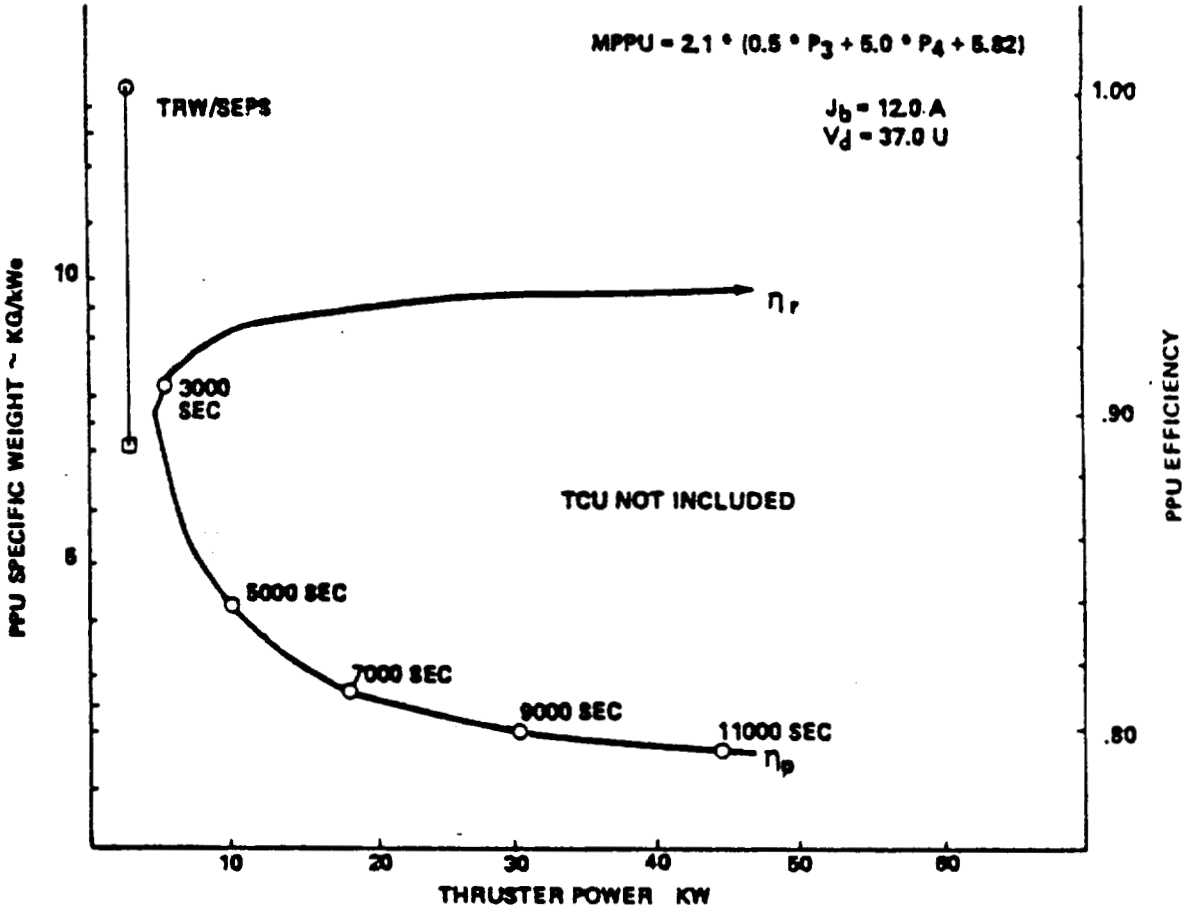

Figure 3.3-9: CDVM PPU for 50-cm Argon Ion Thruster

3.3.2 Colloid Thrusters

Background. The colloid thruster electrostatically accelerates charged aerosol droplets instead of charged molecules. The use of aerosols instead of molecules is prompted by the fact that at a given specific impulse, the power efficiency is greater for more massive ions. For specific impulses in the range of 1500 to 2000 sec (optimum for cislunar transfers), only colloid electric thrusters could operate efficiently.

Description. A candidate colloid thruster is shown schematically in Figure 3.3-10. A liquid propellant is drawn by capillary action to the tips of the

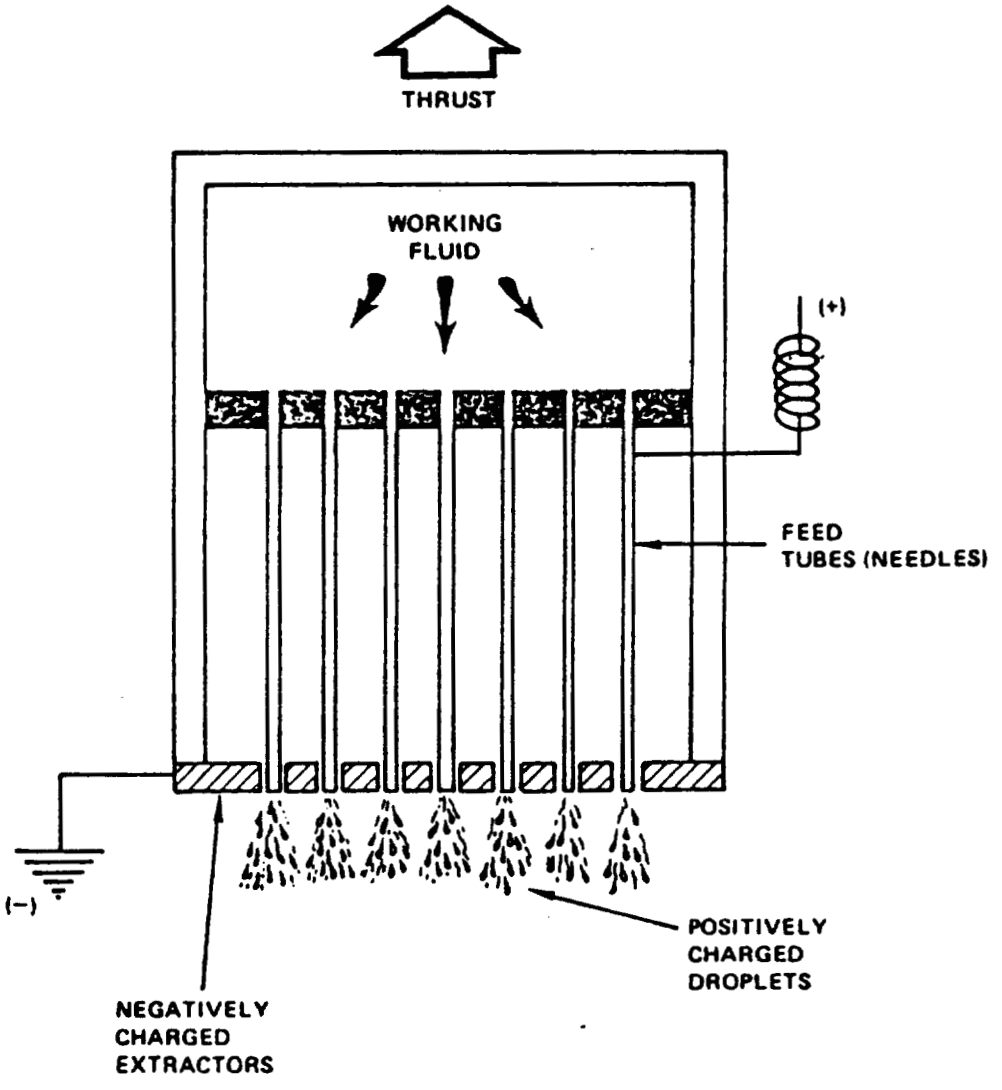

Figure 3.3-10: Colloid Thruster

needles where it is affected by the intense electric field concentrated at the point of the very small needles. The surface of the electrolytic propellant is disrupted by the intense electric field, and uniform submicrometer-sized, electrically charged droplets are ripped from it and accelerated downstream producing thrust. An electron-producing neutralizer would be used to neutralize the beam as on the ion thruster. The typical propellant would consist of a salt (like NaI or LiI) dissolved in a solvent-like glycerol.

Issues. Colloid thrusters have been plagued with poor lifetimes caused by high voltage arcing from the needles to the accelerator grid. The problem seems to be inherent with the design and there is very little work being done on colloid thrusters.

For these reasons, colloid thrusters are not recommended for further development at this time.

3.4 Magnetoplasmadynamic (MPD) Thrusters

MPD thrusters produce thrust by body-force acceleration of a continum plasma in a $\vec{J} \times \vec{B}$ field. The prevalent thruster considered for this application is the self-field pulsed plasma thruster being developed at Princeton University with support from JPL.

3.4.1 Princeton MPD Thruster

This conceptually simple thrust device consists of an axial cathode with a radial anode (Figure 3.4-1). A very strong radial current ($\sim 10^4$A) is used to induce a toroidal magnetic field (self-field) and the two combine to accelerate a plasma which forms during the arc formation (breakdown) process. The power required for this device is quite large so that only pulsed operation is usually considered.

The apparent simplicity of the MPD thruster belies its actual operation. The process of simultaneous plasma formation and acceleration is so complex that no encompassing theory has been sufficiently developed to admit design by analysis. All existing technology is experimental. Performance maps (Figures

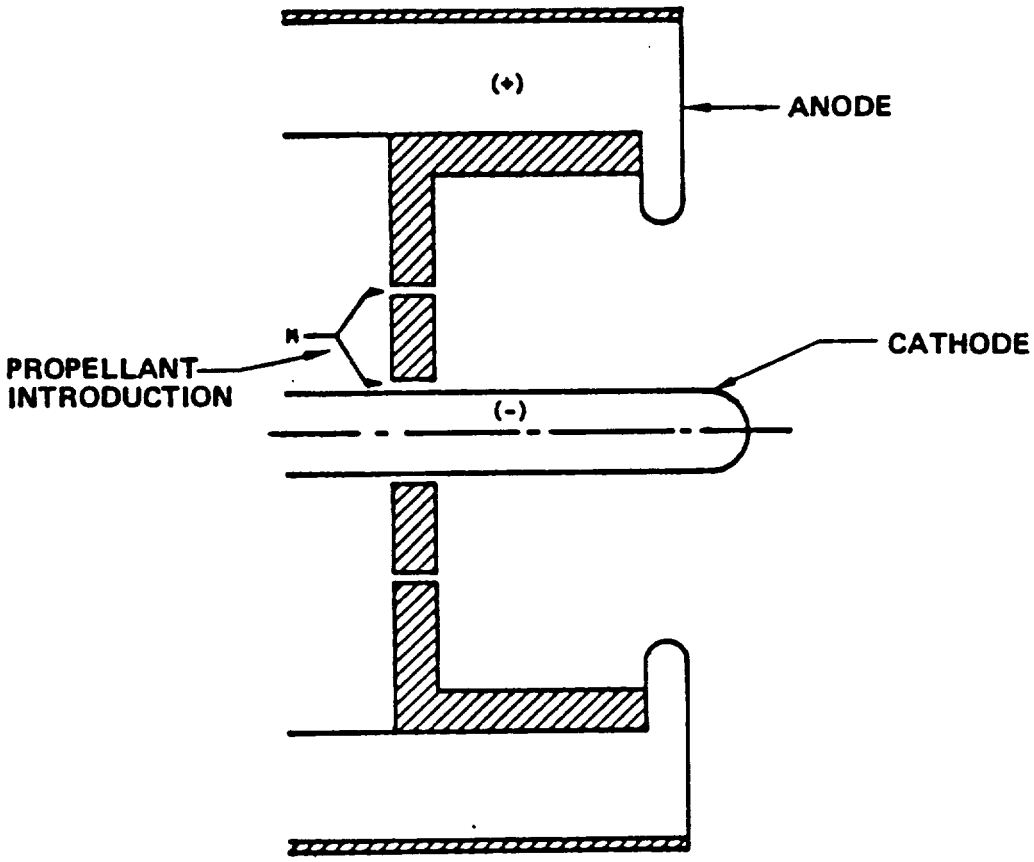

Figure 3.4-1: Princeton Pulsed Self-Field Thruster

3.4-2 and 3.4-3) are based on assumed efficiencies. Measurements of

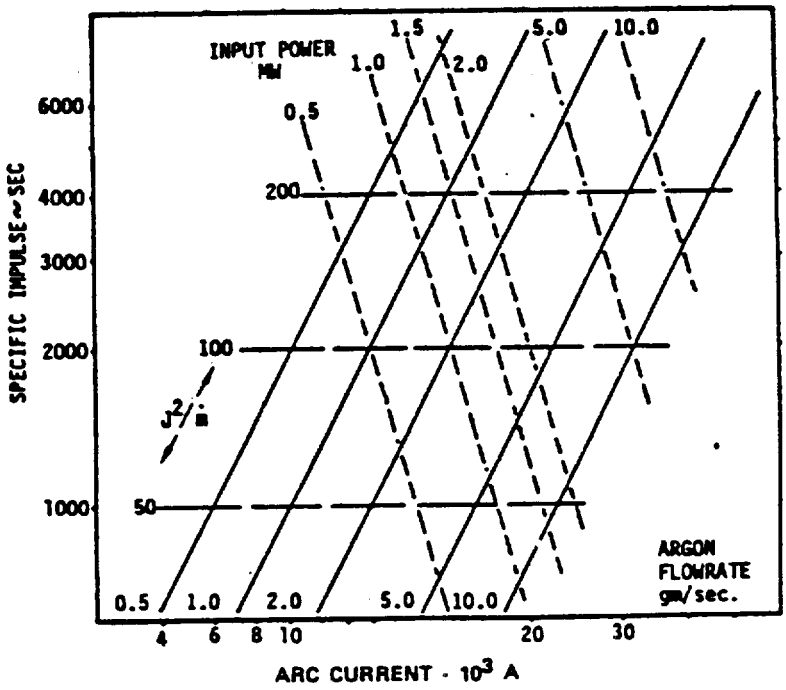

Figure 3.4-2: Self-Field MPD Operating Map

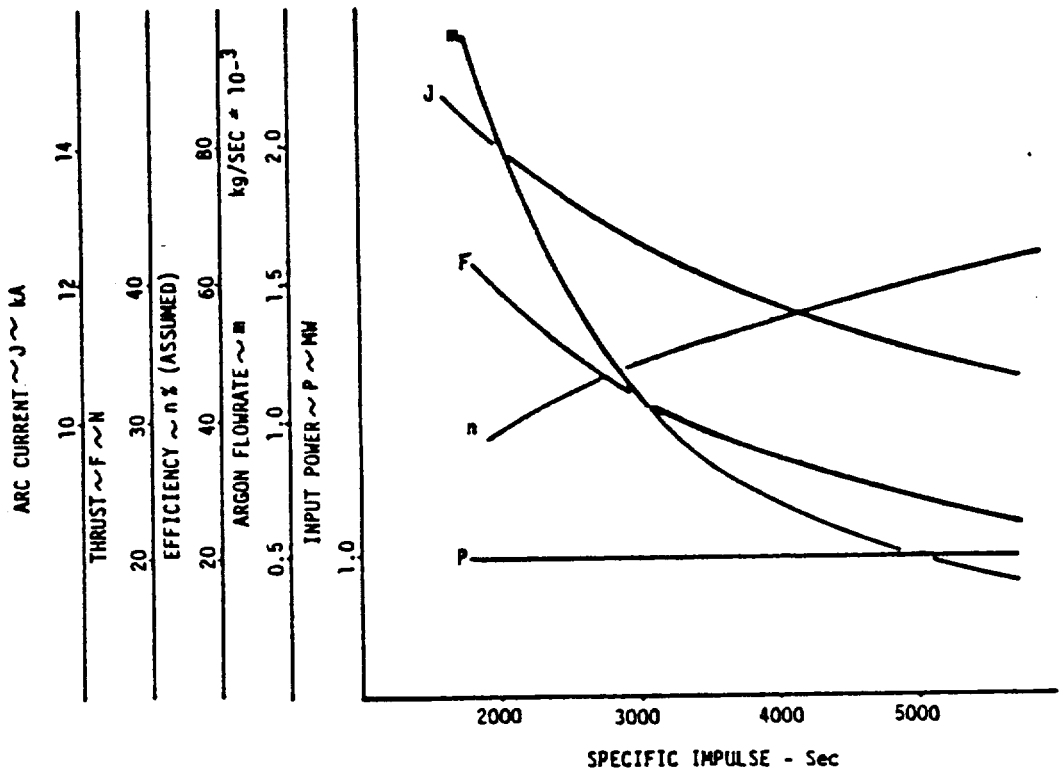

Figure 3.4-3: MPD Thruster Performance Characterization

efficiency have recently been made at Princeton and these data were published at the 15th Electric Propulsion Conference, April 21-23, 1981.

The figures of merit for MPD thrusters are lifetime, achievable I_{sp}, efficiency, average thrust including duty cycle, and thruster mass including TVC and power cabling. Thruster mass is generally negligible with respect to the remainder of the propulsion components (provided natural radiation cooling is adequate). Contemporary MPD thrusters have an I_{sp} limit of about 3000 sec with argon. Estimated efficiencies are shown in Figure 3.4-4. The Princeton data are based on a thrust calculated by integrating plasma acceleration through a $\vec{J} \times \vec{B}$ field; hence their accuracy is not well known.

Most performance estimates assume 100% mass utilization efficiency and based on instantaneous mass flow rate within the arc. In fact, utilization efficiency will be appreciably less than 100%, about 80% to 90%. Because reported efficiencies are based on instantaneous flow, the system efficiency must reflect the square of utilization efficiency. Evidently, additional development will be required to make the MPD concept a competitive option to

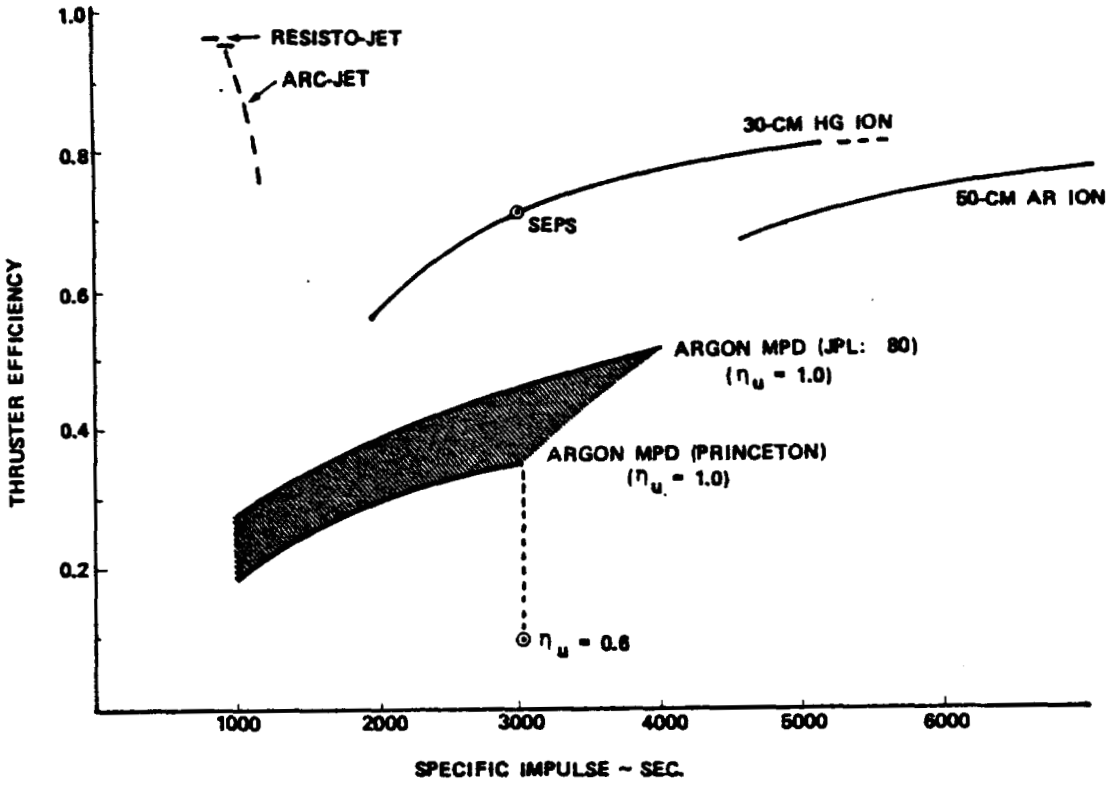

Figure 3.4-4: Comparison of Electric Thruster Options

ion propulsion, but there is motivation. Its thrust density may be 100 to 1000 times that of an ion thruster (at $\sim$ 1 N/m^2). The MPD thruster was recommended for vehicle level assessment in Task 2.

3.4.2 Pulse Formation and Energy Storage Systems

The self-field MPD thruster requires very high arc currents ($\sim$ 10,000A) for efficient operation. As a result, it usually would be operated in a pulsed mode to avoid meltdown from the joule heating in the structure which must carry these currents. Because the power sources under consideration for this study are all continous duty concepts, some form of energy storage device will be required for their efficient use. For instance, if the MPD duty cycle is 1%, direct operation by the power source would require that 99% of its output would have to be wasted; equivalently, it would have to be 100 times as large as it would be if its output could be stored during the off phase of the duty cycle.

To assess the systems requirements involved, an analysis was performed to develop concepts for pulse forming/energy storage subsystems for MPD thrusters

operated in the quasi-steady-state mode. According to available information, the output pulse from the pulse-forming network was to be trapezoidal in shape to match the thruster propellant flow during pulsed operation.

The selected trapezoidal pulse shape is shown in Figure 3.4-5. The thruster operating point for the flat portion of the curve was at a thruster

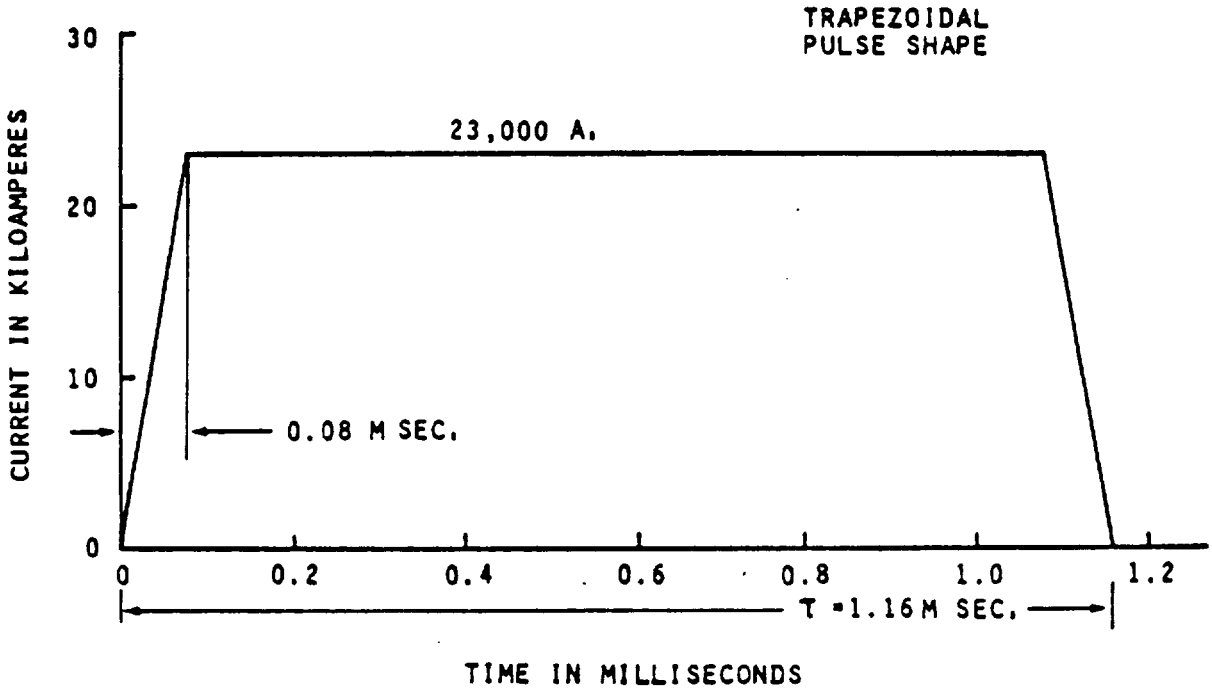

Figure 3.4-5: Trapezoidal Wave Shape Assumed for Five-Section Guillmin Voltage-Fed Pulse-Forming Network

current of 23,000A. This corresponds in Figure 3.4-6 (from ref. 3-3) to a thruster voltage of 220V and a thruster power level of approximately 5 MW. The thruster impedance at this operating point is 9.565mΩ. The power pulse shape shown in Figure 3.4-5 has a 0.08-ms risetime and a flat portion of 1 ms. The pulse repetition rate was 100 per second.

The initial attempt to develop the pulse-forming/energy storage network was an attempt to operate the system (power source, pulse-forming network, and thruster) without a switch in the system. The initial design task was to develop a circuit for the pulse-forming energy storage network. The network was to operate into a load impedance of 10.065 mΩ (9.565 mΩ for the thruster plus 0.5 mΩ for the power conductors from the thruster to network). To transfer maximum power from the pulse-forming network (PFN) to the load, the

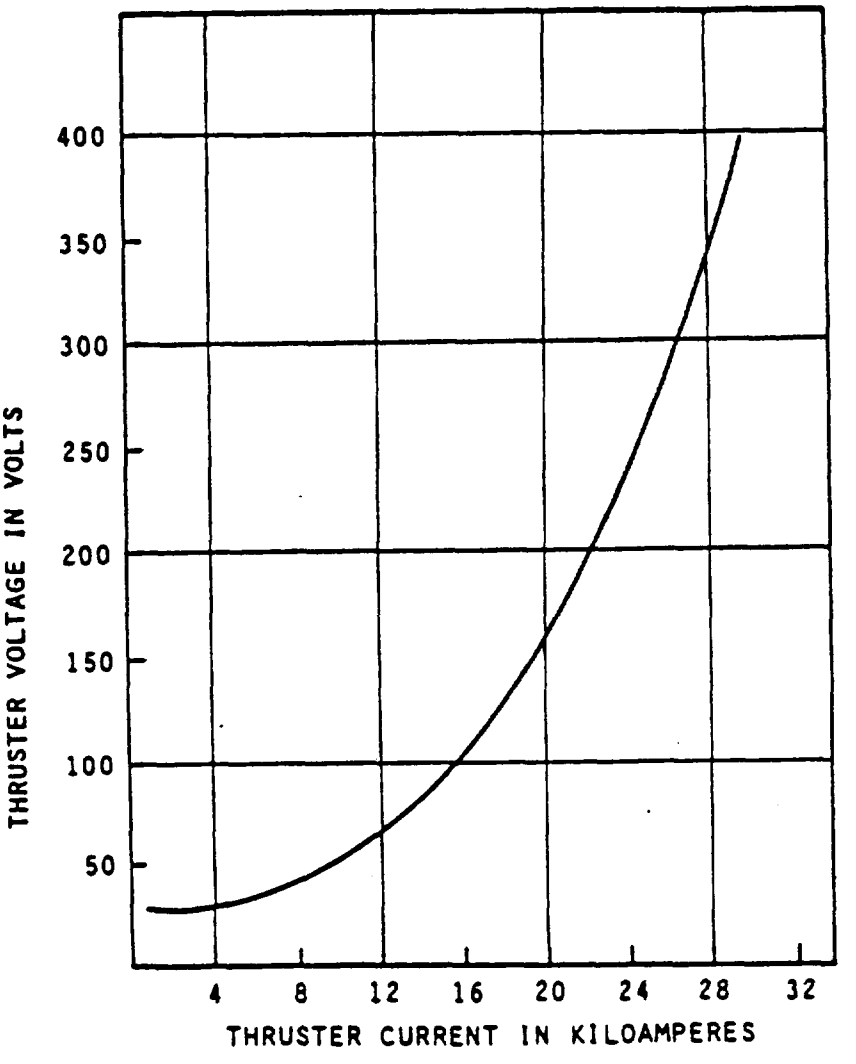

Figure 3.4-6: MPD Thruster Voltage-Current Characteristics

network should have an impedance (Z_N) equal to the load impedance. For this case, the voltage across the load is one-half of the pulse-forming network (PFN) voltage.

Reference 3-4 contains candidate forms for five-section Guillemin voltage-fed PFN's directly applicable to the trapezoidal waveform shown in Figure 3.4-5. For the PFN in that figure, the following parameters apply:

Pulse duration (τ)	=	1.16 ms
Impedance (Z_N)	=	10.065 m
Energy storage in PFN	=	5940 J
PFN voltage	=	463 V

To size the pulse-forming network to store required energy, capacitances are not sized by the technique in reference 3-4; however, the values calculated for energy storage are very near to those calculated by the methods of that reference. The resulting energy storage/pulse-forming network is shown in figure 3.4-7.

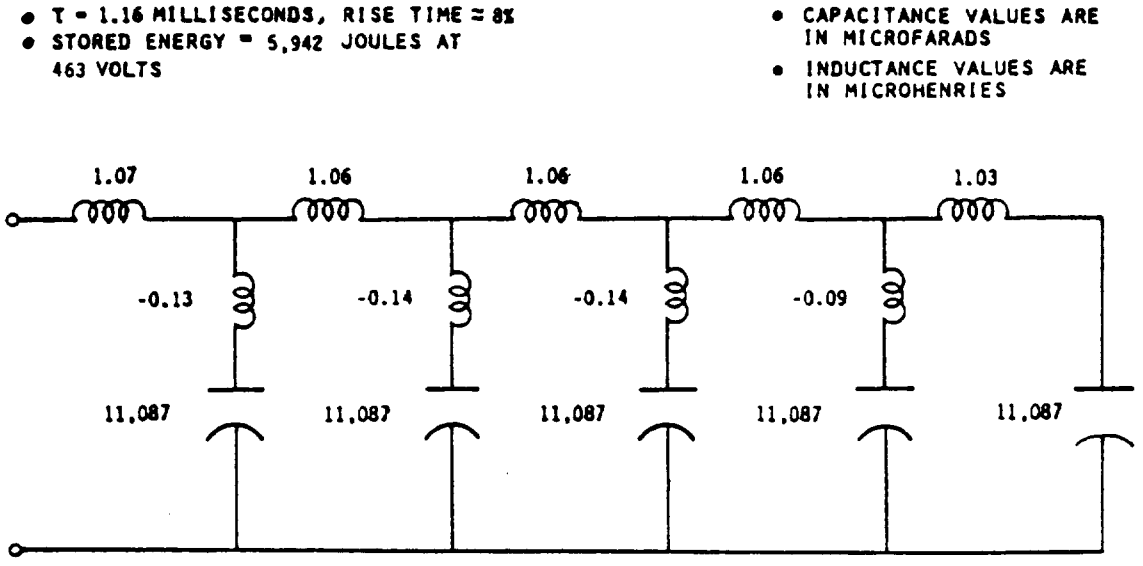

Figure 3.4-7: Five-Section Guillmin Voltage-Fed Pulse – Forming Network for Z_N 10.065 Milliohms, 1-16 Millisecond Pulse Duration

For the purpose of PFN recharging, the following parameters were used:

Pulse repetition rate	=	100/sec
Pulse duration	=	1.16 ms
PFN charging time	=	8.0 ms
Stabilization time	=	0.84 ms

Stabilization was included to ensure thruster operation completion prior to PFN charging. When charging a capacitor back from a voltage source through a resistance, the voltage across the capacitors approaches the supply voltage to within 0.7% in five time constants. For the network shown in Figure 3.4-7, the current during charging is shown in Figure 3.4-8 for a source resistance of 28.8 mΩ . The value of source resistance is required to have five time constants within 8 ms. (The time constant for charging is defined as the product of the source impedance and the total PFN capacitance.)

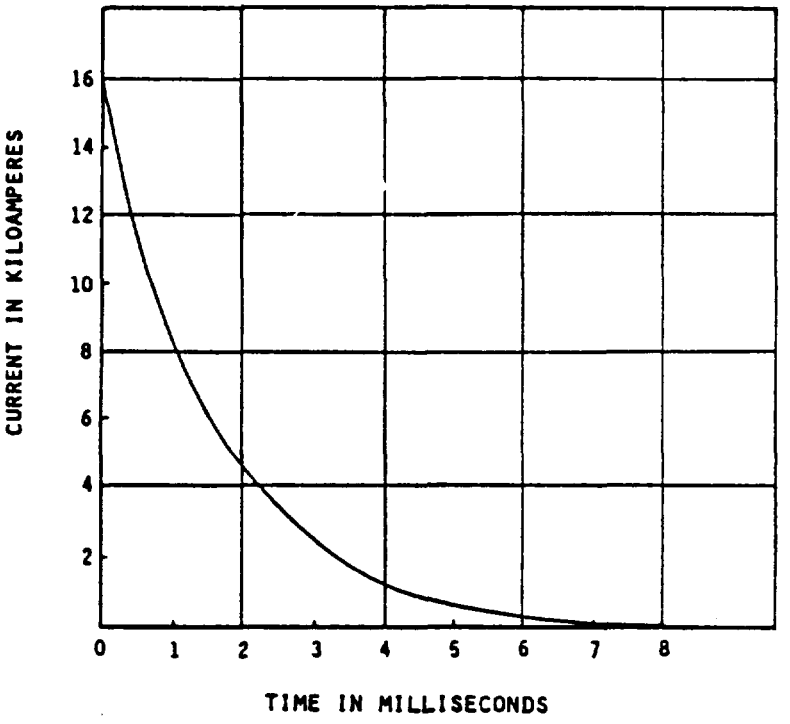

Figure 3.4-8: PFN Charging Current for Low-Voltage System

Because total resistance of the power processing subsystem (conductors, PFN, and thruster) is approximately 40 mΩ , the power source can sustain a current through the thruster of over 10,000A. If the attempt is made to interrupt thruster current by turning off propellant flow, serious damage will occur to the thruster due to erosion caused by the arc. Some means (whether by switch, crowbar, or other method) must be used to isolate the power source from the thruster.

There are several candidates of switches at this low voltage condition. Because the current decays to near zero, a minimum of cummutation circuitry would be required to turn off silicon-controlled reactifiers. Other likely candidates include high-power transistors (such as those being developed for NASA) ganged in parallel (to provide the required maximum current-carrying capability) and the crossed-field switch-tube being developed by Hughes Research Laboratories (Ref. 3-5). The cross-field switchtube has a forward voltage drop in the 20V to 30V range and dissipates considerably power at high-current levels.

Summarie of a candidate low-voltage resistive charge PFN are shown in Figures 3.4-9 and -10. As can be seen, the total value of capacitance for

- PULSE
  - DURATION: 1.16 MILLISECONDS
  - CURRENT AMPLITUDE: 23,000 AMPERES
  - SHAPE: TRAPEZOIDAL
  - REPITION RATE: 100 PULSES/SECOND
- PULSE FORMING NETWORK
  - STORED ENERGY: 5,942 JOULES
  - VOLTAGE: 463 VOLTS
  - TOTAL CAPACITANCE: 55,435 MICROFARADS
  - NUMBER OF SECTIONS: 5
  - TYPE: GUILLEMAN VOLTAGE-FED
  - CHARACTERISTICS IMPEDANCE: 10.065 MILLOHMS
- THRUSTER
  - QUASI-STEADY OPERATION
    - CURRENT: 23,000 AMPERES
    - VOLTAGE: 220 VOLTS
    - IMPEDANCE: 9.565 MILLOHMS
  - LINE RESISTANCE: 0.5 MILLOHMS

PULSE CHARGE TIME (ASSUMED): 8 MILLISECONDS

- CHARGING SWITCH

1) • SWITCH TYPE: LIQUID PLASMA VALVE
   • VOLTAGE DROP: 25 VOLTS
   • AVERAGE POWER DISSIPATION: 64 KW
   • QUANTITY REQUIRED: 1

2) • SWITCH TYPE: TRANSISTOR
   • VOLTAGE DROP (EQUIVALENT): 1.75 VOLTS
   • AVERAGE POWER DISSIPATION: 5 KW
   • QUANTITY REQUIRED: 80

Figure 3.4-9: Characteristics of Low-Voltage Resistive Charge Pulse Forming Network

PARAMETER	CALCULATION	RESULTS
PULSE REPETITION RATE	100 PULSES PER SECOND ASSUMED	1.16 msec PULSE DURATION 8.0 msec CHARGE TIME 0.84 msec STABILIZATION
ENERGY STORED IN PULSE FORMING NETWORK	$W_n = \frac{1}{2}CV^2$ $C = 0.055435$ farad $V = 463$ volts	5,942 JOULES
ENERGY LOSS DURING CHARGING	W_l = RESISTIVE LOSSES + SWITCHING LOSSES $= I^2Rt + V_s It$ WHERE $I = I_o e^{-(t/RC)}$ $W_l = I_o^2 R\int_0^{T_c} e^{-(2t/RC)}dt + V_s I_o \int_0^{T_c} e^{-(t/RC)}dt$ $I_o = 16{,}150$ A $R = 0.02886$ $C = 0.055435$ farad $T_c = 0.008$ sec. $V_s = 25$ volts	6,622 JOULES
AVERAGE POWER REQUIRED FROM SOURCE	$P = \frac{W_l + W_n}{T} = \frac{6{,}622 + 5{,}942}{0.01}$	1.26 Megawatts
ENERGY EFFICIENCY OF THRUSTER SYSTEM	$\eta_e = \frac{\text{THRUSTER ENERGY} \times 100}{W_l + W_n} = \frac{I_t \times V_t \times 100 \times T}{W_l + W_n}$ W_l and W_n are as defined above $V_t = 220$ volts $I_t = 23{,}000$ A T = EFFECTIVE TIME OF $I_t = 1.08$ msec.	43.5%

Figure 3.4-10: Low-Voltage Thruster System Performance Summary (Resistive Direct Charge)

the low-voltage PFN is quite large (55,435 μF). Because stored energy in a capacitor is 1/2 CV^2 and capacitor energy storage per unit mass increases with increasing voltage rating, an alternative design using higher voltage was formulated.

The high-voltage concept requires a pulse transformer for impedance matching. An additional switch (over the low-voltage system) is required for discharging the PFN through the pulse transformer. The high-voltage resistive charge power processing system is summarized in Figures 3.4-11 and -12. The high-voltage system incurs additional losses in pulse coupling (pulse transformer and switch), over the low-voltage system, requiring additional energy storage in the PFN.

- PULSE
  - DURATION: 1.16 MILLISECONDS
  - CURRENT AMPLITUDE: 23,000 AMPERES
  - SHAPE: TRAPEZOIDAL
  - REPETITION RATE: 100 PULSES/SECOND
- PULSE TRANSFORMER
  - TURNS RATIO: 5
  - EFFICIENCY: 95%
- PULSE FORMING NETWORK
  - STORED ENERGY: 6,329 JOULES
  - VOLTAGE: 2,315 VOLTS
  - TOTAL CAPACITANCE: 2,285.5 μFARADS
  - NUMBER OF SECTIONS: 5
  - TYPE: GUILLEMAN VOLTAGE-FED
  - CHARACTERISTIC IMPEDANCE: 252 MILLOHMS
- THRUSTER
  - QUASI-STEADY OPERATION
    - CURRENT: 23,000 AMPERES
    - VOLTAGE: 220 VOLTS
    - IMPEDANCE: 9.565 MILLOHMS
  - LINE RESISTANCE: 0.5 MILLOHMS
  - PULSE CHARGE TIME: 8 MILLISECONDS

- SWITCHES
  - TYPE: LIQUID PLASMA VALVE
  - VOLTAGE DROP: 25 VOLTS
  - AVERAGE DISSIPATION: 14 KW
  - TYPE: TRANSISTOR
  - VOLTAGE DROP (EQUIVALENT): 1.75 VOLTS
  - AVERAGE DISSIPATION: 1 KW

(NOT SUITABLE BECAUSE OF HIGH VOLTAGE)

Figure 3.4-11: High-Voltage Resistive Charge

Figures 3.4-10 and -12 show the PFN charging efficiency, using a resistance in series with the power source, is low. In fact, the maximum achievable charging efficiency is only 50%. The PFN charging efficiency can be improved by inserting an inductance in series with the power source. This charging method takes advantage of the series resonance of L-C circuits to improve the charging efficiency (see Chapter 9 of ref. 3-4). For the case of the PFN capacitances having no charge and the charging inductor having zero current flow, this charging method (called DC resonant charging) can charge the PFN capacitors to about 1.9 times the supply voltage at charging efficiencies of 0.90 for circuit Q's between 7 and 10.

APCS-265

PARAMETER	CALCULATION	RESULTS
PULSE REPETITION RATE	100 PULSES PER SECOND ASSUMED	1.16 msec PULSE DURATION 8.0 msec CHARGE TIME 0.84 msec STABILIZATION
ENERGY STORED IN PULSE FORMING NETWORK	$W_n = \frac{1}{2}CV^2$ $C = 2,258.5$ μfd $V = 2,315$ volts	6,052 JOULES
ENERGY LOSS DURING CHARGING	W_l = RESISTIVE LOSSES + SWITCHING LOSSES $= i^2Rt + V_s i t$ WHERE $i = I_o e^{-(t/RC)}$ $W_l = I_o^2 R \int_0^{T_c} e^{-(2t/RC)} dt + V_s I_o \int_0^{T_c} e^{-(t/RC)} dt$ $R = 0.7084$ $C = 2,258.5$ μfd $I_o = 3,307A.$ $T_c = 0.008$ sec. $V_s = 25$ volts	6,329 JOULES
AVERAGE POWER REQUIRED FROM SOURCE	$P = \frac{W_n + W_l}{T} = \frac{6,052 + 6,329}{0.01}$	1.24 Megawatts
ENERGY EFFICIENCY OF THRUSTER SYSTEM	$\eta_e = \frac{\text{THRUSTER ENERGY} \times 100}{W_n + W_l} = \frac{V_t \times I_t \times 100 \times T}{W_n + W_l}$ W_l and W_n are as defined above $V_t = 220$ volts $I_t = 23,000$ A. T = EFFECTIVE TIME OF $I_t = 1.08$msec	44.1%

Figure 3.4-12: High-Voltage Thruster System Performance Summary; Resistive Direct Charge using Pulse Transformer (N_P/N_S=5; η = 0.95)

A DC resonant charging concept was developed for the low-voltage PFN previously discussed. The concept requires a lower impedance power source than does the resistive charge circuit (14 mΩ versus 28 mΩ) and a charging inductance of 186 MH in series with the power source. The calculated charging efficiency was 0.90 from a 250V power source.

Care must be taken in the design of the charging circuit to minimize charging current for when the switch is activated to isolate the power source from the PFN (see Figure 9-3 of ref. 3-4). Otherwise the problems of interrupting large inductive currents exist.

Conductor grade aluminum was the conductor material selected for main power conductors and for the inductors in the charging reactor and the PFN. This selection, based on the low product of electrical resistivity and specific mass of aluminum, compared to other standard materials.

The capacitance design was based on the K-film capacitor development work funded by the Air Force Rocket Propulsion Laboratory (ref. 3-6). This work aimed at developing long-life capacitors rated at 2,200V. For the low-voltage case, while the specific energy storage density of 40 J/lb at 2,200V for the K-film capacitors does not apply, scaling of capacitance value was accomplished from the K-film data. The design of the K-film capacitors was 80

MF, 2,200V, and weighed 4.75 lb. A conservative factor of 2 was used to scale from 80 MF and 4.75 lb at 2.2 kV to 150 MF at the same weight for the lower voltage case. For the high voltage PFN, 35 J/lb was used to calculate system weight. The reason for the conservatism in the weights of the capacitors is the failures that have occurred in life testing of the K-film capacitors. While the cause of these failures (primarily at the foil edges) will be corrected, it will most likely be at some sacrifice in specific energy-storage density.

The mass of the switches was estimated. The mass of the transistor low-voltage switch was based on 80 high-power transistors in parallel; the cross-field switch was based on earlier SPS studies (ref. 3-7). The mass of the pulse transformer for the high-voltage PFN was estimated at 1.0 kg/kW (average).

A summary of the three PFN networks is shown in Figure 3.4-13. The resonant charge concept requires a considerably smaller power source due to its inherently higher system efficiency. Weights shown are for components only and do not include installation, packaging, thermal control interface, or thermal control provisions.

		POWER SOURCE					
		POWER GENERATOR	SOURCE IMPEDENCE	POWER BUSSES	SWITCH	PULSE FORMING NETWORK	PULSE COUPLING	THRUSTER
RESISTIVE CHARGE LOW V.	POWER IN (KW)		1,224.9		609.6	605.3	575.1	546.5
	POWER LOSS (KW)		615.3		4.3	30.2	28.6	-
	EFFICIENCY		0.498		0.993	0.950	0.948	-
	MASS (KG)		156		200	946	61	-
DIRECT HIGH V.	POWER IN (KW)		1,433		715.9	702.7	667.6	546.5
	POWER LOSS (KW)		717.1		13.2	35.1	121.1	-
	EFFICIENCY		0.499		0.982	0.950	0.819	-
	MASS (KG)		32		300	612	996	-
D.C. RESONANT CHARGE	POWER IN (KW)		677.3		609.6	605.3	575.1	546.5
	POWER LOSS (KW)		67.7		4.3	30.2	0.948	-
	EFFICIENCY		.90		0.993	0.950	0.948	-
	MASS (KG)		898		200	946	61	-

Figure 3.4-13: Pulse-Forming/Energy Storage Concepts Summary

The design example used in this analysis was for a fixed thruster operating point. No attempt was made to optimize the total vehicle. As such, this example does not represent a design for an optimum vehicle operating in the pulsed MPD mode; however, the resonant charging concept offers significant performance improvement over resistive charging. Switching in the power circuit is required. The efficiency and mass of the energy storage and pulse-forming subsystem are significant. The design optimization of the pulse-forming/energy storage subsystem will require an overall vehicle/system optimization analysis.

3.4.3 Magnetohydrodynamic (MHD) Thrusters

The MHD thruster is electromagnetic acceleration in its simplest form (see Figure 3.4-14). A flow of ionized gas in generated in an arc jet or seeded chemical rocket and then subjected to crossed electric and magnetic fields as it expands through the nozzle. If the gas has a scalar conductivity, σ , and velocity, $\vec{u}$, as it enters the accelerator section, then a current density $\vec{j} = \sigma (\vec{E} + \vec{u} \times \vec{B})$ will flow through it. This current is parallel to $\vec{E}$ and will interact with the magnetic field to provide a distributed body force equal to $\vec{J} \times \vec{B}$ which will accelerate the gas in the direction of $\vec{u}$.

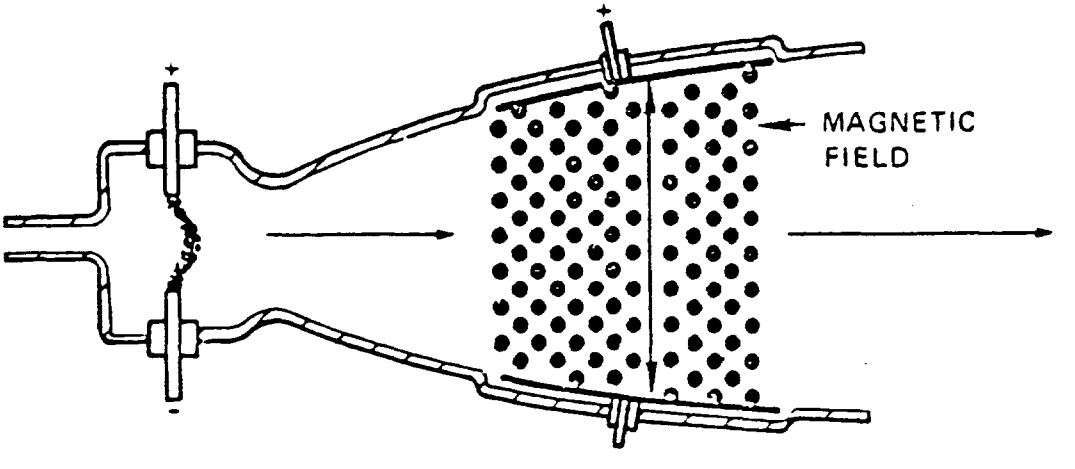

Figure 3.4-14: MHD or Crossed-Field Accelerator

This device, often called the crossed-field accelerator, appeared capable of operating at specific impulses as high as 3000 to 4000 sec with good efficiency (60% to 80%); but work on it was discontinued in the late 1960's to

concentrate on the MPD thruster. This was because the crossed-field accelerator required a substantial external field and therefore a massive electromagnet, whereas the MPD thruster used the plasma current itself to generate the B-field, making for a simpler, lighter system. In addition, MHD thrusters will suffer from most of the same problems associated with MHD generators, namely electrode erosion and shorting. The environment in a space engine should be more benign (cleaner) than in ground-based MHD generators, but the fact that no MHD units are operating on a regular basis after several decades of research and development shows the magnitude of the problems involved.

On the positive side, the crossed-field accelerator requires almost no power processor, operating with unfiltered dc current much as the arc jet thruster; and recent advances insuperconducting magnets could provide the required magnetic field for a small mass and power penalty. It is possible that as propulsion power requirements increase from the 100 kW level discussed today to the multimegawatt level needed for space industrialization, the crossed-field accelerator will make a comeback. This is because the crossed-field accelerator offers increased efficiency and fewer heat rejection problems at higher thrust levels relative to competitive electric thrusters. Also, the weight of the electromagnet becomes insignificant at higher thrust levels compared to the power generating and processing systems required by other thruster concepts.

Recommendation. The MHD thruster was not recommended for Task 2 because (1) the available data base vehicle was felt to be too marginal to support a reasonable level assessment and (2) we had already committed to include a similar concept, the MPD thrusters, and did not want to dilute the study effort.

3.5 Arc-Jet Thrusters

Background. The arc-jet thruster produces thrust by heating hydrogen in an electrical arc and then accelerating it in a conventional expansion nozzle. Hydrogen is the only element which can give the high specific impulse (800 to 1200 sec) required for high payload performance (see section 2.6 for hydrogen performance data). Ordinarily, arc jets have low electrical efficiency because of frozen dissociation and ionization losses originating in the arc

heat process. A downstream mixing chamber might,however, be used to relax these states and thereby achieve high efficiency. A mixing chamber design concept is shown in Figure 3.5-1. Its expected performance is shown in Figure 3.4-4. A possible advantage for the arc jet is that little or no power processing is required provided load impedance can be matched with the source impedance (source must be direct current, but high quality, low ripple, is not required).

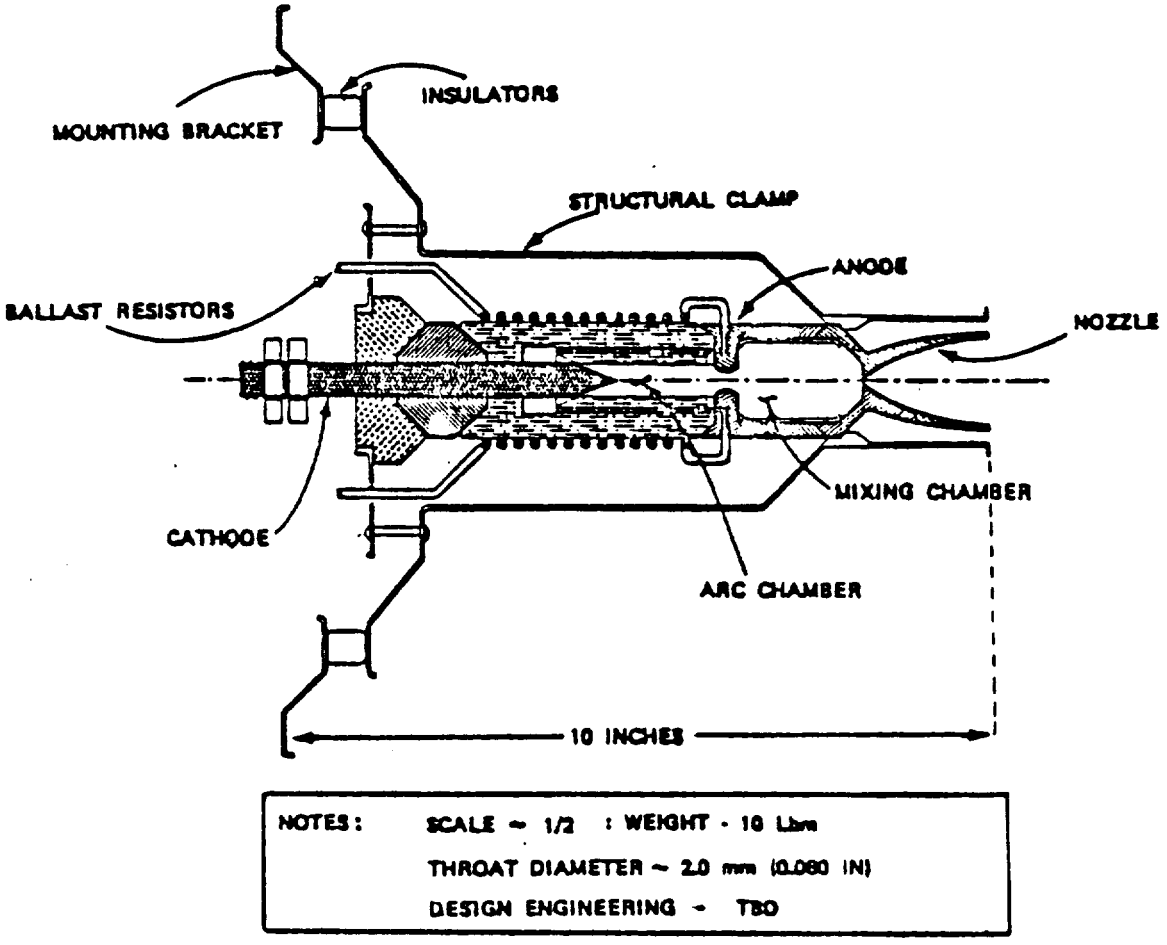

Figure 3.5-1: 25-Kw Thermal Arc-Jet Concept

Issues. Foreseeable issues that may influence the eventual use of arc-jet thrusters are (1) thermal shock survivability of brittle arc-jet components and (2) arc-jet lifetime and efficiency with respect to delivered I_{sp}.

Recommendation. The high thermal efficiency at moderate specific impulse levels makes this concept attractive enough for Task 2 assessment.

3.6 Electromagnetic (EM) Thrusters

Electromagnetic thruster concepts rely on forces generated when a magnetic field interacts with electrical currents to accelerate solid conductors or plasmas to high velocities thereby generating thrust. There are a number of ways to accelerate reaction mass magnetically. One scheme, the mass driver, is a synchronous linear electric motor in disguise where the magnetic field is used to transfer forces between current-carrying wires. Another scheme, the rail gun, uses a single current loop to accelerate a plasma armature with the $\vec{J} \times \vec{B}$ magnetic force. The plasma armature and its confining reaction mass are driven from gun at high velocity to generate thrust. Other less publicized schemes, use the repulsion force between eddy currents generated in a conductor by a time-varying magnetic field and the field itself to accelerate a conducting reaction mass. Examples of these schemes are the direct current induction accelerator proposed by MIT and the pulsed inductive plasma thruster proposed by TRW. Each of these magnetic thruster concepts will be discussed in the following subsections.

3.6.1 Mass-Driver Reaction Engine

In the schemes commonly proposed for the mass driver (refs. 3-8 and 3-9), the reaction mass rides in a magnetically driven moving "bucket" which releases the mass at high velocity, circulates back on a separate return path, and receives a new reaction mass for the next cycle. For the highest efficiency, braking would be regenerative. Because an operational mass-driver condiguration (figure 3.6-1) has many buckets, each with two bucket coils and several thousand drive coils, system complexity is a primary consideration.

Each bucket's superconducting coils would be inside a sealed, well-insulated enclosure and would be bathed in liquid helium. Once the bucket coils are energized, no further action is required except periodic recharging of the liquid helium. The drive coils, however, need fast and accurate switching to ensure proper phasing with the bucket coils to accelerate and decelerate the bucket. Because of the extremely high velocites

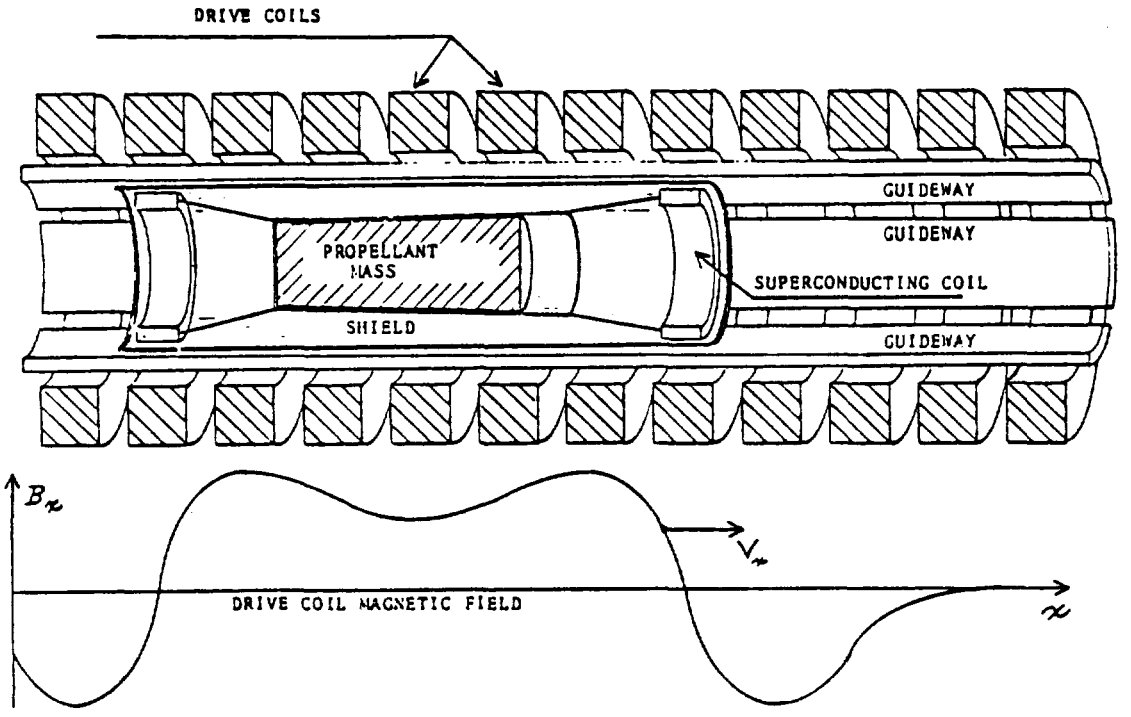

Figure 3.6-1: Mass-Driver Linear Synchronous Motor

involved (up to 10 to 20 km/sec), timing is critical and it is unlikely that bucket driver contacts could be allowed; hence, the system must be very reliable.

The Princeton mass-driver working group has recently published a detailed design study (ref. 3-10) for solar electric orbit transfer vehicles using mass drivers, with an estimated electrical efficiency of 70% to 90%. In their analyses, the mass of the electrical switching, to be done with silicon-controlled rectifiers (SCR), becomes significant as exhaust velocities exceed 10 km/sec (equivalent to 1000 sec of specific impulse). However, a later paper (ref. 3-11) proposes a new type of mass driver with a pull-only drive system in a new tightly coupled bucket configuration that avoids the requirement for rapid current switching at the high-velocity end of the device. This promises exit velocities up to 20 km/sec using state-of-the-art SCR's.

Unfortunately, mass drivers operating at 500g to 1000g acceleration have to be inherently large (5 to 10 km long) to reach velocities or 10 to 20 km/sec. Consequently, they optimize at very large payloads (4000 M to GEO in ref. 3-10) which is beyond the scope of this study. A conceptual configuration of a solar-powered mass-driver reaction engine is pictured in Figure 3.6-2.

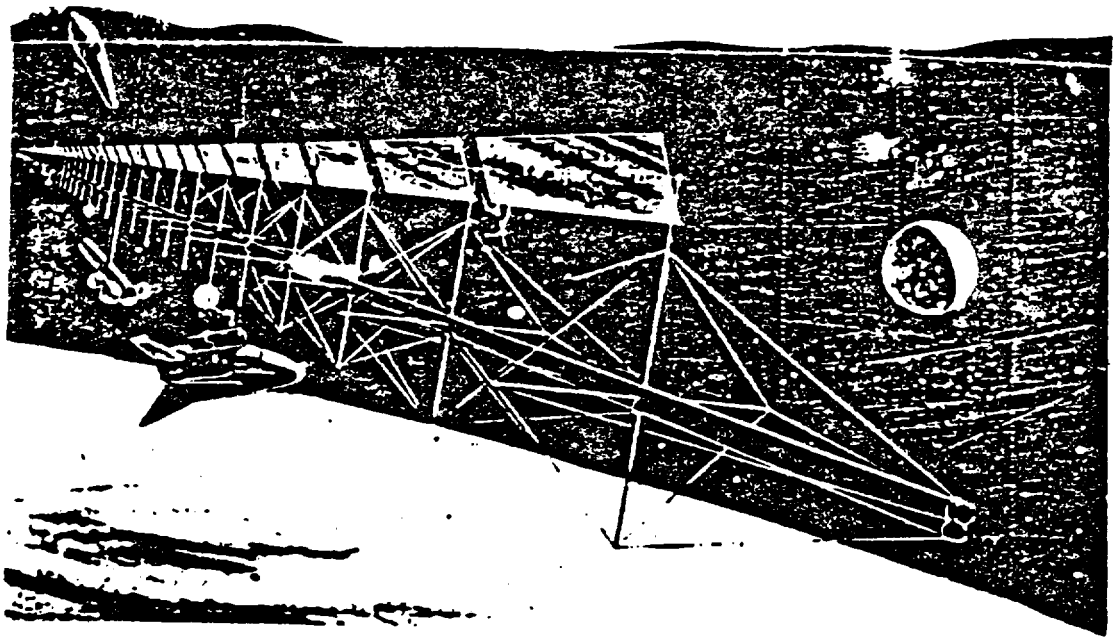

FEATURES

- ISP = 800 - 1500 SECS (OPTIMUM FOR EARTH - MOON SYSTEM)
- INITIAL T/W = 3×10^{-4}
- VERY HIGH ELECTRICAL EFFICIENCY

RISK/FEASIBILITY ISSUES

- LACK OF CHARACTERIZATION/HIGH COMPLEXITY
- REUSABLE BUCKET REQUIRES VERY LARGE SYSTEM (10 KM)

Figure 3.6-2: Mass-Driver Feature and Risks

Recommendation. Because of the very large size required and the extreme complexity of currently proposed systems, the mass-driver reaction engine was not carried into Task 2.

3.6.2 Rail Gun Reaction Engine

A simple parallel rail gun consists of a pair of rigid conducting rails that form two opposite sides of a rectangular accelerator channel. The other two sides consist of a nonconducting refractory material. A rectangular projectile, which seals the accelerator bore, is inserted and an electrically conducting armature placed directly behind it. If an electrical potential was applied across the rails at the breech, the situation shown schematically in figure 3.6-3 would soon develop. Current in the rails would produce a magnetic field between the rails which would interact with the current flowing through the armature and produce a $\vec{J} \times \vec{B}$ force to accelerate the armature and projectile.

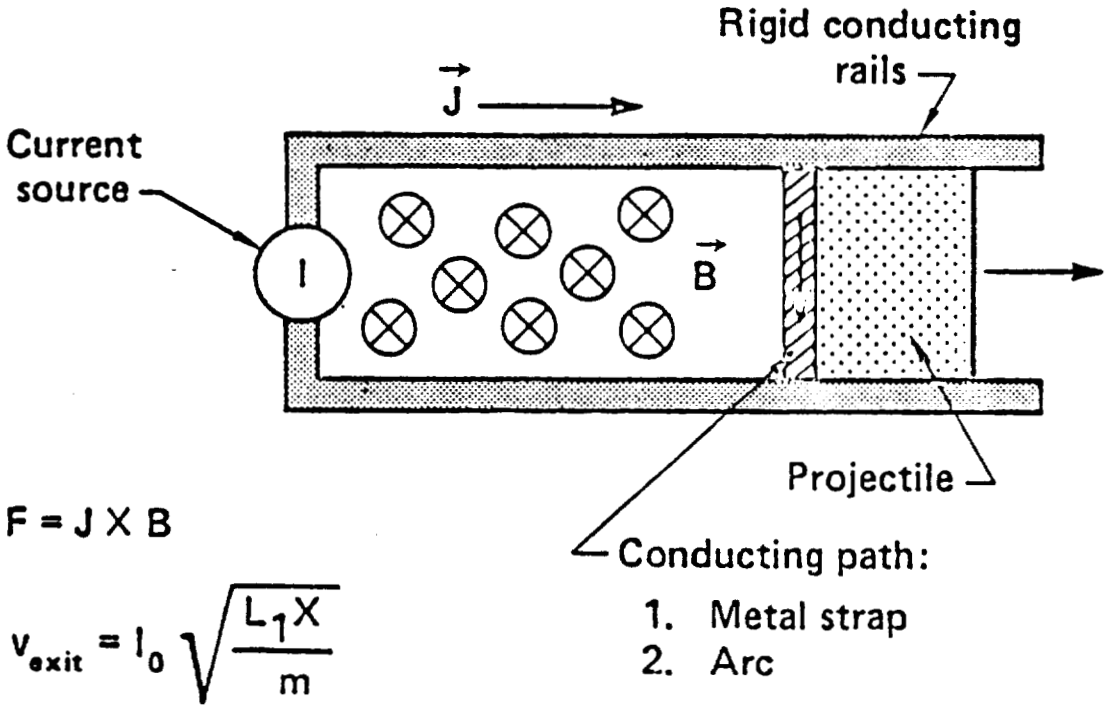

Figure 3.6-3: Simple Rail Gun Schematic

Projectiles can be made from almost any material provided they can be potted in a nonconducting substance. The projectile must possess sufficient strength, however, to withstand the acceleration stresses involved (up to 10,000 g's). It would also be very desirable to leave no permanent reaction mass projectiles in Earth orbit. It should be possible to use a reaction mass material that evaporates or sublimes over a period of minutes. Candidates that might fulfill this requirement are water, ice, and mothballs.

The rail gun is simple, cheap, and known to work (refs. 3-12 and 3-13). Its main technical considerations are high-current switching, keeping projectiles intact during acceleration, rail wear due to projectile friction, and/or arc erosions. Arc erosions is the most serious problem, especially during arc starting when the velocities are low and at the end of the rails as the projectile leaves the gun. It should be possible to tailor the arc current to reduce arc erosion, but more testing and development are necessary to determine rail gun lifetimes.

Recent studies (refs. 3-14 and 3-15) have examined the performance of conceptual electric rail gun propulsion systems (Figure 3.6-4) and show them to be competitive with conventional electric thruster systems for LEO-GEO delivery times of 20 to 120 days.

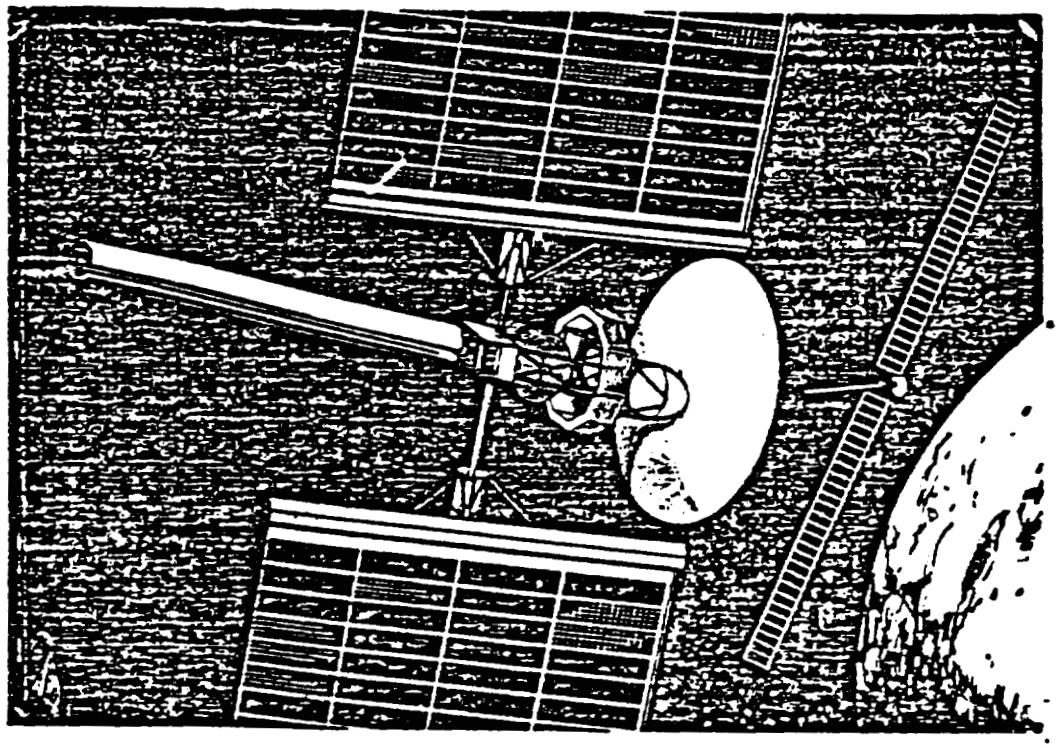

FEATURES

- I_{sp} = 800-1500 SECONDS
- T/W = 10^{-3}–10^{-4}

RISK/FEASIBILITY ISSUES

- ARC EROSION OF BARREL SURFACES
- FINAL DEPOSITION OF FIRED PELLETS

Figure 3.6-4: Solar Electric Rail Gun Rocket

Recommendation. Because the recent rail gun propulsion studies used ground rules compatible with this study, their results have been incorporated directly into Task 2.

3.6.3 Induction Thruster

Induction thrusters use the repulsion force between eddy currents generated in a conductor by a time varying magnetic field and the field itself to accelerate the conductor as the reaction mass. Examples of proposed induction thrusters are the MIT direct current induction accelerator and the TRW pulsed inductive plasma thruster. Of these two, the TRW thruster is further developed and appears to be more practical.

The MIT thruster concept involves accelerating a metal ring with a series of coaxial coils spaced along a nonconducting barrel. By firing a capacitor bank through each coil immediately after the ring has passed through it, a

large repulsive force is generated between the coil and the eddy current in the ring, accelerating the ring to high velocities. The upper limit on velocity is determined by the melting of the ring through the ohmic heating of the eddy currents. Feasibility issues include the need for high-speed, highly accurate switching and the problem of leaving solid projectile reaction masses in Earth orbit. Because sufficient design data were not available for the MIT direct current induction thruster, it was not recommended for vehicle level assessment in Task 2.

The TRW pulsed inductive thruster has been the subject of theoretical analyses and experimental design for almost 20 years, according to reference 3-16. The thruster itself is a large (greater than 1m), flat, spiral coil through which a capacitor bank is fired. Simultaneous with the capacitor bank triggering, a poppet valve releases and lays a cloud of propellant gas just over the coil. The sudden magnetic pulse ionizes some of the neutral gas and forms a thin flat disc of pure j_o current carried only by electrons. The eddy current, driven away from the coil by magnetic repulsion, ionizes and sweeps up the neutral gas ahead of it to provide thrust. A schematic of the pulsed inductive thruster is shown in Figure 3.6-5. One reason for using inductive coupling rather than direct contact through electrodes is to avoid erosion and energy loss mechanisms, which are characteristic of other electric thruster concepts and result in limited thruster lifetimes.

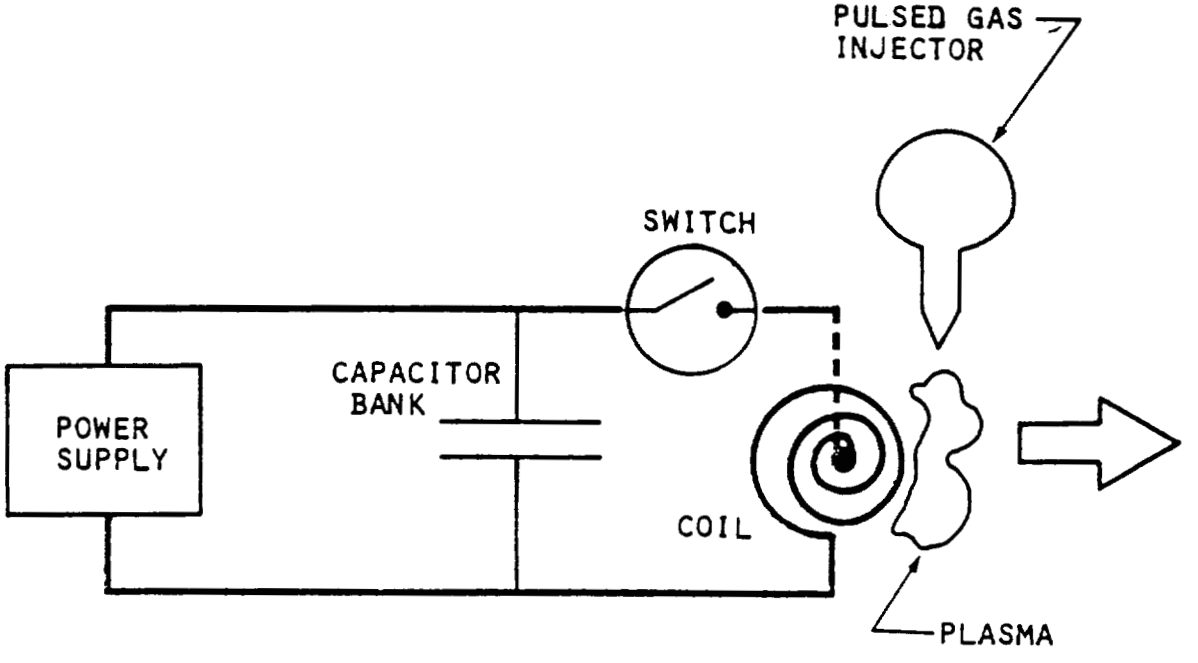

Figure 3.6-5: Schematic of Pulsed Inductive Thruster

The results of a 10-year development program looking at increasing thruster diameters is shown in Figure 3.6-6. The trend of increasing efficiency and specific impulse with increasing diameter agrees with analytical calculations (ref. 3-17), which showed a rapid rise of efficiency with diameters up to about 1m, with a more gradual increase thereafter.

The pulsed inductive thruster has many of the same characteristics and problems of the MPD thruster discussed in section 3.4. Namely, it requires a pulsed propellant injection system and a pulse-forming energy storage system, does as the MPD thruster, and it has about the same efficiency but at lower specific impulse levels. For these reasons it was decided not to pursue the pulsed inductive thruster in Task 2 but to use the MPD thruster because of its further development.

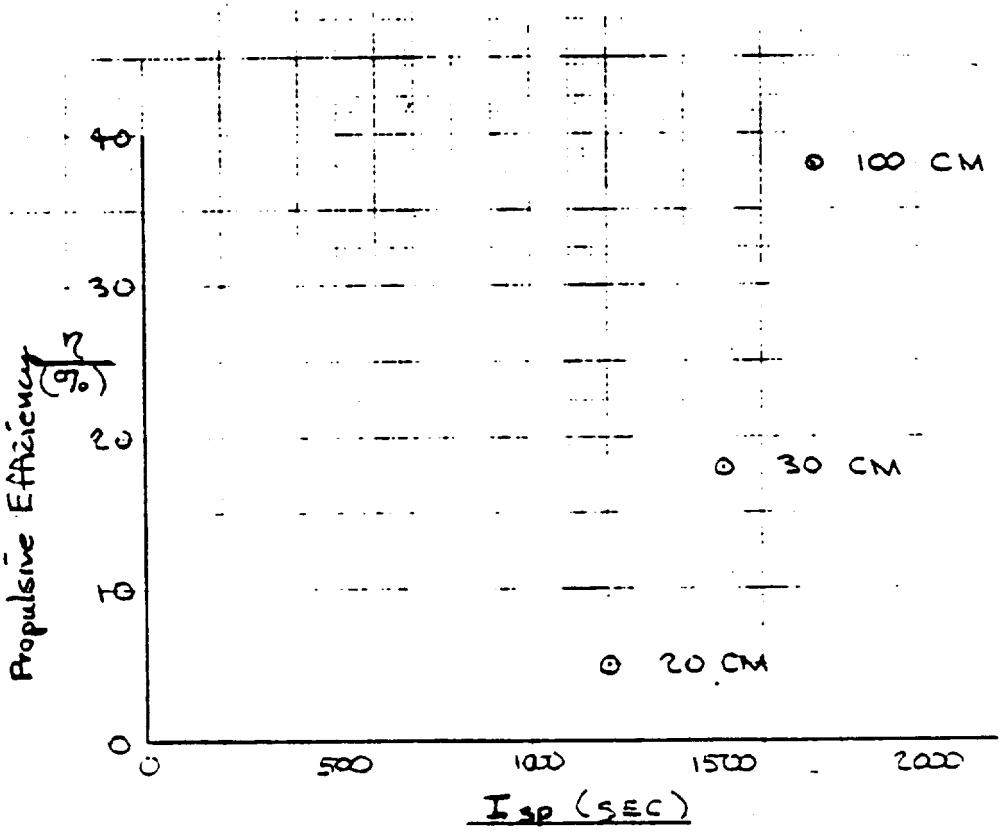

Figure 3.6-6: Effect of Coil Diameter on Efficiency

4.0 OTHER PROPULSION CONCEPTS

In the process of surveying advanced propulsion concepts, a few did not fit into the categories of thermodynamic or electric rockets. Principal exceptions; are the so-called photon rockets: namely the solar sail and the antimatter rocket. Other concepts in this category (e.g., antigravity, gravity screens, reactionless propulsion [Dean Drive], wormholes in the vicinity of a black hole, etc.) are ideas for conversation with no hard data or accepted theory to indicate they will exist. Although photon rockets are far beyond the mission models discussed in this study, a brief description of each follows for the sake of completeness.

4.1 Solar Sail

The solar sail is a conceptually simple device that deploys a large, lightweight reflective surface to intercept and reflect solar radiation, thereby generating thrust on the vehicle. In the vicinity of Earth, a perfectly reflective surface could generate almost 10^{-5} N/m^2. If the vehicle could be made light enough ($\sim$ 0.01 kg/m^2), a usable thrust to weight would result. Recent advances in solar sail technology (ref. 4-1) suggest that 0.1 thick films could be manufactured in quantity in orbit. If assembled into a large solar sail structure and a way to successfully control and steer that structure were devised, a very economic form of deep-space transportation could evolve. The solar sail concept proposed in reference 4-2 would have a 0.003 thrust to weight and would be competitive for LEO-GEO delivery, but it could not overcome air drag below 900 km. The high-performance solar sail configuration proposed in references 4-1 and 4-2 is shown in Figure 4.1-1.

Principal feasibility questions not addressed sufficiently to date, deal primarily with the operational issues of solar sails. Is it possible to process the rotating solar sail rapidly enough to accelerate it out of LEO without distorting its very fragile structure? How many manhours are required

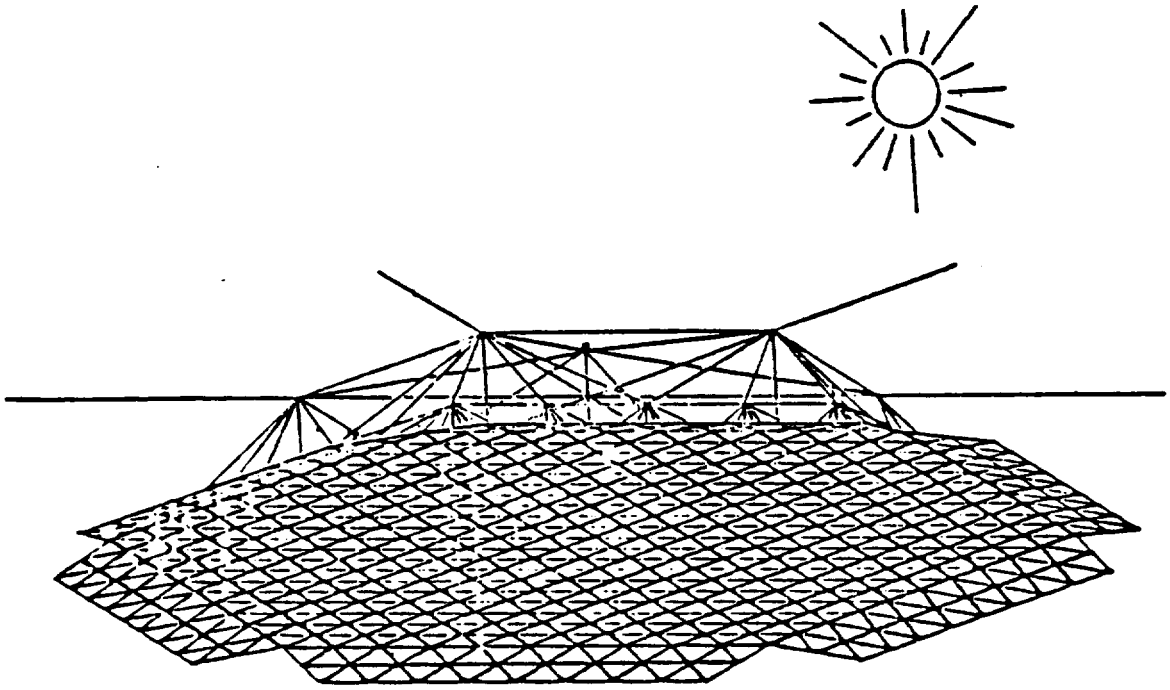

FEATURES

- ISP = ESSENTIALLY INFINITE
- T/W = 10^{-4}

RISK/FEASIBILITY ISSUES

- CANNOT OPERATE BELOW 1000 KM
- FABRICATION AND HANDLING OF VERY THIN (0.1 MICRON) FILMS

Figure 4.1-1: Solar Sail Configuration

to assemble the tens of thousand of fragile subpanels into a working solar sail? Can the assembly and operation of solar sails be automated or is human control necessary?

Because the solar sail was not compatible with LEO-GEO mission requirements of this study, it was not characterized. As a potential contender for low-cost deep-space transportation, however, it should be supported at a level commensurate with other candidate systems.

4.2 Antimatter Rocket

Mass annihilation provides the greatest energy per unit mass and the highest specific impulse of any concept which expels mass to provide thrust. The reaction of antimatter with ordinary matter converts both particles into

energetic photons which could be directed by a very efficient reflector to provide thrust (photon drive). This would result in a specific impulse of 3 x 10^7 sec, which makes the antimatter rocket the only device that could theoretically reach a significant fraction of the speed of light.

Obviously, a detailed analysis of antimatter propulsion is neither possible nor warranted because no way to efficiently produce or store signficant amounts of antimatter has been found. Antimatter propulsion remains technically feasible and desirable; but until a breakthrough in antimatter production and storage is made, no further work is recommended.

5.0 OBSERVATIONS

At the conclusion of the survey and characterization task described in this volume, it was apparent that there were going to be no easy winners. The less data available on any given concept, the better the concept looked; but as holes in data were filled, performance degraded until it was comparable to other advanced concepts. The performance levels attained by the concepts surveyed are shown in Figure 5.0-1; note that all have specific impulses higher than those of chemical rockets.

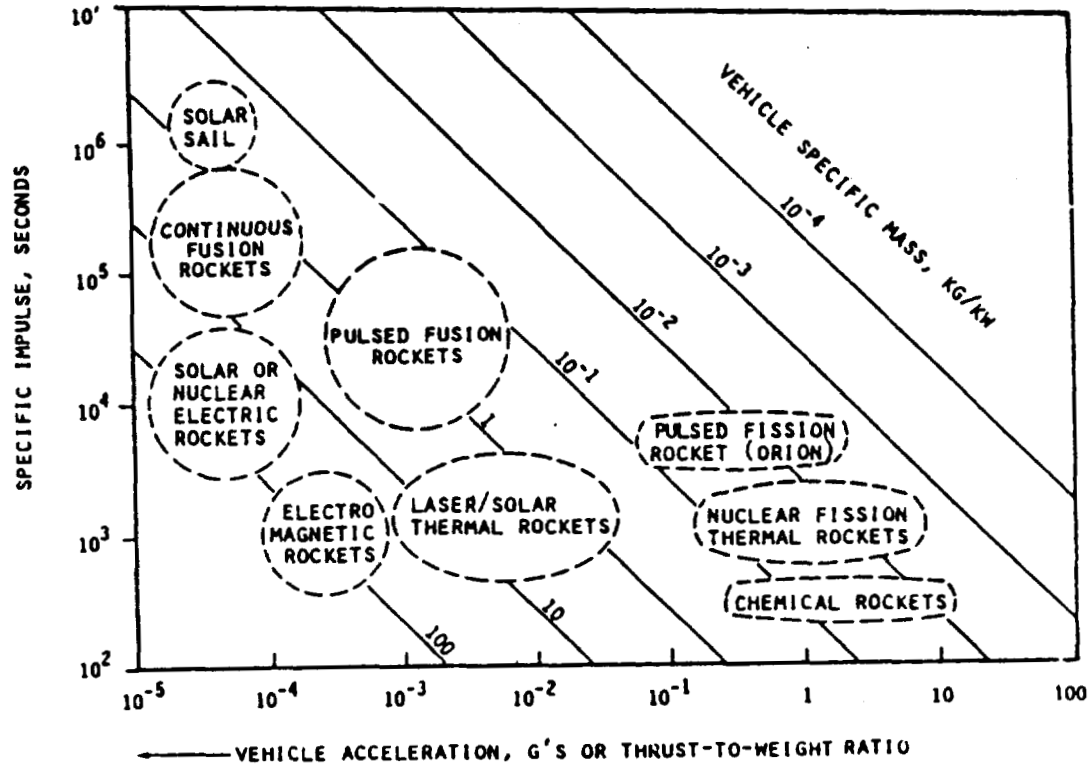

Figure 5.0-1: Propulsion System Performance

Advanced propulsion concepts shown fall into two categories: (1) those that can be developed in the near future using today's design level technology and (2) those appearing to be physically realizable, extrapolating from today's technology, but for which detailed design data do not exist. The first category includes solar and nuclear electric rockets, laser and solar thermal rockets, and fission thermal rockets. These concepts were all recommended for vehicle level assessment in the next part of the study. The second category includes the solar sail, pulsed fission rocket, pulsed fusion

rocket, and continuous fusion rocket. These concepts appear to have tremendous potential for deep-space exploration and exploitation, but they also appear to be unsuitable for LEO to GEO operations (a prerequisite mission of the current study); therefore no concepts from the second category were recommended for assessment in Task 2.

To address the issue of mission models, a chronology of future orbit transfer missions and corresponding vehicle requirements is shown in Figure 5.0-2, starting with the first operational use of the space shuttle. This

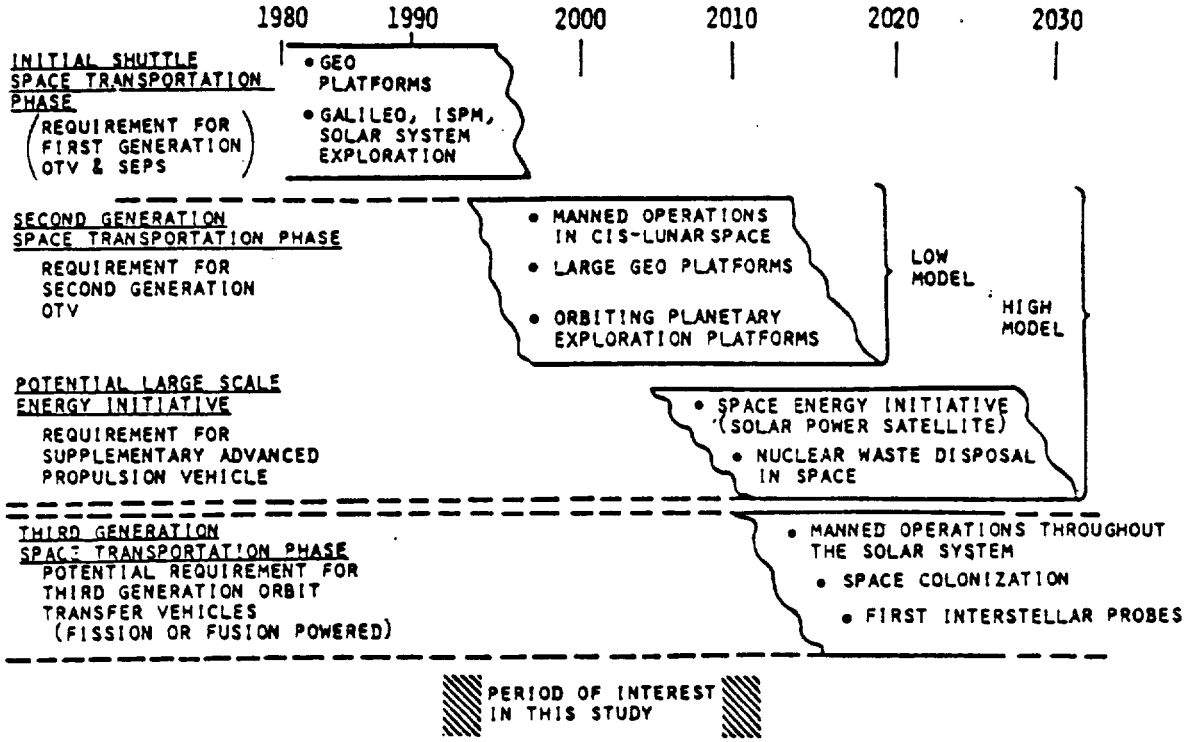

Figure 5.0-2: Upper-Stage Vehicle and Mission Chronology

phase will involve expendable vehicles beginning with IUS and ending with the initial LOX-LH_2 OTV and first-generation SEPS. These vehicles will perform early GEO platform deliveries and solar system exploration missions. From 1992 through about 2010, a series of missions are planned requiring manned presence in GEO and large-scale use of cislunar space for commercial and military applications. These missions require new space transportation vehicles with larger payload capability plus reusability for cost reduction. The advanced propulsion vehicles recommended for vehicle level assessment were recommended with these second-generation missions in mind.

The third-generation phase begins when human technology has advanced to the point where manned exploration and operations outside cislunar space are

possible. Space transportation in this era will require very high delta-V's at relatively high thrust-to-weight ratios (10^{-3} to 10^{-2}) to reduce manned mission times to acceptable limits (1 to 2 years). This will necessitate the use of high-energy fission and/or fusion propulsion to reach the gigawatt power levels required. Requirements for these propulsion systems were to occur some time after 2010. Even though this era is of extreme interest in some circles, it was not a subject of this study and advanced fission and fusion propulsion concepts were not pursued beyond the survey task.

6.0 REFERENCES

1-1 Gabriel, D. S. and Helms, I., "The New Status of Space Nuclear Propulsion in the United States of America," Atomic Energy Review, vol. 12, no. 4, p. 801.

1-2 Moeckel, W. E., "Comparison of Advanced Propulsion Concepts for Deep Space Exploration," J. Spacecraft, December 1972, p. 863.

1-3 Niehoff, J. C. and Friedlander, A. L., "Comparison of Advanced Propulsion Capabilities for Future Planetary Missions," J. Spacecraft, August 1974, p. 566.

1-4 Fishback, L. H. and Willis, E. A., Jr., "Performance Potential of Gas-Core and Fusion Rockets: A Mission Applications Survey," J. Spacecraft, August 1972, p. 569, and NASA TMX-67940.

2-1 Mead, F. B. Jr., "Advanced Propulsion Concepts - Project Outgrowth," AFRPL-TR-72-31, June 1972, p. I-12.

2-2 Ibid, I-26.

2-3 Anon., "Stable Spin-Polarized Atomic Hydrogen," Physics Today, June 1980.

2-4 Cline, R. W., Greytak, T. Y., et al, "Production and Magnetic Confinement of Spin-Polarized Hydrogen," Dept. of Physics, MIT (published in Le Journal de Physique, 1980).

2-5 Papailiou, D. D., "Frontiers in Propulsion Research: Laser, Matter-Antimatter, Excited Helium, Energy Exchange, Thermonuclear Fusion, NASA-CR-142707, p. 120, March 1975.

2-6 Bussard, R. W., and De Lauer, R. D., "Fundamentals of Nuclear Flight," McGraw Hill, 1965.

2-7 Balcomb, J. D., "Nuclear Rocket Reference Data Summary," Los Alamos Scientific Laboratory Report LA-5057-MS, October 1972.

2-8 Durham, F. P., "Nuclear Engine Definition Study," Los Alamos Scientific Laboratory Report LA-5044-MS, vols. I, II, and III, Sept. 1972.

2-9 Altseimer, J. H., and Booth, L. A., "The Nuclear Rocket Energy Center Concept," AIAA paper No. 72-1091, Dec. 1972.

2-10 Balcomb, J. D., "Preliminary Mission Studies for a Small Nuclear Engine," LASL report LA-4890-MS, March 1972.

2-11 TRW Systems Group, "Dual Mode Nuclear Rocket Applications Study, vols. I and II," NASA CR 123934 and CR 123935, September 1972.

2-12 Balcomb J. D., "Mission Performance of a 360-MW Nuclear Rocket Engine." Los Alamos Scientific Laboratory report No. LA-DC-72-1255, October 1972.

2-13 McDonnell Douglas Astronautics Company. "Mission Planning Handbook for Small Nuclear Stage Applications," MDC G4304, February 1973.

2-14 Hatch, L. P., Regan, W. H., and Powell, J. R., "Fluidized Solids as a Nuclear Fuel for Rocket Propulsion," ARS Journal, April 1961, p. 547-548.

2-15 Lindauer, G. C., Tichler, P., and Hatch, L. P., "Experimental Studies on High-Gravity Rotating, Rotating Fluidized Beds," BNL-50013 (T-435), Brookhaven National Laboratory, 1966.

2-16 Hendrie, J. M., Hoffman, K. C., et al, "Rotating Fluidized Bed Reactor for Space Nuclear Propulsion," Brookhaven National Laboratory report No. BNL-50321 (UC-33), August 1971.

2-17 Ludewig, H. and Chernick, J., "Physics Parameters of the Hatch Reactor," Transactions of the American Nuclear Society, vol. 14, No. 1, 1971, p.11.

2-18 Ludewig, H., Manning A. J., and Roseman, C. J., "Feasibility of Rotating Fluidized Bed Reactor for Rocket Propulsion," Journal of Spacecraft, vol. II, No. 2, February 1974, p. 65-71.

2-19 Anderson, L. A., Hasinger, S. H. and Turman, B. N., "Two-Component Vortex Flow Studies of the Colloid Core Nuclear Reactor," Aerospace Research Labs, Wright-Patterson AFB, ARL-72-0096, December 1971.

2-20 Barrett, W. L. Jr., "Preliminary Investigation of the Feasibility and Potential of a Liquid core Nuclear Rocket," Boeing Aerospace Document D2-22111, May 1963.

2-21 Nelson, S. T., Grey, J., and Williams, P. M., "Conceptual Study of a Liquid-Core Nuclear Rocket," Journal of Spacecraft, vol. 2, No. 3., p. 384, June 1964.

2-22 McGuirk, J. P., and Park, C., "Propellant Flow Rate Through Simulated Liquid Core Nuclear Rocket Fuel Bed," Journal of Spacecraft, vol. 9, No. 5, p. 375, May 1972.

2-23 Ragsdale, R. G., "Status of Open-Cycle Gas-Core Reactor Project Through 1970," NASA-TM-X2259, NASA, March 1971.

2-24 Ragsdale, R. G., "High Specific Impulse Gas-Core Reactors," NASA-TM-X-2243, NASA, March 1971.

2-25 Fishback, L. H., "Mission Performance Potential of Regeneratively Cooled Gas-Core Nuclear Rockets," NASA-TM-X 2256, NASA, April 1971.

2-26 Kascak, A. F., "Nozzle and Cavity Wall Cooling Limitations on Specific Impulse of a Gas-Core Nuclear Rocket," NASA-TM-X-67923, NASA, 1971.

2-27 Ragsdale, R. G., et al, "Gas-Core Rocket Reactors: A New Look," NASA-TM-X-67823, NASA, 1971.

2-28 Kascak, A. F. et al, "Bleed Cycle Propellant Pumping in a Gas-Core Nuclear Rocket Engine System," NASA-TM-X-2517, NASA, March 1972.

2-29 Turney, G. E., et al, "Dynamic Analysis of an Open-Cycle Gas-Core Nuclear Rocket," NASA-TM-X-2784, NASA, April 1973.

2-30 Ragsdale, R. G., "Some Fuel Loss Rate and Weight Estimates of an Open-cycle Gas-Core Nuclear Rocket," NASA-TM-X-52775, NASA, 1970.

2-31 Putre, H. A., "Estimates of Fuel Containment in a Coaxial Flow Gas-Core Nuclear Rocket," NASA-TM-X-52838, NASA, 1970.

2-32 Weinstein, H., "Review of Coaxial Flow Gas-Core Nuclear Rocket Fluid Mechanics," NASA-CR-158549, Illinois Institute of Technology, July 1976.

2-33 Rodgers, R. J., et al, "Analytical Design and Performance Studies of the Nuclear Light Bulb Engine," NASA-CR-129296, United Aircraft Corp., Sept. 1972.

2-34 McLafferty, G. H., "Squeezing the Last Drop out of the Gas-core Reactor Part A, Nuclear Light Bulb Rocket Engine," Proceedings of the AFOSR Symposium on Advanced Propulsion Concepts," AFOSR-TR-71-3128, p. 295, March 1972.

2-35 Hutchinson, P. I., "Radiation Exposure to the Orbiting Lunar Station and Lunar Surface Related to Reusable Nuclear Shuttle Operations," NASA-TM-X-2440, p. 264, January 1972.

2-36 Masser C. C., "Crew Radiation Dose from a High-Impulse Gas-Core Nuclear Rocket Plume," J. Spacecraft, vol. 9, No. 8, p. 597, August 1972.

2-37 Rice, E. R., et al, "Technical Report on Analysis of Nuclear Waste Disposal in Space - Phase III," contractor report for NASA Contract NAS8-32391, Battelle-Columbus Laboratories, Columbus, Ohio, March 31, 1980.

2-38 Shipps, P. R., "Manned Planetary Exploration Capability Using Nuclear Pulse Propulsion," GA-6224, N65-30677, March 1965.

2-39 Martin, A. R. and Bond, A., "Nuclear Pulse Propulsion: A Historical Review of an Advanced Propulsion Concept," TBIS, vol. 32, pp. 283-310, 1979.

2-40 Boyer, K. and Balcomb, J. K., "System Studies of Fusion-Powered Pulsed Propulsion Systems, AIAA paper No. 71-636, presented at 7th Propulsion Joint Specialist Conference, 14-18 June 1971 (LA-DC-12520).

2-41 Fowler, T. K.; "Fusion Research in Open-Ended Systems Nuclear Fusion," vol. 9, 1969.

2-42 Post, R. F.; "Fusion Power: Direct Conversion and the Reduction of Waste Heat," TID-25414, 1970.

2-43 Post, R. F.; "Nuclear Fusion by Magnetic Confinement," Proceedings of IEEE Intercon Conference Records (UCRL-74445), New York, 1973.

2-44 Chu, T. K.; Physics Today, Aug. 1980, p. 19.

2-45 Grieger, Renner; International Conference on Plasma Physics and Controlled Nuclear Fusion, Brussels, Belgium, 1980.

2-46 Robinson, C. A. Jr.; "Aerospace Aids Fusion Power Concept," Aviation Week & Space Technology, 12 June 1978, pp. 60-61.

2-47 Boyer, K. & Balcomb, J. D.; "System Studies of Fusion-Powered Pulsed-Propulsion Systems," AIAA paper No. 71-636, June 1971.

2-48 Lubin, M. J.; "Laser-Produced Plasmas for Power Generation and Space Propulsion," Astro. and Aero., vol. 8, No. 11, 1970. pp. 42-48.

2-49 Hyde, R., Wood, L., and Nuckolls, J.; "Prospects for Rocket Propulsion with Laser-Induced Fusion Microexplosions," AIAA paper No. 72-1063, December 1972.

2-50 Winterberg, G.; Nature, No. 286, 24 July 1980, p. 365.

2-51 Project Daedalus Study Group; "Project Daedalus: The Final Report on the BIS Starship Study," JBIS, vol. 31, supplement 1978.

2-52 Martin, A. R. and Bond, A.; "Nuclear-Pulse Propulsion: A Historical Review of an Advanced Propulsion Concept, JBIS, vol. 32, pp. 283-310, 1979.

2-53 Nebolsine, P. E., Pirri, A. N., et al, "Pulsed Laser Propulsion," presented at AIAA Conference on High-Power Lasers, Cambridge, Mass., Oct. 1978.

2-54 Douglas-Hamilton, D. H., Kantrowitz, A. R., and Reilly, D. A., "Laser-Assisted Propulsion Research," AVCO Everett Research Laboratory, Inc., Everett, Mass., 1978.

2-55 Shoji, J. M., "Laser-Heated Rocket Thruster," NASA CR-135128, Rocketdyne Division of Rockwell International, May 1977.

2-56 Kemp, N. H. and Root, R. G., "Analytical Study of Laser-Supported Combustion Waves in Hydrogen," Journal of Energy, vol. 3, No. 1, p. 40, January 1979.

2-57 Fowler, M. C., Newman, L. A., and Smith, D. C., "Beamed Energy Coupling Studies," Final Technical Report AFRPL-TR-79-51, United Technologies Research Center, January 1980.

2-58 Klein, J. F., "Experiments to Simulate Heating of the Propellant in a Nuclear Light Bulb Engine Using Thermal Radiation from a DC Arc Radiant Energy Source," UARL report K-910900-8, September 1971.

2-59 Klein, J. F., "Nuclear Light Bulb Propellant Heating Simulation Using a Tungsten/Argon Aerosol and Radiation from a DC Arc Surrounded by a Segmented Mirror Cavity," UARL report L-910900-13, September 1972.

2-60 Selph, C., and Horning, W., "Laser Propulsion," IAF Paper 76-166, 27th Congress of the International Astronautical Federation (IAF), Oct. 1976.

3-1 "Thermionic/Thermoelectric Energy Conversion Technology Development Program," Volume I Progress Report: May 3, 1979, JPL Report 730-49.

3-2 "Study of Reactor Brayton Systems for Nuclear Electric Spacecraft," Sept. 28, 1979, AiResearch Co., for California Institute of Technology-Jet Propulsion Laboratory, Contract 955008.

3-3 Clark, K. E., von Jaskowsy, W. F., Wolff, M., and Budd, D. W., "MPD Thruster Operation with Inductively Stored Energy," AIAA Paper 79-2073, International Electric Propulsion Conference, Princeton, N. J., 1979.

3-4 Glasoe, G. N. and Lebacqz, J. V., Pulse Generators, McGraw-Hill Book Co., Inc., New York, N. Y., 1948.

3-5 Eckhardt, W. O. and Hofmann, G. A., "A 10-kA, 30-kV Liqui-Metal Plasma Valve Switch for Inductive Energy Storage," IEEE Paper No. 75, CHI 097-5NPS, Sixth Symposium on Engineering Problems of Fusion Research.

3-6 Ramrus, A., White, W., and Palumbo, D., "Development of a High Energy density Capacitor for Plama Thrusters," AIAA Paper No. 79-2084, 1979.

3-7 The Boeing Co., "Microwave Power Distribution Systems," D180-22876-4 SPS Systems Definition, NASA Contract NAS9-15196, December 1977.

3-8 Billingham and Gilbreath, Editors, NASA SP-428, Space Resources and Space Settlements," 1979.

3-9 Snow, W. R. and O'Neill, G. K., "Construction and Testing of the 2.5m Mass Driver," AIAA paper No. 79-2095 (Oct. 30 - Nov. 1, 1979).

3-10 Snow, W. R. and Dunbar, R. S., "Mass Drriver Reaction Engine Characteristics and Performance in Earth Orbital Transfer Missions," Princeton/AIAA/SSI 5th Conference on Space Manufacturing, May 1981.

3-11 O'Neill, G. K., et al, "High Performance Mass Drivers," Princeton/ AIAA/SSI 5th Conference on Space Manufacturing, May 1981.

3-12 Rashleigh, S. C. and Marshall, R. A., "Electromagnetic Acceleration of Macroparticles to High Velocities," J. Appl. Phys., 49, pp 2540-2542, (April, 1978).

3-13 Hawke, R. S. et al, "Results of Railgun Experiments Powered by Magnetic Flux Compression Generators," ARRADCOM/DARPA Conference on Electromagnetic Guns and Launchers, San Diego, Nov. 1980.

3-14 Barber, J. P., AIAA paper No. 2091 (Oct. 30 - Nov. 3, 1979).

3-15 Bauer, D. P. and Barber, J. P., "The Electric Rail Gun for Space Propulsion," NASA CR 165312, Final Technical Report - Contract No. NAS3-22475, Feb. 1981.

3-16 Dailey, C. L. et al, Advanced Electric Propulsion Technology - High Thrust, "Final Report, AFRPL contract No. FO4611-79-C09958, TRW Space Systems, Sept. 1980.

3-17 Dailey C. L. and Lovberg, R. H., "Large-Diameter Inductive Plasma Thrusters," AIAA paper No. 79-2093, Nov. 1979.

4-1 Drexler, K. E., "Design of a High Performance Solar Sail System," MIT Thesis, May 1979.

4-2 Drexler, K. E., "High Performance Solar Sails and Related Reflecting Devices," Fourth Priceton/AIAA Conference on Space Manufacturing Facilities, paper No. 79-1418, May 1979.